Spring 1-1-2012

Experimental Study and Theoretical Modeling of Recycled Aggregate Concrete and Evaluation of Long-Term Performance of Reinforced Concrete Bridge Decks

Yu-chang Liang
University of Colorado at Boulder, yu-chang.liang@colorado.edu

EXPERIMENTAL STUDY AND THEORETICAL MODELING OF RECYCLED AGGREGATE CONCRETE

AND

EVALUATION OF LONG-TERM PERFORMANCE OF REINFORCED CONCRETE BRIDGE DECKS

By

YU-CHANG LIANG

B.S, National Central University, 1998

M.S, National Taiwan University, 2000

A thesis submitted to the

Faculty of the Graduate school of the

University of Colorado for the degree of

Doctor of Philosophy

Department of Civil, Environmental, and Architectural Engineering

2012

This thesis entitled:

EXPERIMENTAL STUDY AND THEORETICAL MODELING OF RECYCLED AGGREGATE CONCRETE

AND

EVALUATION OF LONG-TERM PERFORMANCE OF REINFORCED CONCRETE BRIDGE DECKS

written by Yu-chang Liang
has been approved for the Department of
Civil, Environmental, and Architecture Engineering

Yunping Xi, Committee Chair

Ross Corotis, Committee Member

Mettupalayam Siva, Committee Member

Franck Vernerey, Committee Member

Kevin Rens, Committee Member

Date

The final copy of this thesis has been examined by the signatories, and we find that both the content and the form meet acceptable presentation standards of scholarly work in the above mentioned discipline.

YU-CHANG LIANG (Ph.D., Civil, Environmental, and Architectural Engineering)

Experimental Study and Theoretical Modeling of Recycled Aggregate Concrete

and

Evaluation of Long-Term Performance of Reinforced Concrete Bridge Decks

Thesis directed by Professor Yunping Xi

This dissertation covers two themes: one for experimental and theoretical studies of recycled aggregate concrete (RAC) and the other for the performance evaluation of chemical sealers applied to reinforced concrete (RC) bridge decks.

For the first theme, the research has found that a better mixing approach, better water to cement ratio, and more appropriate surface treatments can improve RAC's mechanical properties. We further checked its durability properties. Also, this research has developed a theoretical model for analyzing and predicting various properties of RACs such as bulk modulus, volume fraction, shear modulus, and shrinkage strain. One of the durability properties, drying shrinkage, was used to modify this multiscale and multiphase model.

The second theme includes: (1) discovering the corrosion initiation time of the rebar embedded in RC bridge decks attacked by the chloride ions from deicers; (2) giving the rankings of four popular sealer products applied to RC bridge decks based on the results of long-term performance monitoring; and (3) deriving diffusion equation models in comparisons with field performance measurements and combining those with concrete composite damage model.

DEDICATION

To all of my family

Ming-Hong Liang,
Tsia-Mei Hsieh,
and Yuan-Hao Liang.

ACKNOWLEDGEMENTS

I would like to gratefully and sincerely thank to my advisor, Professor Yunping Xi, for his guidance, understanding, encouragement, and most importantly, his friendship during my study in the University of Colorado at Boulder.

I am also grateful to Professor Ross Corotis, Mettupalayam Siva, Franck Vernerey, and Kevin Rens for taking the time to serve on my thesis committee and for their expert guidance and invaluable discussions. Special thanks are offered to Professor Yunping Xi and Franck Vernerey, Colorado Department of Transportation, and National Science Foundation for their guidance and financial support, without which my work would not have been possible.

Additionally, I would like to thank the many CDOT personnel that assisted with this study. A special thanks to Aziz Khan of the DTD Applied Research and Development Branch; Ali Harajli, Mark Nord, and Golda Davydov of the Bridge Design and Management Branch; Patrick Kropp and Eric Prieve of the Materials and Geotechnical Branch; Glenn Frieler and Gary DeWitt of Region 4; and Mathew Greer of the Federal Highway Administration.

I would like to extend my gratitude to my friends and colleagues, who have offered fruitful suggestions during this work: Dr. Nattapong Damrongwiriyanupap, Dr. Okpin Na, Dr. Pania Meshgin, for their encouragement and friendship.

Finally, I would like to give my profound appreciation to my parents for their love, unconditional support, and endless encouragement. Their constant love and sacrifices over the years have made it possible to complete my studies in the U. S. I want to share the joy with them.

CONTENTS

TABLE OF TABLES

TABLE OF FIGURES

Chapter 1

Organization

This dissertation covers two themes: one for experimental and theoretical studies of recycled aggregate concrete (RAC) and the other for the performance evaluation of chemical sealers applied to reinforced concrete (RC) bridge decks. The corresponding chapter sections are shown in Figure 1.1.

For the first theme, the research has found that a better mixing approach, better water to cement ratio, and more appropriate surface treatments can improve RAC's mechanical properties. We further checked its durability properties. Also, this research has developed a theoretical model for analyzing and predicting various properties of RACs such as bulk modulus, volume fraction, shear modulus, and shrinkage strain. One of the durability properties, drying shrinkage, was used to modify this multiscale and multiphase model.

The second theme includes: (1) discovering the corrosion initiation time of the rebar embedded in RC bridge decks attacked by the chloride ions from deicers; (2) giving the rankings of four popular sealer products applied to RC bridge decks based on the results of long-term performance monitoring; and (3) deriving diffusion equation models in comparisons with field performance measurements and combining those with concrete composite damage model.

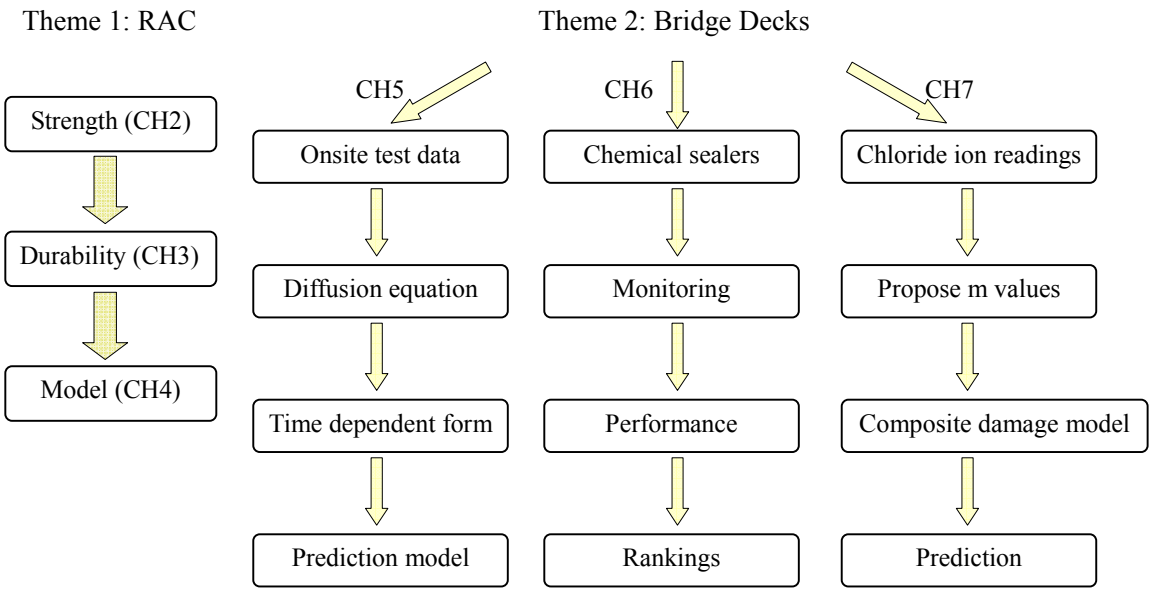

Figure 1.1 Outline

Chapter 2 presents a systematic experimental study on various properties of RAC. The study aims to find a better mixing approach, better water to cement ratio, and more appropriate surface treatment methods for improving mechanical properties of RAC.

Chapter 3 uses the best RAC mixture obtained from Chapter 2 and checks its durability properties including freeze-thawing cycle tests, drying shrinkage, and rapid chloride permeability tests.

Chapter 4 describes a multiscale chemomechanical coupled analytical model for characterizing mechanical and transport properties of RAC. The RAC will be considered as multiphase composites at both meso-scale and micro-scale levels. Composite mechanics models will be used at the selected scale levels to characterize effective properties of RAC. The volume fractions of different constituents in the old and new concrete will be calculated based on the degrees of hydration of old and new cements.

Chapter 5 focuses on the experimental study and theoretical analysis of chloride penetration in five bridge decks with different topical protection systems. The goal is to determine the service life of the decks in terms of corrosion initiation time of the rebar under different topical protection systems. In the theoretical analysis, the degradation of diffusion coefficient of the concrete with time was considered in

the model. By calibrating the model parameters in the analytical model with the chloride concentration profiles obtained from the bridges, a more reliable prediction model for corrosion initiation time of the bridges was established.

Chapter 6 concentrates on the long-term monitoring and performance comparisons of four chemical sealer products. In this section, these sealants are applied on selected RC bridge decks and by comparing four parameters: skid resistance, temperature, moisture, and chloride concentration; we rank their performance to find the better chemical sealer.

Chapter 7 continues the derivations of time dependent diffusion equations from Chapter 5 and uses the on-site test data of chloride ion concentration in Chapter 6 to derive a certain m value for each chemical sealer product. In this section, the bridge deck's damage status can be represented based on its certain m value. In addition, we combine the composite damage model of concrete with the above equations and give the prediction of chloride concentration profiles and rebar's corrosion initiation time.

Chapter 2

Recycled aggregate concrete

2.1. Motivations

Due to the growing difficulty in obtaining natural aggregate concrete (NAC) and taking into consideration the environmental issues as well as the high social cost, the construction industry needs to find a feasible alternative. Construction and demolition waste (CDW) constitutes a major portion of all generated solid waste, with 200 to 300 million tons generated annually in the United States alone (Meyer 2009). Therefore, a possible feasible alternative is to reuse construction and demolition waste as aggregates to incorporate into the production of new concrete or totally replace new concrete.

Recycled aggregate concrete (RAC) has become one of the sustainable technologies in concrete industry in past decades due to its great environmental advantages (Mueller et al. 2008; Ann et al. 2008; Limbachiya et al. 2008; Rahal 2007; Tu et al. 2006; Oikonomou 2005). In the USA, about 30 million tons of concrete has to be discarded each year (Jiusu et al. 2009). Although the extensive use of RAC in the construction industry has environmental benefits, only a very small portion of the concrete waste is reused as aggregate in new concrete construction (Abbas et al. 2006). The main reason is the poor quality of RAC. As a result, RAC has not been used as a structural material.

The poor quality of RAC results from high water absorption capacity, high porosity, and weak bond of interfacial transition zone between recycled aggregate (RA) and new cement mortar. Also, the lack of technical data, lack of specifications and quality control guidelines are some of the reasons responsible for the limited usage of RAC.

In some countries, like Japan, even though the standard specification was drafted by the Ministry of Construction in 1996, it has still hardly been applied to actual structures because of the high cost for

production (K. Eguchia et al. 2007). In Hong Kong, various governmental departments of the Hong Kong Special Administrative Region (HKSAR) are encouraging the use of RA in the local construction industry by issuing various guidelines and specifications. Owing to uncertainty about its properties, practitioners are skeptical of using it as a substitute (Tam, V. W. Y., and Tam, C. M. 2009). Even ACI-555R (Lamond et al. 2002) provides some guidelines for proportioning of concrete mixes made with RAC, henceforth termed RAC concrete. Neither it nor any other source gives a specific mix design method for achieving targeted fresh and hardened properties for recycled aggregate concrete.

RAC has been studied by applying conventional mix proportioning methods (Dhir et al. 1999); (Limbachiya et al. 2000); (Mandal et al. 2002); (Gomez Soberon 2002 a,b,c), treating RAC as a homogenous material, like the natural aggregate, but with its own absorption capacity, density, and other pertinent properties. In previous studies, researchers investigating the strength growth of RAC found it could be 10-25% lower than that of conventional concrete made with natural coarse aggregate (Tabsh and Abdelfatah 2009). Furthermore, concrete made with 100% recycled aggregate coarse aggregates has 20-25% less compressive strength than the conventional concrete at 28 days after being mixed, with the same effective water to cement ratio (water to cement ratio = 0.50) and cement quantity (Etxeberria et al. 2007). Recycled aggregate is well acknowledged for its poorer quality due to the higher porosity resulting from cement mortar remaining attached to its surface.

Tam et al. 2005 proposed a two-stage mixing approach (TSMA) for improving the strength of RAC made of up to 30% RA replacement. Experiments achieved improvements in strength of recycled aggregate concrete. Another new approach in mixing concrete extends this work by exploring RA substitutions ranging from 0% to 100% and comparing their performance with the traditional mixing procedure (Tam et al. 2007). The test results were then optimized using general regression neural networks (GRNN) and RA replacements of 25% to 40% and 50% to 70% were found to be optimal when the TSMA was adopted.

Water to cement ratio is one of the important factors in controlling the casting quality as well as

the mechanical properties of RAC, which due to its higher porosity, results in cement mortar remaining attached to its surface, thus hampering the recycling rate of concrete waste. In order to solve the major problem of replacing 100% of natural coarse aggregates with recycled aggregate in construction sites, we applied a surface treatment with cement slurry or with cement slurry plus silica solution before mixing and compared their performances.

This surface treatment method of adding silica solution was used to treat regular aggregate (Shah and Li, 1992). Natural aggregates were coated with cement slurry plus silica fume prior to mixing with cement and water. It was shown that the bonding strength of the treated natural aggregate increased. A similar method was used for recycled aggregates (Katz 2004). It was also shown that impregnation of the recycled aggregate with a 10% by weight silica fume solution can increase compressive strength by 23-33 % and 15% at ages 7 and 28 days respectively.

Other studies (Otsuki et al. 2003); (Tam et al. 2005) showed that recycled aggregates can be coated with mortar of a lower water-binder ratio than the rest of the concrete mix and improvements can be achieved in terms of strength, chloride penetration and carbonation resistances of RAC. Kou et al. (2007) showed that adding fly ash in recycled concrete can reduce chloride permeability of RAC but also reduces the strength of the concrete. All previous studies did not compare the performances of different surface treatment methods and did not come up with an optimum method. As a result, the potential users of RAC do not have specific guidelines to follow. Furthermore, the reduced compressive strength of RAC is often used as the only reason for not using it, while multiple criteria (strength, workability, and durability) have been used in practice for selection of regular concrete mixes.

Some researchers also developed two different mixing approaches. In the first, called TSMAs (silica fume), they added silica fume into certain percentages of recycled aggregate in the pre-mixing procedure. In another approach, called two-stage mixing approach (silica fume and cement) (TSMAsc) (Tam, V. W. Y., and Tam, C. M. 2008), they added silica fume and proportional amounts of cement into certain percentages of RA in the first mix. They concluded that TSMAs and TSMAsc can provide

alternative methodologies for further improvement in the quality of this recyclable material.

2.2. Pretest

In order to get an idea of which water to cement ratio could lead to better casting quality as well as high compressive strength when using 100% recycled coarse aggregate, the pretest was preformed before the main test. The pretest can also be divided into two sets of experiments. The first one was conducted by fixing the water to cement ratio at 0.5 and applying different surface treatments. From the test results, we realized keeping the water to cement ratio at 0.5 for 100% recycled coarse aggregate was not a good option. The specimen was too dry to achieve acceptable compressive strength. Therefore, we added more water in the mixing process during the second part of the pretest and hoped that would improve its slump and workability.

In the first part of the pretest, each group contained three cases of 4×8 concrete cylinders and the compressive test was performed after 14 days. Group 1 was the control batch and had regular concrete cylinders. In Group 2, 100% of coarse aggregate was replaced with recycled coarse aggregate and all other variables were kept equal to the proportions of Group 1. In Group 3, the cement slurry was first used to cover the surface of recycled coarse aggregate and left for two days, then mixed with treated coarse aggregate with fine aggregate (sand), cement, and water. The proportions of all other materials followed Groups 1 and 2. In Group 4, the silica fume was added into the cement slurry to administer the surface treatment. The treatments and mix designs are detailed in Tables 2.1 and 2.2. The process is shown in Figures 2.1 through 2.4.

From Figure 2.5, it is obvious the specimen that keeps the water to cement ratio at 0.5 for 100% recycled coarse aggregate replacement would be too dry to achieve acceptable compressive strength. Therefore, more water was added in the mixing process in hopes of improving the slump and workability in the second part of the pretest.

Table 2.1 Treatments (first part of pretest)

	Treatments
Group 1	Natural coarse aggregate + sand + cement + water
Group 2	Recycled coarse aggregate + sand + cement + water
Group 3	Step 1: recycled coarse aggregate + cement+ water; then wait for two days. (surface treatment)
	Step 2: The materials from Step 1 + cement + sand + water
Group 4	Step 1: recycled coarse aggregate+ cement+ silica fume+ water; then wait for two days. (surface treatment)
	Step 2: The materials from Step 1 + cement + sand + water

Table 2.2 Mix designs (first part of pretest)

Group 1	Natural coarse aggregate	1012.72 (kg/m^3)
	Fine aggregate (Sand)	871.52 (kg/m^3)
	Cement	355.97 (kg/m^3)
	Water	177.98 (kg/m^3)
Group 2, 3	Recycled coarse aggregate	974.23 (kg/m^3)
	Fine aggregate (Sand)	871.52 (kg/m^3)
	Cement	355.97 (kg/m^3)
	Water	177.98 (kg/m^3)
Group 4	Recycled coarse aggregate	974.23 (kg/m^3)
	Fine aggregate (Sand)	871.52 (kg/m^3)
	Cement	355.96 (kg/m^3)
	Silica fume	101.27 (kg/m^3)
	Water	177.98 (kg/m^3)

Figure 2.1 Recycled coarse aggregate

Figure 2.2 Material preparation

Figure 2.3 Surface treatments with cement slurry in Group 3

Figure 2.4 Surface treatments with cement slurry plus silica fume in Group 4

Figure 2.5 Casting of Group 2

In the second part of the pretest, three sets of concrete cylinders were cast belonging to Group 5, Group 6, and Group 7. In Group 5, more water (w/c=0.78) was added based on experience to make sure the workability of these specimens was good enough, but a concern was that the higher water to cement ratio might lead to lower compressive strength. Therefore, in Group 7, we added less water (w/c=0.64) in the mixing process and hoped to improve the strength as well as the casting quality. In Group 6, the concrete cylinder was composed with regular coarse aggregate and the water to cement ratio was kept at 0.5 just like in the first part of the pretest. The purpose of Group 6 was to compare the compressive strength after 3 days with the other two groups. For each group, we cast three 4×8 concrete cylinder and performed compressive tests after 3 days. The mix designs and final water to cement ratio are shown in Table 2.3.

Table 2.3 Mix designs (second part of pretest)

Group 5	Natural coarse aggregate	1012.72 (kg/m^3)
	Fine aggregate (Sand)	871.52 (kg/m^3)
	Cement	355.97 (kg/m^3)
	Water	283.57 (kg/m^3)
	Water to cement ratio	0.78
Group 6	Recycled coarse aggregate	974.23 (kg/m^3)
	Fine aggregate (Sand)	871.52 (kg/m^3)
	Cement	355.97 (kg/m^3)
	Water	177.98 (kg/m^3)
	Water to cement ratio	0.5
Group 7	Recycled coarse aggregate	974.23 (kg/m^3)
	Fine aggregate (Sand)	871.52 (kg/m^3)
	Cement	355.97 (kg/m^3)
	Silica fume	101.27 (kg/m^3)
	Water	233.24 (kg/m^3)
	Water to cement ratio	0.64

2.3. Experimental results of pretest

The curing time for the first part of the pretest was 3 days and the compressive test results are shown in Figure 2.6. Several pictures of the compressive test are shown in Figures 2.7 through 2.10.

In Group 2, the water absorption was much higher than expected and the bad casting quality led to lower compressive strength. In Group 3, the 3-day compressive strength was higher than Group 2. That means the surface treatment using cement slurry apparently improves the strength. In Group 4, adding silica fume into the cement slurry seemed to increase the ratio of water absorption in the covering process.

Its quality was the worst among the four.

After casting the four groups, we reconsidered the water to cement ratio and adopted different surface treatments to decrease the water absorption in the mixing process. So, in the second part of the pretest, we added more water in the beginning to make sure the specimens had enough slump and workability and then decreased the amount of water to achieve higher compressive strength. With this, we could obtain a more appropriate water to cement ratio to take care of both casting quality and strength. The compressive test results in 14 days are shown in Figure 2.11 and the specimens' failure modes are shown in Figure 2.12.

You can see from Figure 2.12 that the casting quality of Groups 5 to 7 was much better than previous cases. This was also verified by test results. The difference between Group 5 and Group 7 was the water to cement ratio. In Group 5, the final water to cement ratio was 0.78. In Group 7, we added less water in the process and finally we got the higher compressive strength which was close to the quality of the specimen with natural coarse aggregate in Group 6.

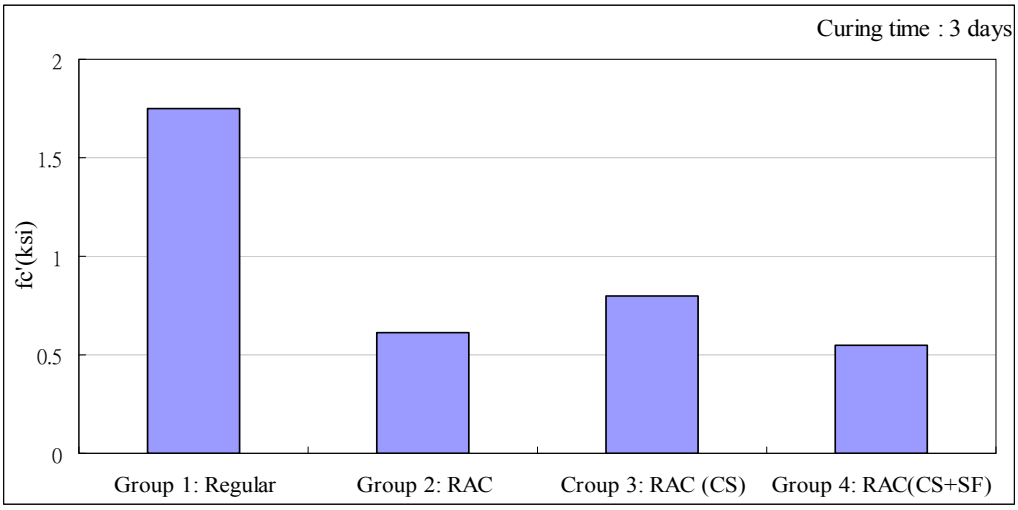

(CS: cement slurry; SF: surface treatment)

Figure 2.6 Comparisons (3-day compressive strength of pretest)

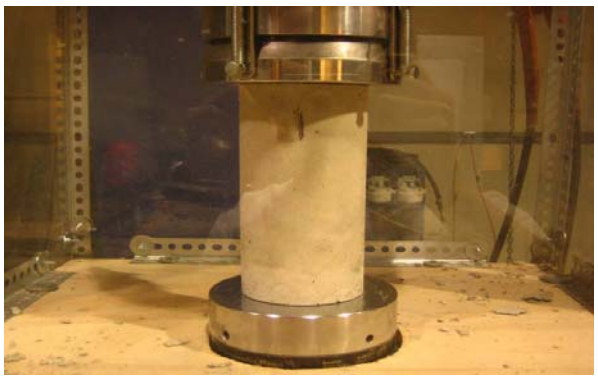

Figure 2.7 Compressive tests (Group 1)

Figure 2.8 Compressive tests (Group 2)

Figure 2.9 Failure modes (Group 1 and 2)

Figure 2.10 Failure modes (Group 3)

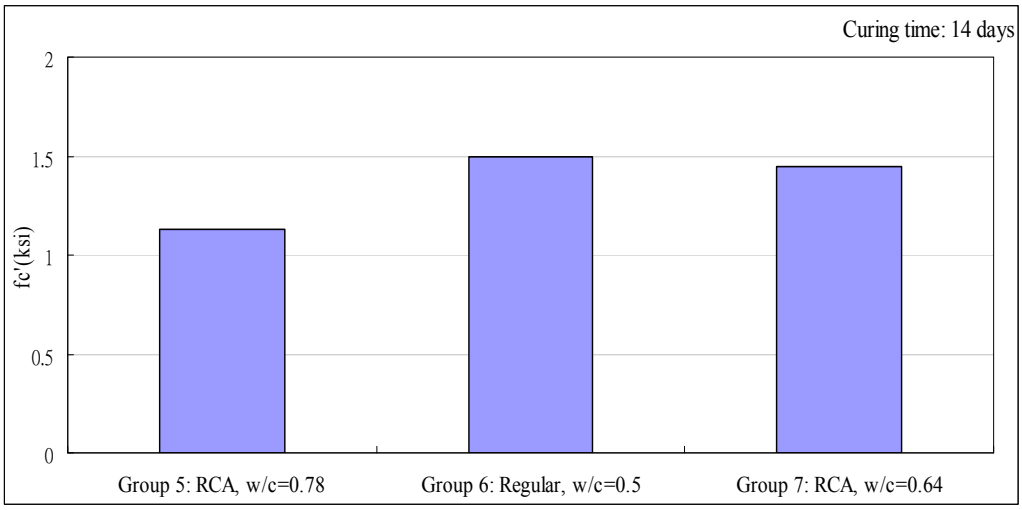

Figure 2.11 Strength comparisons (Groups 5 through 7)

Figure 2.12 Failure modes (Groups 5 through 7)

2.4. Main test

The shaking table was used in the main test, so as expected the casting quality was better than

what resulted in the pretest. Based on previous test results, we found that keeping the water to cement ratio at around 0.49 leads to better casting quality as well as higher compressive strength. So, we used a water to cement ratio closer to 0.49 in our starting set. The main test had four groups and aimed to compare the effects of several factors.

In Group 8, three mixing approaches were adopted and compared for their compressive strengths after 3, 7, and 28 days. They were divided into Groups 8-1 through 8-3. In Group 8-1, we mixed sand, cement, and 3/4 of the total water together for 90 seconds. Then, we added recycled coarse aggregates with the rest of the water and mixed it for another 90 seconds. Because the mortar forms in the beginning, it is called the mortar mixing approach (MMA).

In Group 8-2, we mixed sand and 3/4 of the water together for 30 seconds. Then, we added cement and mixed it for 45 seconds. In the last stage, we mixed recycled coarse aggregate with the rest of water for 90 seconds. Because the sand is enveloped by water in the first stage, we call it the sand enveloped mixing approach (SEMA).

In Group 8-3, we mixed sand and recycled aggregates together for 60 seconds. Then, we added 1/2 of the total water and mixed it for 60 seconds. Then, we mixed the cement for 30 seconds. In the last stage, we mixed the rest of the water for 120 seconds. The approach is called the two-stage mixing approach (TSMA) (Tam 2008).

After comparing the test results for all three sets in Group 8, we realized the compressive strength of Group 8-3 was the lowest. So, we removed this mixing approach (TSMA) in the following sets and applied the SEMA in Group 9 and the MMA in Group 10.

In Group 9, four different water to cement ratios (0.45, 0.47, 0.49, and 0.51) were chosen for Groups 9-1 through 9-4. All sets in Group 9 used the SEMA. Test results of compressive strength at three days in Group 9-4 (water to cement ratio=0.51) showed acceptable workability, but the compressive strength was the lowest. Due to this, we decided not to use this water to cement ratio in Group 9-4. We used three different water to cement ratios (0.45, 0.47, and 0.49) for Groups 10-1 through 10-3. All the

sets in Group 10 used the MMA.

For Group 11 and Group 12, we compared the effects of different surface treatments using cement slurry and cement slurry plus silica product (liquid) for Groups 11 and 12.

From previous experience (Groups 3 and 4 in the first part of the pretest), we found that waited two days after surface treatment was applied might not be long enough, so we extended the waiting time to seven days until the hydration reaction was complete in Group 11 and Group 12. In Group 11, five sets were tested. The water to cement ratios for Groups 11-1 through 11-5 were 0.37, 0.37, 0.39, 0.41, and 0.45. Groups 11-1 and 11-2 used the same water to cement ratio (0.37), but different mixing approaches, and compared their compressive strengths after 3, 7, 14, and 28 days.

In Group 12, four sets were tested. The water to cement ratios for Groups 12-1 through 12-4 were 0.47, 0.43, 0.45, and 0.49. From Group 11, we noticed the water to cement ratio was too low to attain acceptable casting quality; therefore more water was added in Group 12 with the goal of improving both workability and strength. The test designs and treatments from Groups 8 through 12 are shown in Table 2.4.

Table 2.4 Test designs of main test (Groups 8 to 12)

	Mixing approaches	Surface treatment	W/C
Group 8-1	1	N	0.49
Group 8-2	2	N	0.49
Group 8-3	3	N	0.49
Group 9-1	2	N	0.45
Group 9-2	2	N	0.47
Group 9-3	2	N	0.49
Group 9-4	2	N	0.51
Group 10-1	1	N	0.45
Group 10-2	1	N	0.47
Group 10-3	1	N	0.49
Group 11-1	1	CS, 0.4	0.37
Group 11-2	2	CS, 0.4	0.37
Group 11-3	2	CS, 0.4	0.39
Group 11-4	2	CS, 0.6	0.41
Group 11-5	2	CS, 0.6	0.45
Group 12-1	2	CS+SS, 0.4	0.47
Group 12-2	2	CS+SS, 0.4	0.43
Group 12-3	2	CS+SS, 0.6	0.45
Group 12-4	2	CS+SS, 0.6	0.49

Mixing approach 1: mortar mixing approach (MMA)

Mixing approach 2: sand enveloped mixing approach (SEMA)

Mixing approach 3: two stage mixing approach (TSMA)

CS: cement slurry

SS: silica solution

The numbers right after CS and CS+SS mean the water to cement ratio of the surface treatment.

2.5. Experimental results of main test

The main test included Group 8 (8-1, 8-2, and 8-3), Group 9 (9-1, 9-2, 9-3, and 9-4), Group 10 (10-1, 10-2, and 10-3), Group 11 (11-1, 11-2, 11-3, 11-4, and 11-5), and Group 12 (12-1, 12-2, 12-3, and 12-4). In Group 8, we used different approaches shown in Figures 2.13 through 2.15. The purpose of the whole test was to compare strength using different mixing approaches. The test results are shown in Table 2.5 and Figure 2.16.

In Group 9, the same mixing approach (SEMA) and different water to cement ratios were used. The purpose was to compare the effect of the water to cement ratio on compressive strength while using the SEMA. The test results are shown in Table 2.6 and Figure 2.17.

In Group 10, the same mixing approach (MMA) and different water to cement ratios were used. The purpose was to observe the effect of the water to cement ratio on compressive strength while using the MMA. The test results are shown in Table 2.7 and Figure 2.18.

In Group 11, we applied the surface treatment of cement slurry with different water to cement ratios (0.4 and 0.6). Then, we waited for 7 days until the hydration was complete and used different water to cement ratios in the casting process. All sets in Group 11 were made using the same mixing approach (SEMA) except Group 11-1. The only difference between Group 11-1 and Group 11-2 is the mixing process. We aimed to compare the compressive strength from different mixing processes (1 and 2) with surface treatments. The main purpose of the Group 11 was to discover the effect of water to cement ratios on both surface pretreatment stage and casting stage. The test results are shown in Table 2.8 and Figure 2.19.

In Group 12, we applied the surface treatment of cement slurry plus silica solution with different

water to cement ratios (0.4 and 0.6). Then, we waited for 7 days until the hydration was complete and used different water to cement ratios in the casting process. The whole group was tested using the SEMA and the purpose was to discover the effects of water to cement ratios on both surface pretreatment stage and casting stage. The test results are shown in Table 2.9 and Figure 2.20.

Slump partly reflects the workability properties of recycled aggregate concrete being used in constructions. In the mixing process, slump test results are shown in Figure 2.21 and Table 2.10.

Table 2.5 Compressive strength (Groups 8-1 through 8-3)

Group 8 (w/c=0.49)	Group 8-1 Mixing approach 1 (MMA)	Group 8-2 Mixing approach 2 (SEMA)	Group 8-3 Mixing approach 3 (TSMA)
3 days	3701	2898	2820
7 days	3646.5	3323	3067.7
28 days	4597.9	3813.7	3582.8

Table 2.6 Compressive strength (Groups 9-1 through 9-4)

Group 9 (Mixing approach 2) (SEMA)	3 days	7 days	14 days	28 days
Group 9-1 (w/c=0.45)	3662.4	3113	3991.3	4025
Group 9-2 (w/c=0.47)	2707	3387	2830	2930
Group 9-3 (w/c=0.49)	2953.8	3067.7	3269.1	3662
Group 9-4 (w/c=0.51)	1992.8	2808.9	2867.8	3406.8

Table 2.7 Compressive strength (Groups 10-1 through 10-3)

Group 10 (Mixing approach 1) (MMA)	3 days	7 days	14 days	28 days
Group 10-1 (w/c=0.45)	2012	1084	1301	1351
Group 10-2 (w/c=0.47)	2103	3423	2278.6	3657
Group 10-3 (w/c=0.49)	3701	3646.5	4212.3	4597.9

Table 2.8 Compressive strength (Groups 11-1 through 11-5)

Group 11(Cement slurry)	3 days	7 days	14 days	28 days
Group 11-1, MMA (w/c=0.4 0.37)	209	269	367	283
Group 11-2, SEMA (w/c=0.4 0.37)	835	1713	2125	3304
Group 11-3, SEMA (w/c=0.4 0.39)	498	533	742	778
Group 11-4, SEMA (w/c=0.6 0.41)	432	2580	4858	5150
Group 11-5, SEMA (w/c=0.6 0.45)	2861	3198	2639	3364

Table 2.9 Compressive strength (Groups 12-1 through 12-4)

Group 12 (Cement slurry+ Silica solution)	3 days	7 days	14 days	28 days
Group 12-1 (w/c=0.4 0.45)	3833	3202	3814	3610
Group 12-2 (w/c=0.4 0.43)	4826	4960	5872	6277
Group 12-3 (w/c=0.6 0.45)	2769	3025	2959	2906
Group 12-4 (w/c=0.6 0.47)	2117	2019	3208	3406

Table 2.10 Slump measurements

	Mixing approaches	Surface treatments	W/C	Slump (mm)
Group 8-1	1	N	0.49	125
Group 8-2	2	N	0.49	150
Group 8-3	3	N	0.49	75
Group 9-1	2	N	0.45	0
Group 9-2	2	N	0.47	0
Group 9-3	2	N	0.49	125
Group 9-4	2	N	0.51	195
Group 10-1	1	N	0.45	105
Group 10-2	1	N	0.47	65
Group 10-3	1	N	0.49	125
Group 11-1	1	CS, 0.4	0.37	130
Group 11-2	2	CS, 0.4	0.37	90
Group 11-3	2	CS, 0.4	0.39	100
Group 11-4	2	CS, 0.6	0.41	95
Group 11-5	2	CS, 0.6	0.45	95
Group 12-1	2	CS+SS, 0.4	0.47	85
Group 12-2	2	CS+SS, 0.4	0.43	0
Group 12-3	2	CS+SS, 0.6	0.45	20
Group 12-4	2	CS+SS, 0.6	0.49	85

Mixing approach 1: mortar mixing approach (MMA)

Mixing approach 2: sand enveloped mixing approach (SEMA)

Mixing approach 3: two stage mixing approach (TSMA)

CS: cement slurry

SS: silica solution

The numbers right after CS and CS+SS mean the water to cement ratio of the surface treatment.

Figure 2.13 Mixing approach 1: mortar mixing approach (MMA)

Figure 2.14 Mixing approach 2: sand enveloped mixing approach (SEMA)

Figure 2.15 Mixing approach 3: two-stage mixing approach (TSMA)

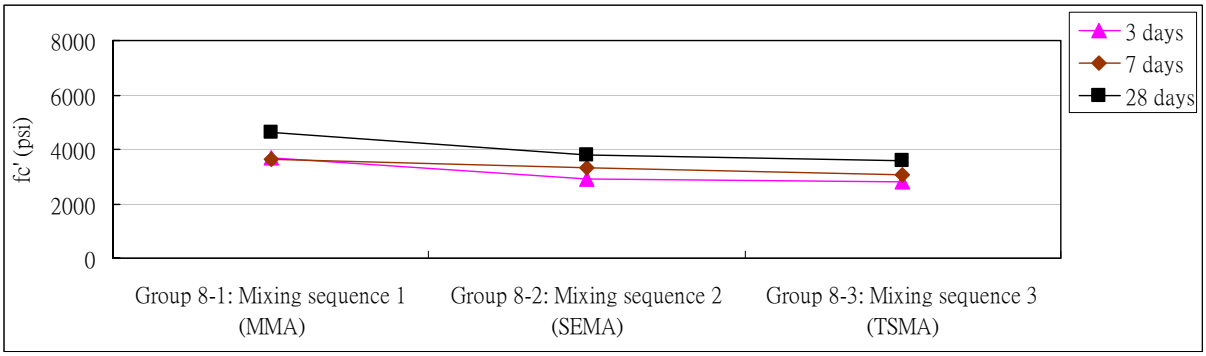

Figure 2.16 Compressive strength (Groups 8-1 through 8-3)

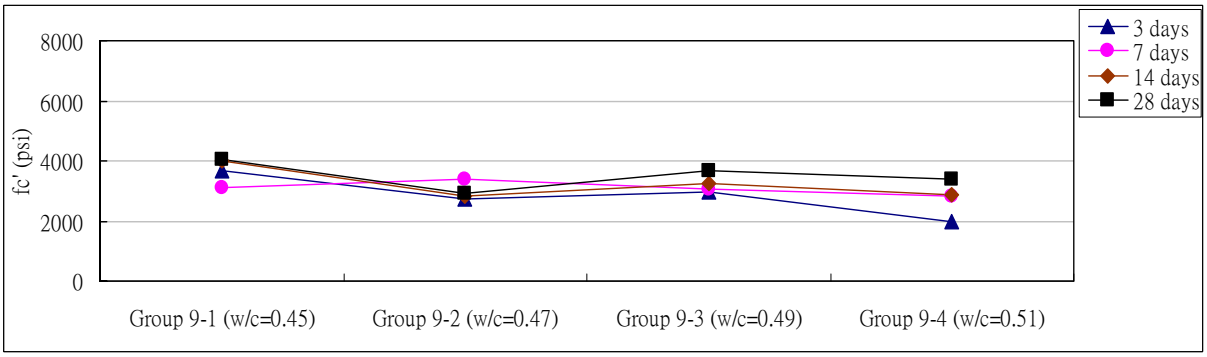

Figure 2.17 Compressive strength (Groups 9-1 through 9-4)

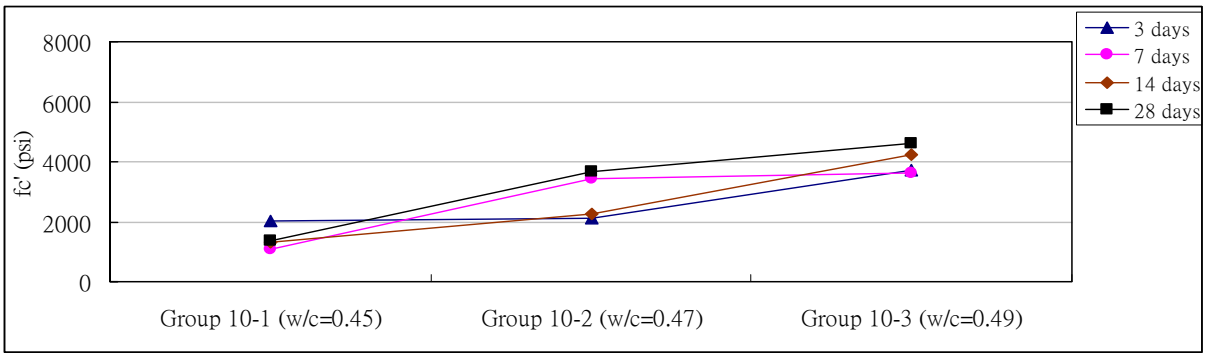

Figure 2.18 Compressive strength (Groups10-1 through 10-3)

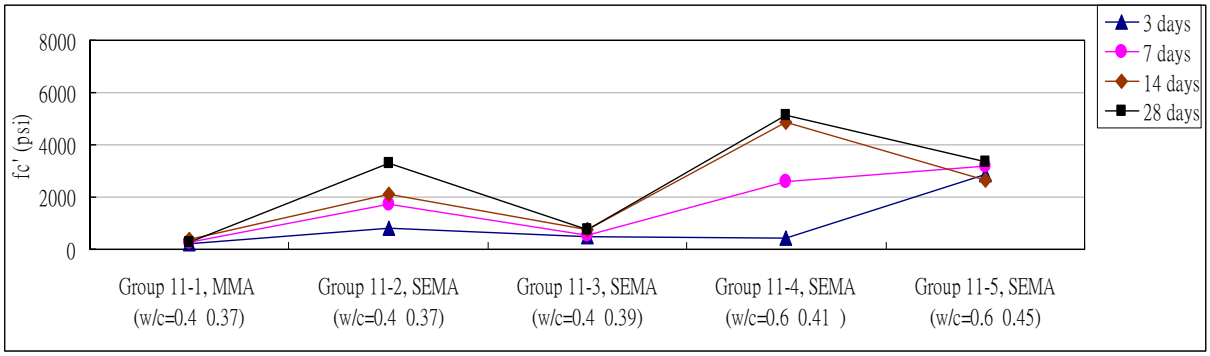

Figure 2.19 Compressive strength (Groups 11-1 through 11-5)

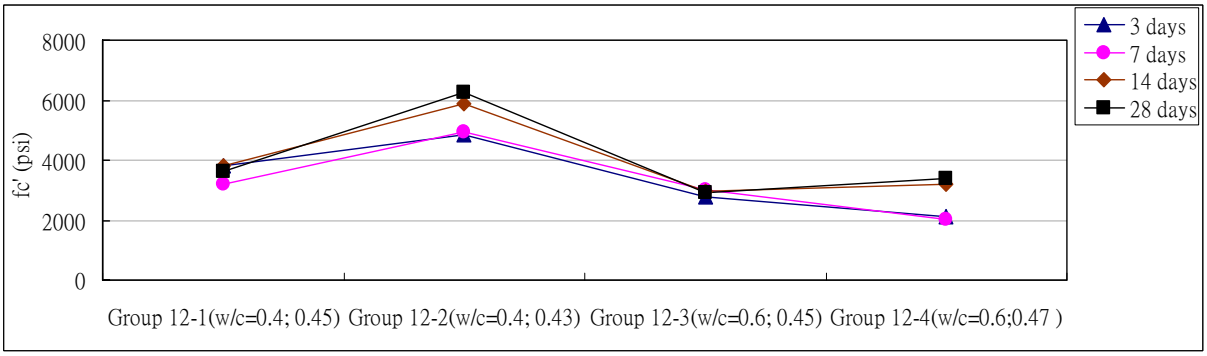

Figure 2.20 Compressive strength (Groups 12-1 through 12-5)

Figure 2.21 Slump test

2.6. Comparisons

We were curious as to which casting would have the highest strength, whether it would be castings with or without surface treatment applied in advance, and which water to cement ratio would result in the highest 28-day compressive strength. The comparisons are shown in Table 2.11 and Figure 2.22. Silica solution indeed improved the strength of the casting and the 28-day compressive strength reached 6277 psi. Without surface treatment, only a compressive strength of around 4000-4500 psi was able to be achieved.

In order to evaluate the performance of different surface treatment approaches, we used the same water to cement ratio in each group. Those comparisons are shown in Table 2.12 and Figure 2.23. Using the same water to cement ratio (0.45) without any surface treatment led to higher compressive strength (4025 psi), but the difference between these sets (Groups 2 and 3) is not significant. The low strength might be a result of the low water to cement ratio.

Mixing approaches as well as the surface treatments were the top concerns. We kept all the other conditions the same, and did the comparisons set by set; results of these tests are displayed in Table 2.13 and Figure 2.24. Without any surface treatment, the MMA was better than the SEMA. However, the results were totally opposite when the surface treatment with cement slurry was employed.

Table 2.11 Comparisons (the highest compressive strength in each group)

	3 days	7 days	14 days	28 days
Group 9-1, SEMA, w/c=0.45, no surface treatment	3662.4	3113	3991.3	4025
Group 10-3, MMA, w/c=0.49, no surface treatment	3701	3646.5	4212.3	4597.9
Group 11-5, SEMA, w/c=0.45; Cement slurry (w/c=0.6)	2861	3198	2639	3364
Group 12-2, SEMA, w/c=0.43; Cement slurry +silica solution(w/c=0.4)	4826	4960	5872	6277

Table 2.12 Comparisons (different surface treatments under same water to cement ratio)

	3 days	7 days	14 days	28 days
Group 9-1, SEMA, w/c=0.45, no surface treatment	3662.4	3113	3991.3	4025
Group 10-1, MMA, w/c=0.45, no surface treatment	2012	1084	1301	1351
Group 11-5, SEMA, w/c=0.45, Cement slurry (w/c=0.6)	2861	3198	2639	3364
Group 12-1, SEMA, w/c=0.45; Cement slurry +silica solution(w/c=0.4)	3833	3202	3814	3610
Group 12-3, SEMA, w/c=0.45, Cement slurry +silica solution(w/c=0.4)	2769	3025	2959	2906

Table 2.13 Comparisons (different mixing approaches)

	3 days	7 days	14 days	28 days
Group8-1 (No surface treatment, MMA, w/c=0.49)	3701	3646.5		4597.9
Group8-2 (No surface treatment, SEMA, w/c=0.49)	2898	3323		3813.7
Group11-1 (Cement slurry (w/c=0.4), MMA, w/c=0.37)	209	269	367	283
Group11-2 (Cement slurry (w/c=0.4), SEMA, w/c=0.37)	835	1713	2125	3304

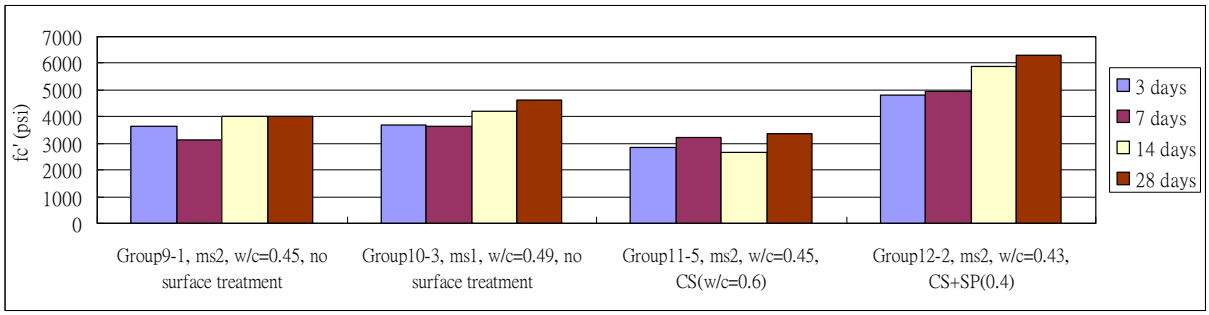

Figure 2.22 Comparisons (the highest compressive strength in each group)

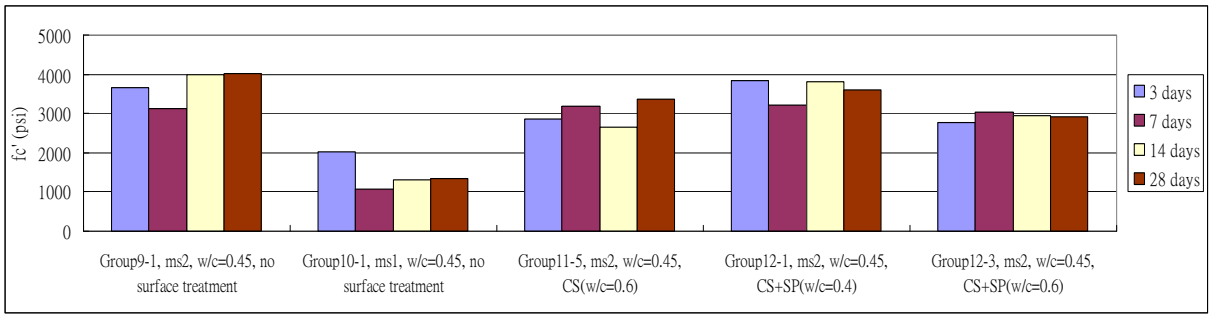

Figure 2.23 Comparisons (different surface treatments under same water to cement ratio)

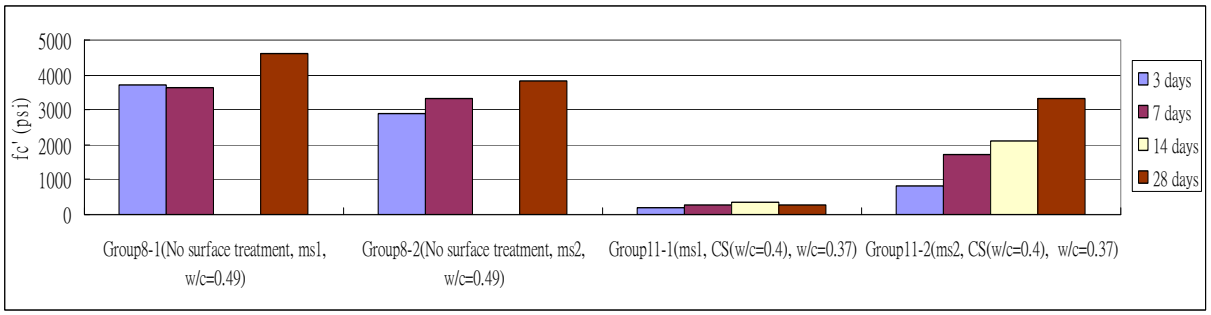

Figure 2.24 Comparisons (different mixing approaches)

2.7. Micrographs

The micrographic images provide better understanding of recycled aggregate concrete at the microstructure level. Figure 2.25 shows the texture of the samples of conventional concrete, RAC without surface treatment, RAC with cement slurry surface treatment, and RAC with cement slurry plus silica solution surface treatment respectively.

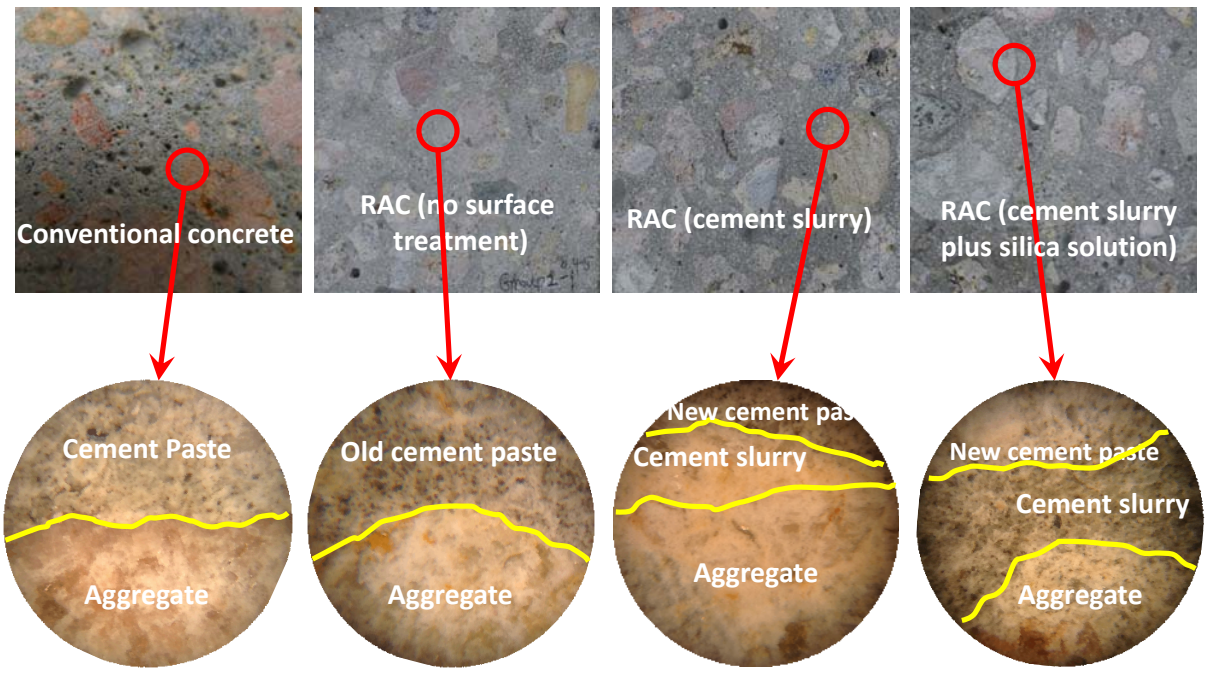

(a) (b) (c) (d)

Figure 2.25 Micrographic images

The curing time of RAC (no surface treatment) is much longer than conventional concrete. From the Figures 2.25 (a) and (b), the difference of cement paste and old cement paste is significant from their textures and colors of microstructures. With surface pretreatment one week before the mixing, the cement slurry formed a condensed layer to cover the surface of the recycled coarse aggregate (Figure 2.25 (c)); therefore, less water was absorbed in the final mixing, which led to higher compressive strength. In Figure 2.25 (d), further using silica solution in surface pretreatment stage changed the microstructure of the pure cement slurry related to Figure 2.25 (c) and showed a finer-grained covering, which further enhanced the strength improvement.

2.8. Discussions and conclusions

From the experimental study, we can conclude the following:

(a) The water to cement ratio used in the surface treatment stage is suggested to be 0.6 for pure cement slurry and 0.4 for cement slurry plus silica solution.

(b) Surface treatments indeed improve the casting quality, but the water to cement ratio should

be closely monitored. When adopting cement slurry as the surface treatment material, the best water to cement ratio is 0.41 because the 28-day compressive strength can reach 5150 psi. Furthermore, when adding silica solution into cement slurry as surface treatment materials, the most effective water ratio is 0.43 as the compressive strength reaches a strong 6277 psi.

(c) Using cement slurry or cement slurry plus silica solution as surface treatments at least one week before mixing can produce a very fine layer to cover the surface of recycled coarse aggregate. The characteristics of this new layer are totally different from the old cement mortar inside the coarse recycled aggregate. The new layer has lower water absorption and partly stops the water absorbed into recycled coarse aggregate. This is a major benefit gained from using surface treatments in advance of mixing.

(d) Test results prove that surface treatments can efficiently reduce the amount of required water in the mixing process. Without any surface treatments, the minimum water to cement ratio for 100% replaced recycled coarse aggregate is around 0.49. With this ratio, the specimen is too dry to be of acceptable casting quality and the 28-day strength is just around 4000-4500 psi. However, when we adopt the surface treatment with cement slurry plus silica solution in advance of mixing, the 28-day compressive strength can reach 6277 psi and the water to cement ratio can be reduced to 0.43.

(e) Using different mixing approaches might lead to different strengths. Among the three approaches, the SEMA is obviously better than the other two procedures (the mortar mixing approach (MMA) and the two-stage mixing approach (TSMA)), in terms of the compressive strength of RAC.

(f) One of the possible reasons as to why the SEMA performs the best is the improvement of cohesion between cement mortar and recycled coarse aggregate. Mixing sand and 3/4 of the total water together in the beginning completely saturates all the sand, allowing the wet sand

to mix more readily with the cement that is added, with only a few big cement mortar particles forming in the process. The high diversity of ingredients in the cement mortar is very helpful in the hydration reaction. Therefore, we can attain a higher 28-day compressive strength with this approach.

(g) Another benefit from the sand enveloped mixing approach (SEMA) is that when recycled coarse aggregate is mixed with the highly diverse cement mortar, the cement mortar will have a lower water to cement ratio interface to cover the surface of recycled coarse aggregate. The interface will provide a much stronger cohesion between the cement mortar and the recycled coarse aggregate, thus improve the compressive strength of RAC.

(h) From micrographic images, we found that the surface pretreatments of recycled coarse aggregate show significant impacts on the regeneration of microstructures. The improvement benefitting the strength development can be proved as well from the experimental test results.

Chapter 3

Durability properties of recycled aggregate concrete

3.1. Rapid chloride permeability test

3.1.1. Setup

The recycled aggregate concrete specimens should have a certain resistance to the penetration of moisture and aggressive chemicals from the environment, which represents a relatively lower permeability. This test was conducted by following ASTM C 1202 and the apparatus used in this study based on requirements of ASTM standard was commercially produced by Prove-It Instruments.

For the preparation, first the specimens were prepared by using a water-cooled diamond saw to cut the faces of specimens into 50 mm thickness and 100 mm diameter pieces, so each specimen could have four pieces and the middle two were used in the permeability test. Second, in order to prevent chemical solutions from leaking through the sidewalls of the disc and to create a linear flow of electrical current, the cylinder walls of specimens were sealed with a coating of silicone and allowed to dry for 12 hours. Third, after drying, they were then vacuumed for 3 hours. De-aerated water filled a container to cover the specimens and a vacuum pump was maintained to run for one additional hour. Finally, the specimens were submerged in water for 18 hours. Each specimen was then immediately loaded into Prove-It to record the passing of coulombs, which can be seen in Figure 3.1 (Stanish et al., 1997).

After the preparation, chemical solutions were added to the two chambers: one with 3% solution of NaCl and the other with 0.3 NaOH. The capability of chloride ions to pass through faces of concrete specimens was measured and recorded in terms of the impedance in coulombs over the total time of the test from the supplied software. Once the test cycle started, a 60 Volt of DC voltage was imposed across the concrete specimens for six hours. The experimental setup is shown in Figure 3.2.

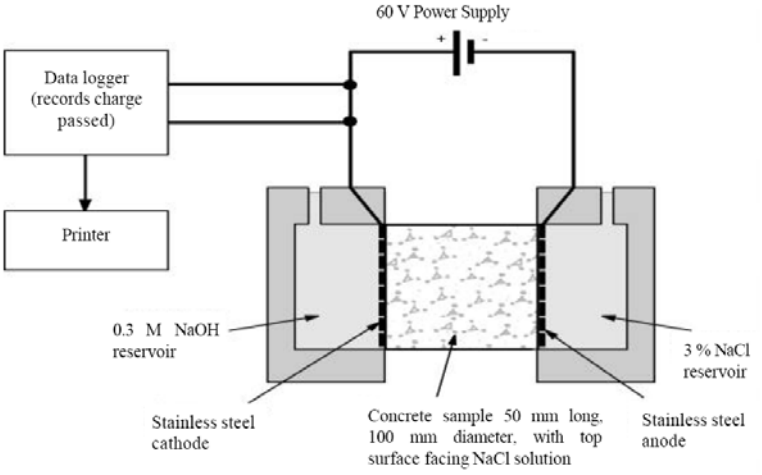

Figure 3.1 Rapid chloride permeability test (setup (1))

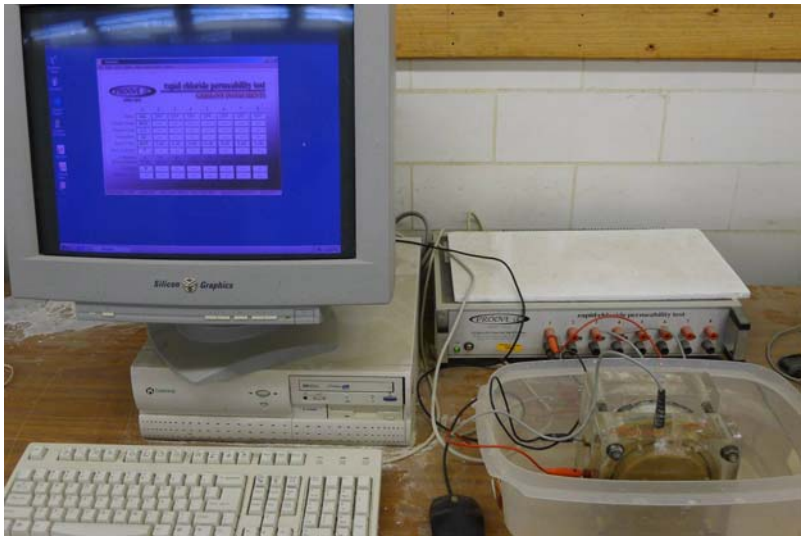

Figure 3.2 Rapid chloride permeability test (setup (2))

3.1.2. Experimental results

The mixture of recycled aggregate concrete specimens used in this test and the experimental results are given in Table 3.1 and Table 3.2. This experiment measured the electrical conductivity of the specimens, which can be considered an indicator of the permeability of recycled aggregate concrete. The permeability depends on total porosity of the material and the connectivity of the pores.

From Table 3.2, it can be concluded that the total charges passing through the recycled aggregate

concrete specimens are higher than conventional ones when compared with the ASTM standard shown in Table 3.3. However, Group 4, in which the surface was pretreated with cement slurry plus silica solution, shows higher resistance to penetration of moisture and aggressive chemicals and represents relatively lower permeability.

Table 3.1 Mix designs (first part of pretest)

Group 1	Natural coarse aggregate	1012.72 (kg/m^3)
	Fine aggregate (Sand)	871.52 (kg/m^3)
	Cement	355.97 (kg/m^3)
	Water	177.98 (kg/m^3)
Group 2, 3	Recycled coarse aggregate	974.23 (kg/m^3)
	Fine aggregate (Sand)	871.52 (kg/m^3)
	Cement	355.97 (kg/m^3)
	Water	177.98 (kg/m^3)
Group 4	Recycled coarse aggregate	974.23 (kg/m^3)
	Fine aggregate (Sand)	871.52 (kg/m^3)
	Cement	355.96 (kg/m^3)
	Silica fume	101.27 (kg/m^3)
	Water	177.98 (kg/m^3)

Table 3.2 RCPT test results

Group number	Coulombs	Chloride ion penetrability
Group 1 #1	5344	High
#2	4820	High
Group 2 # 1	4345	High
# 2	5592	High
Group 3 # 1	6969	High
# 2	6956	High
Group 4 # 1	4584	High
# 2	5097	High

Table 3.3 RCPT concrete permeability ratings

Charge Passed (Coulombs)	Chloride Ion Penetrability
> 4000	High
2000 – 4000	Moderate
1000 – 2000	Low
100 -1000	Very Low
< 100	Negligible

3.2. Drying shrinkage

3.2.1. Setup

Drying shrinkage is one of the most important factors in durability properties. Inadequate allowance for the effects of drying shrinkage in the application of recycled aggregate might lead to cracking or warping of elements of the structure due to the restraints presented during shrinkage.

This test was conducted by following ASTM C 157 (Standard Test Method for Length Change of

Hardened Hydraulic-Cement Mortar and Concrete) to measure the longitudinal length change of recycled aggregate concrete specimens. After mixing and then leaving the specimens in the curing room (at a temperature of 67 degrees F and 96% relative humidity) for seven days, the prisms were removed from the curing room and placed in the lab (at a temperature of 71 degrees F and relative humidity at 32%). Due to the loss of moisture, the specimens showed significant drying shrinkage as times went by. Figure 3.3 shows the hardened recycled aggregate concrete specimens with the screws embedded into the specimens.

Figure 3.3 Drying shrinkage measurements

By using a comparator as shown in Figure 3.4, the length change of specimens was measured every day in the first week, every three days in the second and third week, and every seven days in the following sixteen weeks.

Figure 3.4 The comparator reading for length change measurement

3.2.2. Experimental results

Length change of recycled aggregate concrete specimens can be calculated as equation (3.1). We adopted the specimens from five sets (Groups 9-1, 9-3, 9-4, 12-3, and 12-4) in Table 3.4 and the measurements were shown in Figures 3.5 through 3.9. The number in Table 3.4 following CS and CS+SS indicates the water to cement ratio in the surface treatment process. The column of w/c represents the water to cement ratio at the final mixing process.

$$L_c = \frac{(L_2 - L_1)}{L_1} \times 100 \qquad \text{Eq. (3.1)}$$

L_c = Length change of specimen (%)

L_1 = Length comparator reading at 0 days

L_2 = Length comparator reading at C days

Table 3.4 Drying shrinkage measurements

	Mixing approaches	Surface treatments	W/C
Group 9-1	2	N	0.45
Group 9-3	2	N	0.49
Group 9-4	2	N	0.51
Group 12-3	2	CS+SS, 0.6	0.45
Group 12-4	2	CS+SS, 0.6	0.49

Mixing approach 2: sand enveloped mixing approach (SEMA)

CS: cement slurry

SS: silica solution

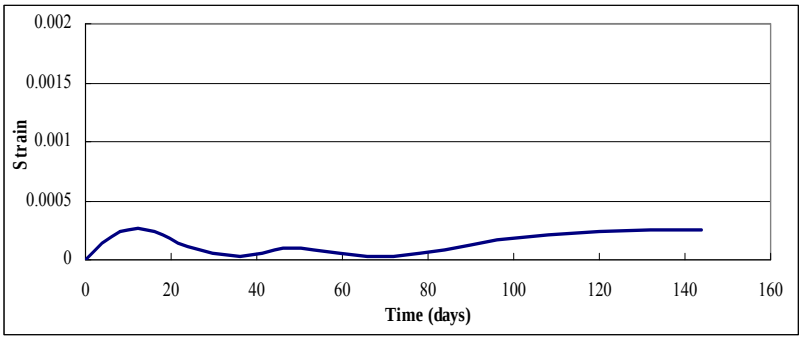

Figure 3.5 Drying shrinkage (Group 9-1)

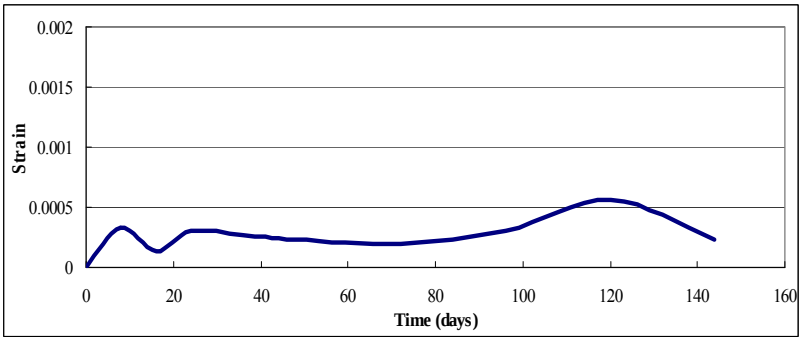

Figure 3.6 Drying shrinkage (Group 9-3)

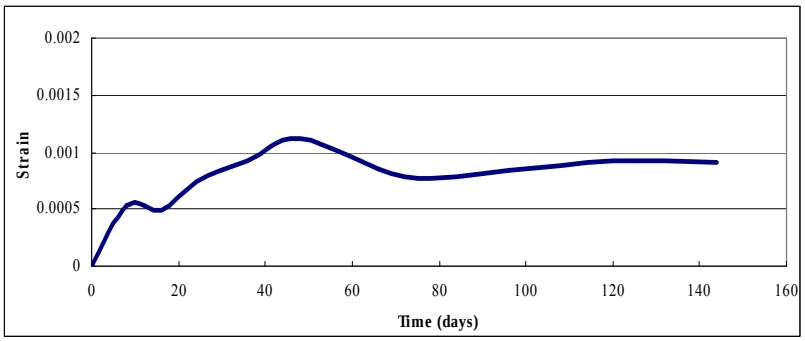

Figure 3.7 Drying shrinkage (Group 9-4)

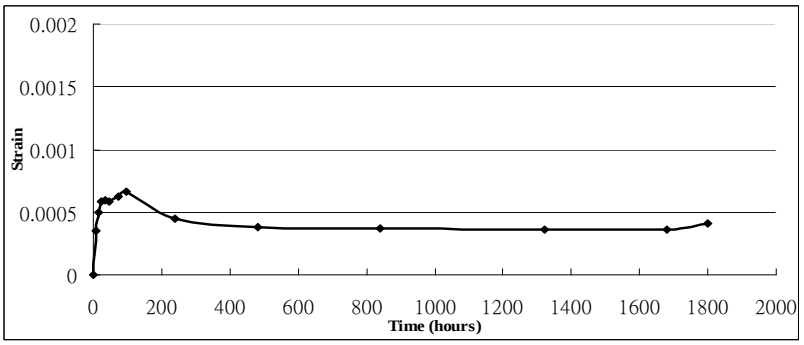

Figure 3.8 Drying shrinkage (Group 12-3)

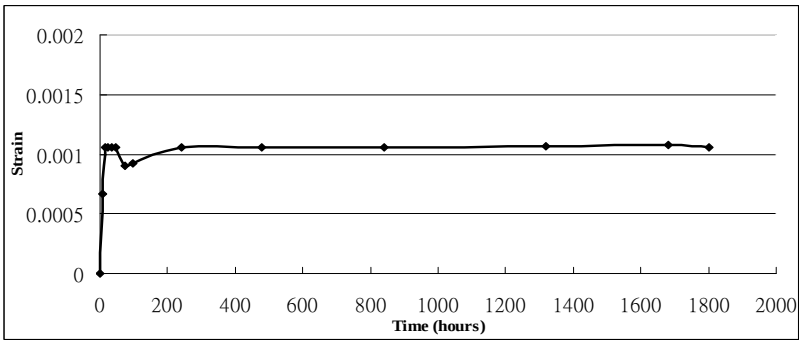

Figure 3.9 Drying shrinkage (Group 12-4)

The normal drying shrinkage value of conventional concrete specimens has a range between 0.00035 and 0.00065 and the maximum value can reach as high as 0.0015. From Figure 3.5 through Figure 3.9, the trend of drying shrinkage development for recycled aggregate concrete with or without surface treatment can be observed. With surface treatment (Group 12-3 and Group 12-4), the specimens reached the highest drying shrinkage value much earlier than the other three (Group 9-1 through Group 9-

3). In addition, with a higher water to cement ratio, the drying shrinkage increased significantly. The specimens with surface pretreatment (Groups 12-3 and 12-4) had higher drying shrinkage values than others.

3.3. Freeze-thawing cycle test

3.3.1. Setup

The purpose of the freeze-thawing cycle test is to investigate the resistance of recycled aggregate concrete under 300 repeated cycles of the freeze and thawing process under standardized conditions. The test was conducted with a Logan Rapid Freeze-Thaw Chest (Figure 3.11) and follow ASTM C 666. This machine uses a 3 inch by 6 inch freezer plate beneath containers to cool the specimens and uses the electric heaters placed between the containers to warm the specimens.

The freeze-thawing cycle test was controlled following the standards, which define the raising temperature range from 0 degrees F to 40 degrees F and the descending temperature range from 40 degrees F to 0 degrees F. It also states that at the end of the cooling period, the temperature at the center of the specimen is 0 ± 3 degrees F (-17.8 ± 1.7 degrees C) and at the end of thawing period, the temperature at the center of the specimen is 40 ± 3 degrees F (4.4 ± 1.7 degrees C). In addition, a full cycle must be completed between 2-5 hours. The new digital controlling panel is installed to control the temperature range and duration of time accurately as Figure 3.12.

Figure 3.11 Logan Rapid Freeze-Thaw Chest

Figure 3.12 Digital controlling panels

To make sure the temperature inside the concrete specimen matched the requirements, two thermal couple sensors were left in the cabin to calibrate the temperatures for the environment and inside the concrete. The sensor was installed in the center of the specimen as seen in Figure 3.13 (Hamel, 2005). For the temperature calibration, Figure 3.14 shows that the complete cycle is approximately 2 hours and 26 minutes, which is within the limit specified by ASTM standards. Before the test, water filled each container no more than 1/8" over the top of the specimen's surface. The test program was operated a total of 300 cycles which was divided into 10 intervals. The length change, weight loss, and dynamic elastic modulus were measured at each interval.

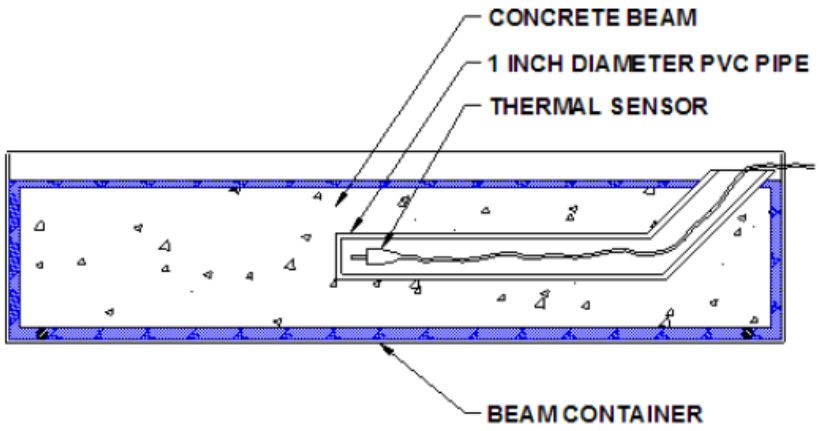

Figure 3.13 Thermal sensor installed at the center of concrete specimen

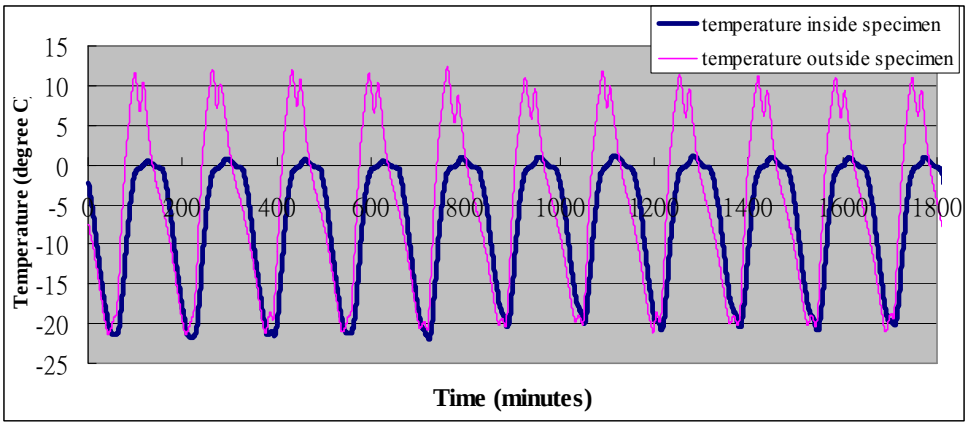

Figure 3.14 Temperature of freeze-thawing cycles

3.3.2. Experimental results

This experiment is categorized into three types of measurements, including weight loss, length change, and ultrasonic pulse velocity. The length change measurement was conducted based on ASTM C 157/C 157M-04. Weight loss of specimens was measured based on ASTM standards as well. The ultrasonic pulse velocity measures the speed at which a frequency pulse travels through concrete specimens. This method is specified by ASTM C 597 and covers the determination of the propagation velocity of longitudinal stress wave pulses through concrete.

The pulse velocity can be calculated by dividing the length of the pulse by its transit time. The setup is shown in Figure 3.15. By using the definition of pulse velocity, the damage in concrete can be estimated with higher velocity meaning less damage. Damage in concrete is presented in terms of dynamic elastic modulus and can be defined as equation (3.2),

$$E_d = \rho V^2 \frac{(1+\mu)(1-2\mu)}{(1-\mu)} \qquad \text{Eq. (3.2)}$$

in which

E_d = The dynamic elastic modulus (Pa)

μ = Poisson's ratio

ρ = Density of specimen (kg/m^3)

v = Pulse velocity (m/s).

Figure 3.15 Ultrasonic pulse velocity measurements

The specimens we used in the experiment are from eight sets in Table 3.5 and the measurements are in Figure 3.16 through Figure 3.18. The number in Table 3.5 right after CS and CS+SS means the water to cement ratio in the surface treatment process. The last column represents the water to cement ratio at the final mixing process.

Table 3.5 Specimens (freeze-thawing cycle test)

	Mixing approach	Surface treatment	W/C
Group 9-1	2	N	0.45
Group 9-2	2	N	0.47
Group 9-3	2	N	0.49
Group 9-4	2	N	0.51
Group 12-1	2	CS+SS, 0.4	0.47
Group 12-2	2	CS+SS, 0.4	0.43
Group 12-3	2	CS+SS, 0.6	0.45
Group 12-4	2	CS+SS, 0.6	0.49

Mixing approach 2: sand enveloped mixing approach (SEMA)

CS: cement slurry

SS: silica solution

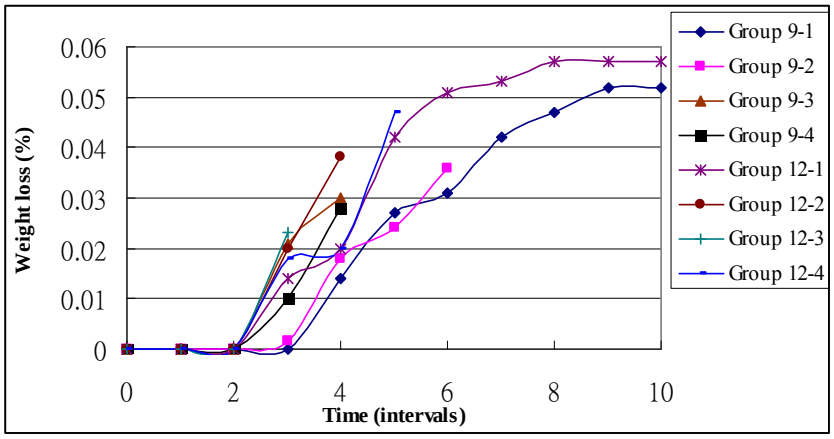

Figure 3.16 Weight loss

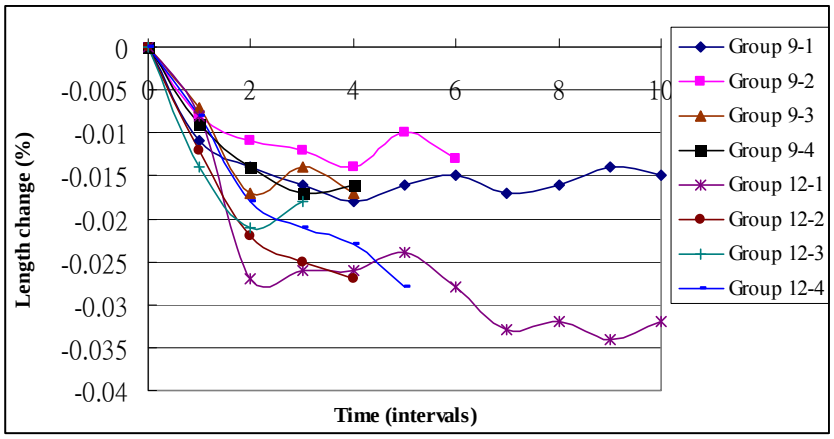

Figure 3.17 Length change

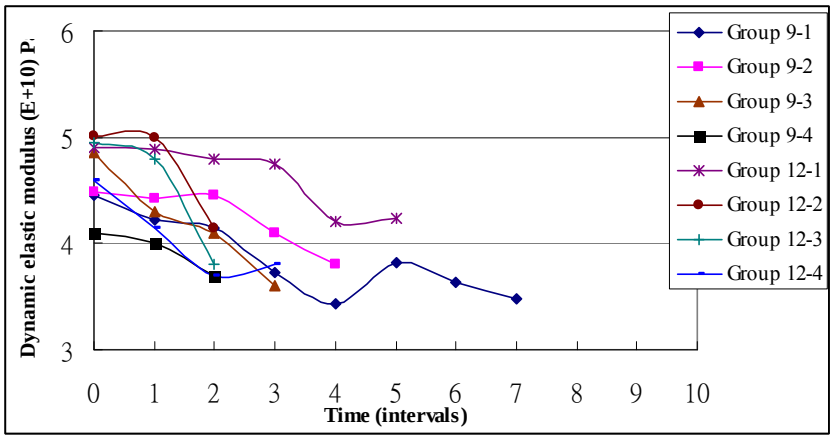

Figure 3.18 Ultrasonic pulse velocities

During the 300 freeze-thawing cycles, the spalling of recycled aggregate concrete was serious; we could not even remove the specimens from the containers to measure their weight loss, length change, and dynamic elastic modulus. Therefore, we lost a lot of information from Figure 3.16 through Figure 3.18. The spalling in concrete specimens led to huge mass losses in the process. For the length change, the specimens with pretreated surface treatment showed higher length change than others.

For dynamic elastic modulus, this parameter is relevant to damage inside concrete. More seriously damaged concrete must spend a longer travelling time to transverse it. From Figure 3.18, we realize the dynamic elastic modulus decreased with increasing time, which implies the freeze-thawing cycles seriously damage the concrete. In addition, with surface pretreatment, the recycled aggregate concrete specimens have better performance.

Chapter 4

Multiscale chemomechanical model

4.1. Motivations

Shrinkage is an important factor in the application of recycled aggregate concrete. From the test results in Chapter 3, we realize it involves a very complicated mechanism. In order to explain, analyze, and even predict shrinkage, we must have an appropriate theoretical model. From this model, we can control the shrinkage and some other mechanical properties of recycled aggregate concrete and extend its application to more important elements of infrastructure or buildings.

The shrinkage of cement paste involves different mechanisms acting over a broad range of scales, from the nanometer to the meter level. Therefore, multiscale mathematical modeling is inevitable.

A multiscale model for shrinkage of cement paste and concrete that links properties at the nanometer, micrometer and millimeter level is proposed. Each parameter of the model at a particular scale level has fundamental physical meaning. The model is used to determine values of shrinkage, bulk modulus, and volume fraction of the constituent phases, and these values are then used to model shrinkage of concrete.

Review of the literature shows that the most notable lack of test results of shrinkage has been at the micrometer level. To fill the gap, the application of the technique to shrinkage of cement paste has produced valuable new microscopic test results (Jennings, H.M., and Xi, Y. 1993); (Bergstrom, T.B. et al 1997), providing a basis for multiscale mathematical modeling.

The two major advantages of multiscale modeling are: 1) It follows the inherent logic of physical phenomena to be described and 2) It separates controlling parameters for shrinkage of cement paste into several components such that each parameter has specific physical meaning (Xi, Y., and Jennings, H.M.

1997). The model at each scale level is based only on mechanisms which are active on that level, and models at different scale levels serve as links in the entire chain of the multiscale model.

The first step in multiscale modeling is to break the whole range of scales into several ranges. The following four scale levels have been partitioned based on these reasons: (1) nanometer level: many currently accepted mechanisms for shrinkage of calcium silicate hydrate (C-S-H) are considered to be active at this level; (2) micrometer level: microstructural features such as the size of cement particles and hydration products are observed at this scale level; (3) millimeter level: most materials' properties are obtained from samples at this level; and (4) meter level: practical problems in structural engineering are solved at this level.

The most commonly used parameter to describe microstructure is the volume fraction of each constituent phase. Besides, even though many researchers would like to describe or predict the elastic properties of materials based on various arrangements of constituent phases, a model has yet to be developed which includes the influence of microstructural features of cement paste, such as particle size distribution and the association between constituent phases. Some researchers conclude that the effective elastic modulus of a three-phase composite can be calculated by using the four-phase sphere model and by a two-step method (Wijeyewickrema A.C. and Leungvichcharoen S. 2003).

Recent years many researchers pay more attention on the study of concrete diffusivity property and have been developed analytical solutions for predicting the chloride diffusivity of hardened cement paste. Zheng J. and Zhou X. 2008 verified the analytical solution with experimental results obtained from the literature, the effects of two key factors, i.e., water to cement ratio and degree of hydration on the chloride diffusivity of hardened cement paste. Sun Y. M. et al 2010 investigated the physical and chemical processes that control the transport of chloride ions into concrete structures, and then an analytical solution of a diffusion reaction model is presented for determining the time-depth dependent chloride diffusivities considering both diffusion process and binding mechanism of chloride occur simultaneously.

Our research focuses on the mathematical modeling of shrinkage of cement paste at the

micrometer level, and attempts to establish links with shrinkage mechanisms at the millimeter level and at the micro- and nanometer levels. The model takes into account effects of water to cement ratios, surface treatments, and aging behaviors on both elastic properties and shrinkage of cement paste.

We would like to develop a general multiphase model for shrinkage of heterogeneous composite materials based on Christensen's three-phase model (Christensen, R.M., 1979); (Christensen, R.M., and Lo, K.H., 1979). In this model, the changes in volume fractions of constituent phases are based on the microstructural model of Jennings and Tennis (Jennings, H.M., and Tennis, P.D., 1995). The elastic properties of each phase are determined by the model as well. From this model, we can predict effective shrinkage and effective bulk modulus of heterogeneous composite materials for recycled aggregate concrete including the influences of aging behavior and surface treatments.

4.2. Generalized self-consistent model

We consider a heterogeneous composite material with a microstructure, the structure of the material can be divided into many regions, or elements, such that the volume fraction of each phase in an element is the same. The partitions may be made so that the elements approach spherical surfaces. This kind of internal structure of the basic element is typical for many engineering materials. The basic element of the microstructure is then a composite sphere composed of three different phases; the ratios of radius are constants, independent of the absolute size of the spheres as a result of constant volume fractions.

The three-phase model mentioned above in Figure 4.1 has been developed by Christensen (Christensen, R.M., 1979); (Christensen, R.M., and Lo, K.H., 1979) to determine effective elastic properties of a two-phase composite. This generalized self-consistent model was originally developed for elastic properties only, but Herve and Zaoui (Herve, E., and Zaoui, A., 1990) have shown that the model can be extended to nonlinear materials.

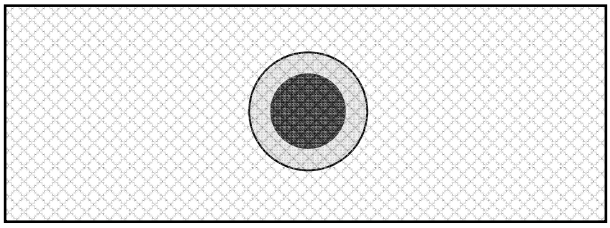

Phase 1

Phase 2

Effective homogenous medium

Figure 4.1 Three-phase effective media model

4.3. Elastic solution of the generalized self-consistent model

According to elasticity, for any single phase that shrinks, for example phase i, the equilibrium equation is:

$$U_{i,rr} + \frac{2}{r} U_{i,r} - \frac{2U_i}{r^2} - \frac{1+\nu_i}{1-\nu_i} \varepsilon_{i,r}^{sh} = 0 \qquad \text{Eq. (4.1)}$$

where U_i : displacement of the phase i in radial direction;

r : location coordinate in radial direction;

$U_{i,r}$: derivative of U_i with respect to r;

ν_i : Poisson's ratio of the phase i;

$\varepsilon_{i,r}^{sh}$: linear shrinkage of the phase i.

The differential shrinkage $\varepsilon_{i,r}^{sh}$ can be neglected (micrometer level), so equation (4.1) can be simplified as equation (4.2). When all phases shrink, each one has its own shrinkage value as equation (4.3).

$$U_{i,rr} + \frac{2}{r} U_{i,r} - \frac{2}{r^2} U_i = 0 \qquad \text{Eq. (4.2)}$$

$$U_i = C_i r + \frac{D_i}{r^2} \qquad \sigma_i = 3K_i C_i - 4G_i \frac{D_i}{r^3} - 3K_i \varepsilon_i^{sh} \qquad \text{Eq. (4.3)}$$

where σ_i : stress of the phase i in radial direction;

K_i : bulk modulus of the phase i ;

G_i : shear modulus of the phase i ;

C_i , D_i : both are constants with $D_1 = 0$ to avoid singularity at $r = 0$.

From equation (4.3) and using continuity condition, we get $U_1(r = R_1) = U_2(r = R_1)$, $\sigma_1(r = R_1)$, and $\sigma_2(r = R_1)$. Also, we have $C_1 R_1 = C_2 R_1 + D_2 / R_1^2$ and $3K_1C_1 - 3K_1\varepsilon_1^{sh} = 3K_2C_2 - 4G_2\left(D_2 / R_1^3\right) - 3K_2\varepsilon_2^{sh}$. There is a displacement δ along radial direction at boundary $r = R_2$, which gives us $U_2\left(r = R_2\right) = C_2R_2 + D_2 / R_2^2 = \delta$.

The three constants C_1 , C_2 , and D_2 can then be solved from the three equations in terms of displacement. Then, consider the continuity conditions at boundary $r = R_2$, the displacement and stress should be the same at $r = R_2$. From the stress continuity condition, $\sigma_{eff}(r = R_2) = \sigma_2(r = R_2)$, combined with equation (4.3) and σ_{eff} , we can get the results as equation (4.4). The subscript "*eff* " stands for effective homogeneous medium.

$$3K_{eff}\frac{\delta}{R_2} - 3K_{eff}\varepsilon_{eff}^{sh} = 3K_2C_2 - 4G_2\frac{D_2}{R_2^3} - 3K_2\varepsilon_2^{sh} \qquad \text{Eq. (4.4)}$$

In equation (4.4), K_{eff} can be solved by taking all shrinkages ε_1 , ε_2 , and ε_{eff} as zero, and then we use equation (4.3) and equation (4.4) to solve for C_2 and D_2 . Finally equation (4.5) can be obtained,

$$K_{eff} = \frac{K_2(3K_1 + 4G_2) - 4c_{12}G_2(K_2 - K_1)}{(3K_1 + 4G_2) + (3K_2 - 3K_1)c_{12}} \qquad \text{Eq. (4.5)}$$

where $C_{12} = R_1^3 / R_2^3$ is the volume fraction of phase 1. Substituting equation (4.5) into equation (4.4), the shrinkage of the effective homogeneous medium can be determined:

$$\varepsilon_{eff}^{sh} = \frac{K_1\varepsilon_1^{sh}c_{12}(3K_2 + 4G_2) + K_2\varepsilon_2^{sh}(1 - c_{12})(4G_2 + 3K_1)}{K_2(3K_1 + 4G_2) - 4c_{12}G_2(K_2 - K_1)} \qquad \text{Eq. (4.6)}$$

4.4. Generalization of generalized self-consistent model

The derivation above can be extended to multiphase materials. Actually, the effective

homogeneous parameters for the multiphase model can be obtained simply by substitution in equation (4.5) and equation (4.6), and then the expression for effective bulk modulus of a three-phase composite can be obtained as:

$$K_{eff}=K_3+\frac{(f_1+f_2)(K_{eff}^{12}-K_3)}{1+(1-f_1-f_2)\dfrac{K_{eff}^{12}-K_3}{K_3+\frac{4}{3}G_3}} \qquad K_{eff}^{12}=K_2+\frac{\frac{f_1}{f_1+f_2}(K_1-K_2)}{1+(1-\frac{f_1}{f_1+f_2})\dfrac{K_1-K_2}{K_2+\frac{4}{3}G_2}} \qquad \text{Eq. (4.7)}$$

where K_{eff}^{12} is the effective bulk modulus for the composite made of phases 1 and 2. By the same manner, the expressions for the effective shrinkage of the three-phase composite can also be obtained:

$$\varepsilon_{eff}^{sh}=\frac{K_{eff}^{12}\left(\varepsilon_{eff}^{sh}\right)_{12}(f_1+f_2)(3K_3+4G_3)+K_3\varepsilon_3^{sh}(1-f_1-f_2)(4G_3+3K_{eff}^{12})}{K_3(3K_{eff}^{12}+4G_3)-4(f_1+f_2)G_3(K_3-K_{eff}^{12})} \qquad \text{Eq. (4.8)}$$

$$\left(\varepsilon_{eff}^{sh}\right)_{12}=\frac{K_1\varepsilon_1^{sh}\dfrac{f_1}{f_1+f_2}(3K_2+4G_2)+K_2\varepsilon_2^{sh}(1-\dfrac{f_1}{f_1+f_2})(4G_2+3K_1)}{K_2(3K_1+4G_2)-4G_2\dfrac{f_1}{f_1+f_2}(K_2-K_1)} \qquad \text{Eq. (4.9)}$$

where K_{eff}^{12} is from equation (4.7), and $\left(\varepsilon_{eff}^{sh}\right)_{12}$ is the effective shrinkage of the composite made of phases 1 and phase 2. Equation (4.7) and equation (4.8) can be used for the shrinkage of cement paste. Furthermore, the recursive method applied for the three-phase composite can be used for the problem with any number of phases. A N-phase composite is described as follows:

$$\left(K_{eff}\right)_i=K_i+\frac{c_{i-1,1}\left[\left(K_{eff}\right)_{i-1}-K_i\right]}{1+(1-c_{i-1,1})\dfrac{\left(K_{eff}\right)_{i-1}-K_i}{K_i+\frac{4}{3}G_i}} \qquad \text{Eq. (4.10)}$$

$$(\varepsilon_{eff}^{sh})_i=\frac{\left(K_{eff}\right)_{i-1}\left(\varepsilon_{eff}^{sh}\right)_{i-1}c_{i-1,i}(3K_i+4G_i)+K_i\varepsilon_i^{sh}(1-c_{i-1,i})\left[4G_i+3\left(K_{eff}\right)_{i-1}\right]}{K_i\left[3\left(K_{eff}\right)_{i-1}+4G_i\right]-4c_{i-1,i}G_i\left[K_i-\left(K_{eff}\right)_{i-1}\right]} \qquad \text{Eq. (4.11)}$$

where $N\geq i\geq 2$; $\left(K_{eff}\right)_1=K_1$ and $\left(\varepsilon_{eff}^{sh}\right)_1=\varepsilon_1^{sh}$. Parameters $c_{i-1,i}$ and $c_{N-1,N}$ are:

$$c_{i-1,i}=\sum_{j=1}^{i-1}f_j\Big/\sum_{j=1}^{i}f_j \quad (N>i\geq 2) \text{ and } c_{N-1,N}=\sum_{j=1}^{N-1}f_j=1-f_N \quad (i=N) \qquad \text{Eq. (4.12)}$$

4.5. Shrinkage of cement paste

The major constituents of cement paste are calcium silicate hydrate (C-S-H), calcium hydroxide (CH) and other crystalline products, anhydrous cores, and pores. From the particle illustration (Xi, Y., and Jennings, H.M. 1997), except anhydrous cores and pores, all the remaining phases are hydration products. The denser region surrounding the anhydrous core is called the inner product of hydration, and the less dense regions are called the outer product (Diamond, S. and Bonen, D., 1993).

Among all the constituents of cement paste, C-S-H is the only phase that shrinks (or expands), therefore, the measured bulk shrinkage of cement paste is actually the shrinkage of C-S-H with reductions due to the constraints of all other phases.

Anhydrous cores CH and other crystals are non-shrinking phases and they together form phase 1, the inner product is phase 2, and the outer product with capillary pores compose phase 3:

$$V_{total}=V_1+V_2+V_3$$

$$V_1=V_{core}+V_{CH}+V_{AFm}\ V_2=V_{inner}V_3=V_{outer}+V_{cp} \qquad \text{Eq. (4.13)}$$

where V_{core} , V_{ch} , V_{inner} , V_{outer} , and V_{cp} are volumes of the anhydrous core, CH crystals and other crystalline phases, inner product, outer product, and the capillary pore, respectively. V_{total} is the total volume.

There are four parameters for each phase, namely elastic modulus, E_i , Poisson's ratio, ν_i (or alternatively, bulk modulus, K_i , and shear modulus, G_i), shrinkage strain, ε_i^{sh} , and volume fraction, f_i . Only eleven of the parameters above in the present model are independent since $f_3=1-f_1-f_2$. Next, we must determine the volume fraction, elastic properties, and shrinkage for each phase, respectively.

4.6. Volume fraction

In order to determine volume fractions of constituent phases f_1 , f_2 , and f_3 , the specific volumes V_{core} , V_{CH} , V_{inner} , V_{outer} , and V_{cp} in equation (4.13) need to be evaluated. These specific volumes can be calculated by using a microstructural model (Jennings, H.M., and Tennis, P.D., 1995). Thus, the ratio is:

$$f_{core} = \frac{V_{core}}{V_{total}} = \frac{1-\alpha}{1+\frac{w}{c}\frac{\rho_c}{\rho_w}} = c\frac{1-\alpha}{\rho_c} p \qquad \text{Eq. (4.14)}$$

where $c = 1/(1+w/c)$ and $p = (1+w/c)\rho_c / [1+w/c(\rho_c/\rho_w)]$; $\rho_c/\rho_w = 3.15$.

In equation (4.14), the volume fraction of unreacted cores can be obtained from initial water to cement ratio (w/c) and degree of hydration of the cement paste (α). The volume of unreacted cores $V_{core} = (1-\alpha)V_{c0}$, where V_{c0} is the initial cement volume, and the total volume is $V = [1+(w/c)(\rho_c/\rho_w)]V_{c0}$, where ρ_c and ρ_w are densities of cement and water, respectively. The degree of hydration of each compound can be taken as a weighted average:

$$\alpha = \alpha_{C_3S} W_{C_3S} + \alpha_{C_2S} W_{C_2S} + \alpha_{C_3A} W_{C_3A} + \alpha_{C_4AF} W_{C_4AF} \qquad \text{Eq. (4.15)}$$

where W_i : initial percentage of weight for each reacting compound, $i = C_3S, C_2S, C_3A$, and C_4AF;

α_i : degree of hydration of each compound, $i = C_3S, C_2S, C_3A$, and C_4AF.

The individual degree of reaction for each of the reacting compounds is $\alpha_i = 1 - \exp\left[-a_i(t-b_i)^{c_i}\right]$, where the time is in days. The constants a_i, b_i, and c_i are determined by Taylor (Taylor and H.F.W (1987)) for pure compounds. The volume fraction of CH and other crystals, f_{CH}, needs to be evaluated based on products of the chemical reactions at hydration:

$$f_{CH} = c(0.189\alpha_{C_3S} W_{C_3S} + 0.058\alpha_{C_2S} W_{C_2S})p$$

$$f_{AFm} = c(0.849\alpha_{C_3A} W_{C_3A} + 0.472\alpha_{C_4AF} W_{C_4AF})p \qquad \text{Eq. (4.16)}$$

Phase 1 is the sum of anhydrous cores, CH, and other crystalline phases, which are approximated here by AFm, thus, from equations (4.13), (4.14), and (4.16) we get

$$f_1 = f_{core} + f_{CH} + f_{AFm} \qquad \text{Eq. (4.17)}$$

From direct microscopic observation, the outer product is the primary shrinking phase. Thus, the C-S-H inaccessible to nitrogen (but accessible to water) is regarded as the gel pore in the inner product. Parameter V_3 is therefore taken as the volume of outer product and V_{N2} has been formulated with respect to V_{C-S-H}, where $V_{C-S-H} = V_{inner} + V_{outer}$. From the definition in equation (4.13), f_3 can be written as:

$$f_3=\frac{V_{outer}+V_{cp}}{V_{total}}=\frac{V_{N2}}{V_{total}}+f_{cp}$$

$$=\frac{V_{N2}}{V_{C\text{-}S\text{-}H}}\frac{V_{C\text{-}S\text{-}H}}{V_{total}}+f_{cp}=f_r\frac{V_{total}-V_1-V_{cp}}{V_{total}}+f_{cp} \qquad \text{Eq. (4.18)}$$

$$=f_r(1-f_1-f_{cp})+f_{cp}$$

where f_{cp} represents the volume fraction of capillary pores and can be calculated as $f=[(1-c)-c\Omega]p$, then $\Omega=0.437\alpha_{C_3S}W_{C_3S}+0.503\alpha_{C_2S}W_{C_2S}+0.397\alpha_{C_3A}W_{C_3A}+0.136\alpha_{C_4AF}W_{C_4AF}$ and $f_r=V_{N2}/V_{C-S-H}=0.706(w/c)+0.131$. This equation is based on measurements made on well-hydrated pastes, which means it is accurate only for highly reacted cement paste. Finally, the volume fraction of inner product can be obtained simply from f_1 and f_3, then $f_2=1-f_1-f_3$.

4.7. Elastic properties

Concrete is first treated as a two-phase material composed of cement paste and aggregate, and then the cement paste is treated as a three-phase material of unreacted cement, inner and outer product. Each component of the cement paste is further considered to be a two-phase material: hydration solid and pore. The major advantages of this multiscale and multiphase model is that the six elastic properties of the three phases in cement paste can be reduced to two elastic parameters of the hydration solid: elastic modulus and Poisson's ratio, which can be evaluated by calibration based on experimental results obtained at the millimeter level.

In Phase 1 (cement paste), we assume that the solid C-S-H, unreacted cores, and CH and other crystals together form the hydration solid have average elastic properties, $E_1=E_s$, and $\nu_1=\nu_s$, which are the unknowns to be determined. From equations (4.10) and equation (4.11), both bulk modulus and shear modulus of each phase are involved in the model, where bulk modulus for phase 2 and 3 can be evaluated by equation (4.5) or equation (4.7), and shear modulus can be determined by the model from Christensen (Christensen, R.M., and Lo, K.H., 1979).

In order to apply the model to phases 2 and 3 (cement paste,) the porosities of f_p^2 and f_p^3 need to

be derived as follows,

$$f_p^2 = \frac{V(\text{inner gel pore})}{V_2} = \frac{f_{total}^{p2} V_{total}}{f_2 V_{total}} = \frac{f_{total}^{p2}}{f_2} \quad \text{Eq. (4.19)}$$

$$f_p^3 = \frac{V(\text{outer gel pore}) + V_{cp}}{V_3} = \frac{f_{total}^{p3} V_{total} + V_{cp}}{f_3 V_{total}} = \frac{f_{total}^{p3} + f_{cp}}{f_3} \quad \text{Eq. (4.20)}$$

where f_{total}^{p2} and f_{total}^{p3} are volume fractions of gel pores inside phase 2 and 3, in terms of total volume.

From Taylor (Taylor, H.F.W., 1987), the volume fraction of total gel pore, f_{gel}, is as shown in equation (4.21). From equation (4.20), we have $f_{total}^{p2} = f_p^2 - f_2$, and then insert it to equation (4.21), we can get $f_{total}^{p3} = f_{gel} - f_p^2 f_2$. By substituting it into equation (4.21), finally we get equation (4.22).

$$f_{gel} = f_{total}^{p2} + f_{total}^{p3} = 0.22\, c(0.278\alpha_{C_3S} W_{C_3S} + 0.369\alpha_{C_2S} W_{C_2S})\, p \quad \text{Eq. (4.21)}$$

$$f_p^3 = \frac{f_{gel} - f_p^2 f_2 + f_{cp}}{f_3} \quad \text{Eq. (4.22)}$$

Among these parameters, only f_p^3 and elastic properties of the phase 3, K_3 and G_3 are functions of age. The volume fractions of capillary pore and gel pore, f_{cp} and f_{gel} (equation (4.18) and equation (4.21)) can be evaluated by $f_{cp} = (w/c - 0.36\alpha)/(w/c + 0.32)$ and $f_{gel} = (0.19\alpha)/(w/c + 0.32)$. The coefficient α can be obtained from equation (4.15).

Based on the known properties of the hydration solid, evolutions of bulk modulus of the cement paste and its constituent phases, i.e. phases 2 and 3, can be obtained. We can see that bulk modulus of the hydration solid and phase 2, K_1 and K_2, are time independent, while K_3 and K_{eff} are both time dependent. Also, shear modulus of constituent phases, G_2 and G_3, are needed in order to evaluate the effective bulk modulus and shrinkage of cement paste. G_2 and G_3 could be determined by Christensen's method.

4.8. Application (Conventional concrete)

Shrinkage and several diffusivity properties of concrete involve different mechanisms acting over a broad range of scales, from the nanometer to the meter level. Therefore, multiscale mathematical modeling is inevitable. The first step for the analysis is to break the whole range of scales into several

ranges as follows:

(a) Nanometer level: many currently accepted mechanisms for shrinkage of calcium silicate hydrate (C-S-H) are considered to be active at this level;

(b) Micrometer level: microstructural features such as the size of cement particles and hydration products are observed at this scale level;

(c) Millimeter level: most materials' properties are obtained at this level;

(d) Meter level: practical problems in structural engineering are solved at this level.

For conventional concrete, we first treat it as a two-phase material composed of aggregate and cement paste. Secondly, among the two phases, because the shrinkage of aggregate is negligible, only the cement paste must be treated as a three-phase material composed of unreacted cement, inner and outer product. Furthermore, the inner and outer product are individually considered as a two-phase material: hydration solid and pore. The mechanism is shown in Figure 4.2. The same composite model of concentric spheres is used at all scale levels and that is why this model is called a multiscale and multiphase model.

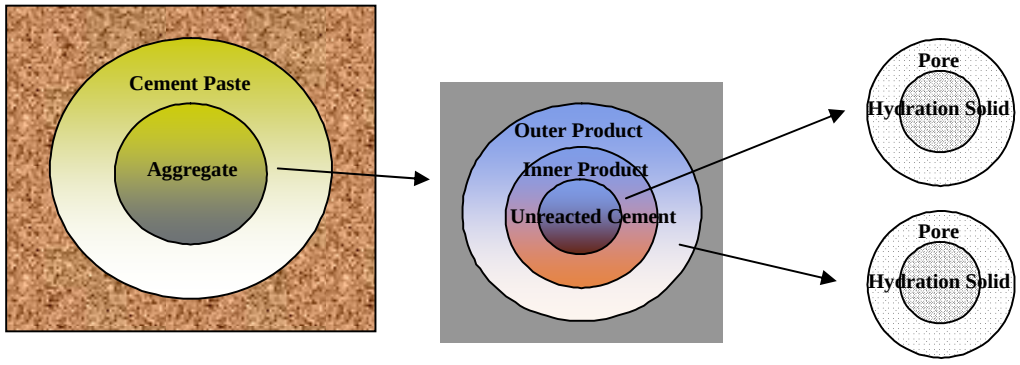

Figure 4.2 Mechanism of conventional concrete

For the theoretical analysis of conventional concrete as shown in Figure 4.2, we should start from a three-phase model (a generalized self-consistent model) which is developed by Christensen, and then the model can be generalized to multiphase problem.

With known properties of the hydration solid, evolutions of bulk modulus of the cement paste and

its constituent phases, i.e. phases 2 and 3, can be obtained. We realize that bulk modulus of the hydration solid and phase 2, K_1 and K_2, are time independent, while K_3 and K_{eff} are time dependent. In the model, shear modulus of constituent phases, G_2 and G_3, are needed in order to evaluate the effective bulk modulus and shrinkage of cement paste through equations. The values of G_2 and G_3 could be determined by Christensen's method.

From environmental scanning electron microscopy test results (Torquato, S., and Stell, G., 1982; Torquato, S., 1986; Allais, L., et al. 1992), shrinkage of unreacted grains and CH crystals can be considered to be zero. The shrinkage of inner product (phase 2) is very small, so that could also be considered as zero. Finally, the shrinkage of outer product is the only source of shrinkage in cement paste and that can be calculated by equations.

4.9. Application (Recycled aggregate concrete)

For recycled aggregate concrete, the mechanism is more complicated than the conventional model. In order to decrease water absorption in the mixing process to improve the 28-day compressive strength of recycled aggregate concrete, different surface treatments needed to be applied before mixing. Besides, the old natural aggregate is covered by existing cement paste. Therefore, with the surface treatments, the model must be modified to a five-phase model (Figure 4.3) and each phase has its own physical meaning as follows,

Phase 1 – Natural aggregate

Phase 2 - Existing cement paste (residual, old cement paste), the curing time is long (several years)

Phase 3 - Surface treatment layer (cement slurry and/or polymer), the curing time is young (35 days)

Phase 4 - New cement paste, the curing time is young (28 days)

Phase 5 - Effective media

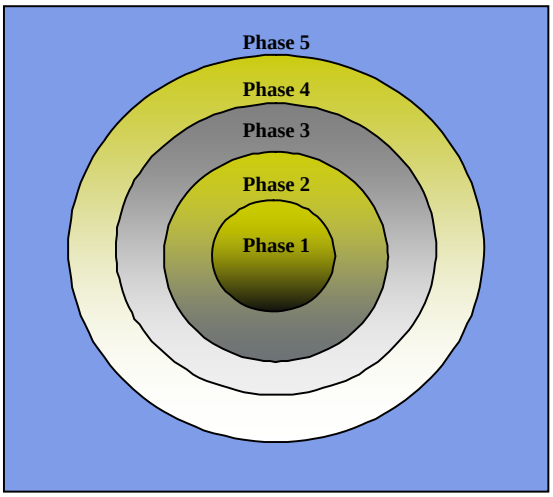

Figure 4.3 Five-phase model (recycled aggregate concrete)

In Figure 4.3, Phase 2 to Phase 4 can be further decomposed into several sub Phases as shown in Figure 4.4. Among them, Phase 3 represents the surface treatment, which varied with different curing time and different water to cement ratios in cement slurry.

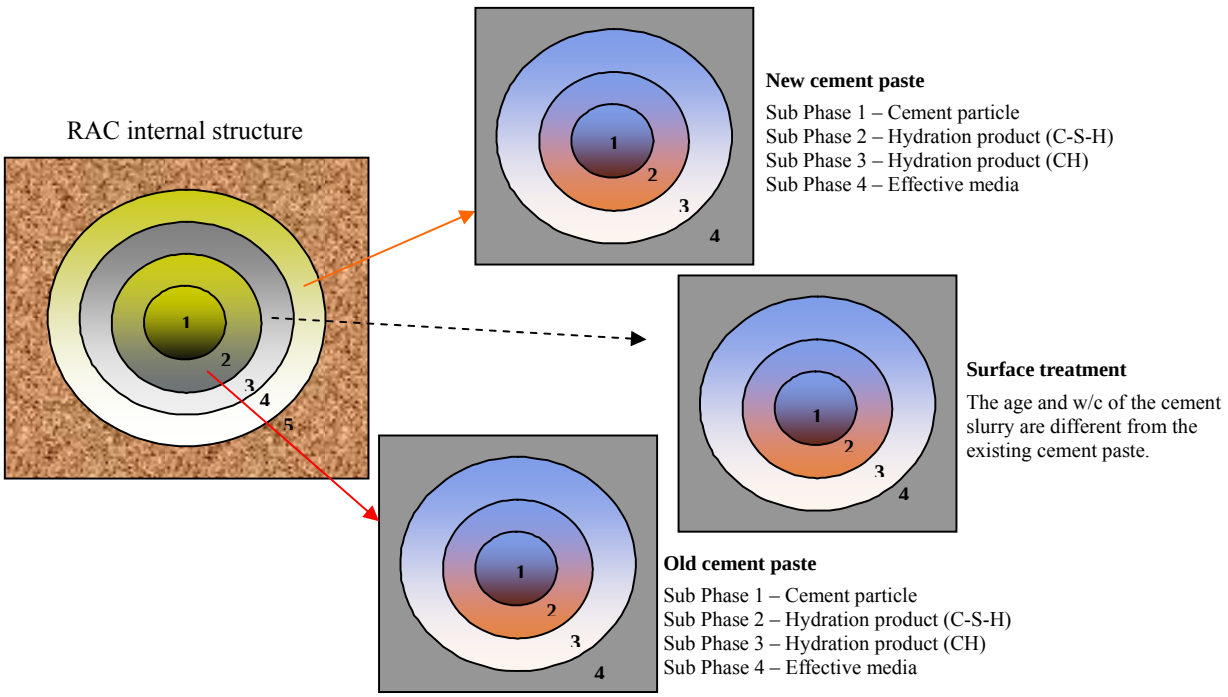

Figure 4.4 Model (recycled aggregate concrete)

4.10. Volume fraction (Recycled aggregate concrete)

In our five–phase model, with different water to cement ratio and curing time, the different degree of hydration reaction will cause the change of volume fraction in the process. Therefore, we should treat it as a time dependent parameter in this model. In order to determine the volume fractions of constituent phases f_1, f_2, and f_3 (three four-phase models in Figure 4.2), the specific volumes V_{core}, V_{CH}, V_{inner}, V_{outer} and V_{cp} in equation (4.13) need to be evaluated. The evolutions of the three parameters in Phase 1 with increasing time are shown in Figure 4.5. The volumes of the inner and outer products may be distinguished by adsorption test results with different gases. Therefore, from the definition, f_3 can be solved following equation (4.18). Finally, the volume fraction of inner product can be obtained simply from f_1 and f_3. The evolutions of volume fractions with increasing time are shown in Figure 4.6.

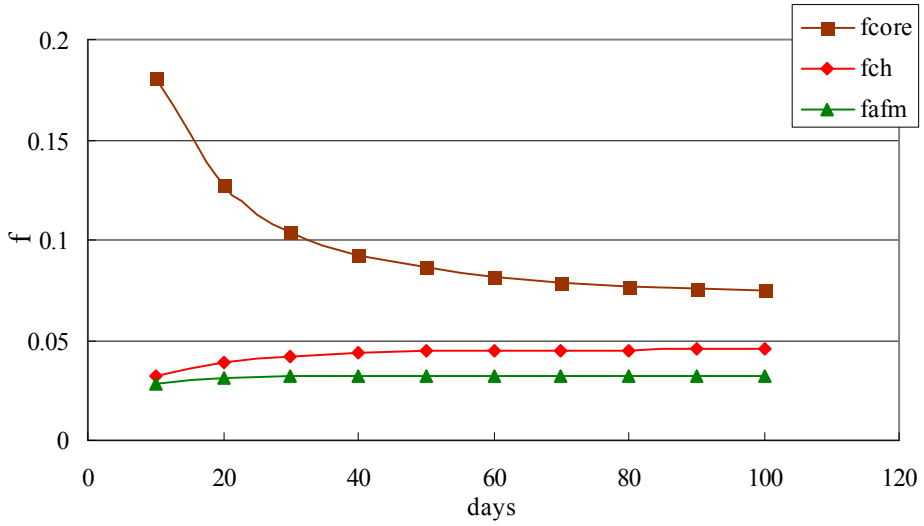

Figure 4.5 Evolutions of three parameters in phase 1

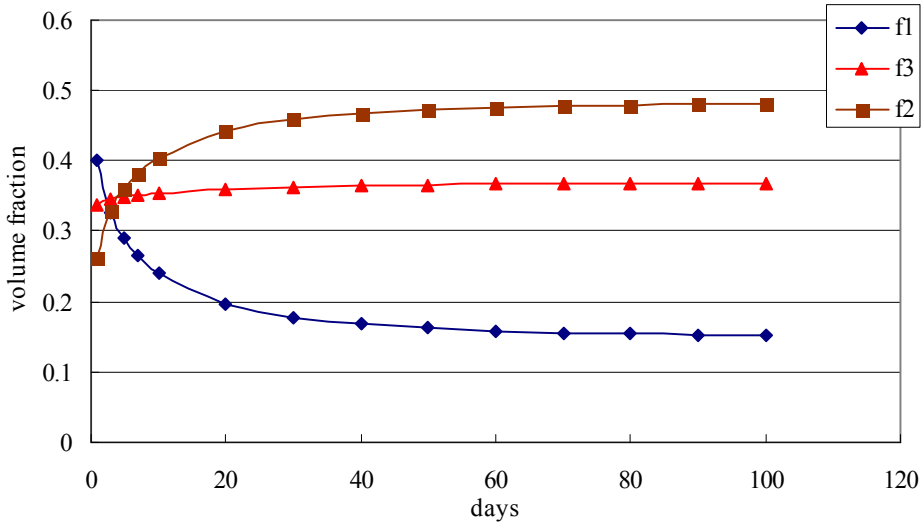

Figure 4.6 Evolution of volume fractions for f1, f2, and f3, with increasing time

4.11. Case study of recycled aggregate concrete (Surface treatment-cement slurry plus silica solution)

The multiscale and multiphase model varies with different water to cement ratio, hydration reaction time, and surface treatment. Combined with the experimental study in Chapter 3.2, the model can be categorized in the following three cases.

Case 1 –recycled aggregate with surface treatment (cement slurry plus silica solution)

Case 2 –recycled aggregate with surface treatment (cement slurry)

Case 3 –recycled aggregate without surface treatment

Among the three cases, Case 1 can be denoted as the most complicated one. We take it as an example and compare its analytical solution with experimental results later. In Case 1, the five–phase model is shown in Figure 4.7. At the left, from the inner layer to outer layer, phase 1 represents natural aggregate, phase 2 represents existing cement paste (residual or old cement paste on surface of aggregate), phase 3 represents surface treatment layer (cement slurry plus silica solution), phase 4 represents new cement paste, and phase 5 represents effective media.

Then, phases 2 through 4 can be decomposed as three four-phase models. Anhydrous cores, CH,

and other crystals are non-shrinking phases and form the phase 1 together. The inner product is the phase 2, and the outer product with capillary pores is the phase 3.

Finally, each component of the cement paste is considered to be a two-phase material, hydration solid and pore. The same composite model of concentric spheres is used at all scale levels and that is why this model is called multiscale and multiphase model.

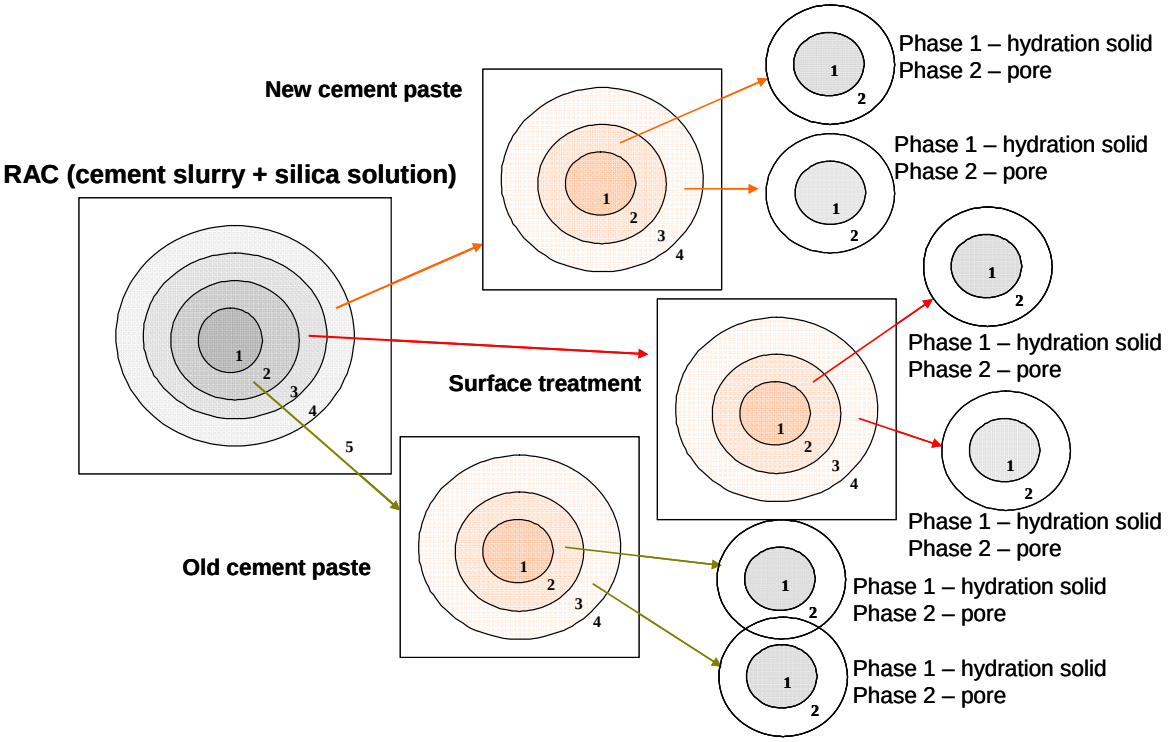

Figure 4.7 Theoretical model (Case1)

In Chapter 3.2, we adopted the specimens from five sets (Groups 9-1, 9-3, 9-4, 12-3, and 12-4) in Table 4.1. The number in Table 4.1 following CS and CS+SS indicates the water to cement ratio in the surface treatment process. The column of w/c represents the water to cement ratio at the final mixing process. Among the five groups, we apply the information of Group 12-4, including the material properties, pretreatment, and mixing process, in our model and compare its analytical solution with the test results (Figure 4.8).

Table 4.1 Drying shrinkage measurements

	Mixing approaches	Surface treatments	W/C
Group 9-1	2	N	0.45
Group 9-3	2	N	0.49
Group 9-4	2	N	0.51
Group 12-3	2	CS+SS, 0.6	0.45
Group 12-4	2	CS+SS, 0.6	0.49

Mixing approach 2: sand enveloped mixing approach (SEMA)

CS: cement slurry

SS: silica solution

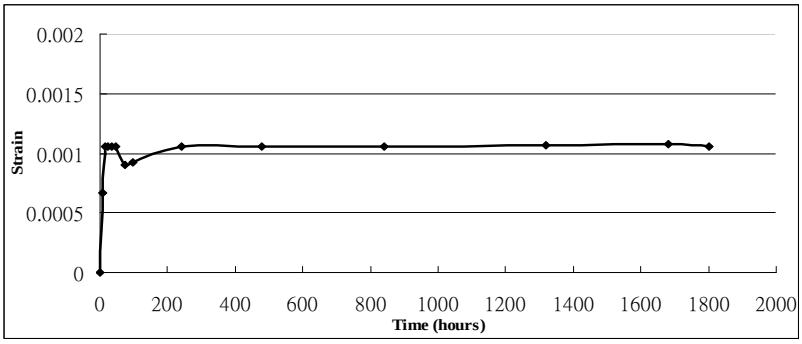

Figure 4.8 Drying shrinkage (Group 12-4)

Apply the concept and equations we mentioned above, several important parameters can be calculated in the process, such as the prediction of bulk modulus in Figure 4.9, and then finally the shrinkage can be obtained as the red line in Figure 4.10.

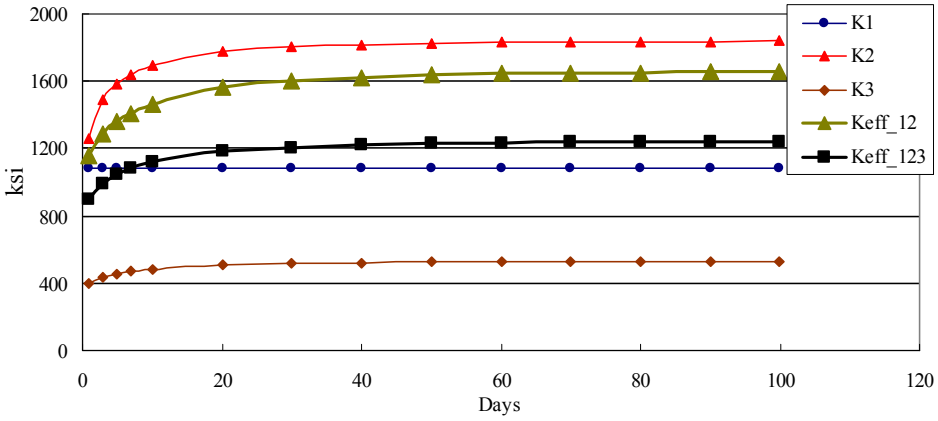

Figure 4.9 Bulk modulus (recycled aggregate concrete)

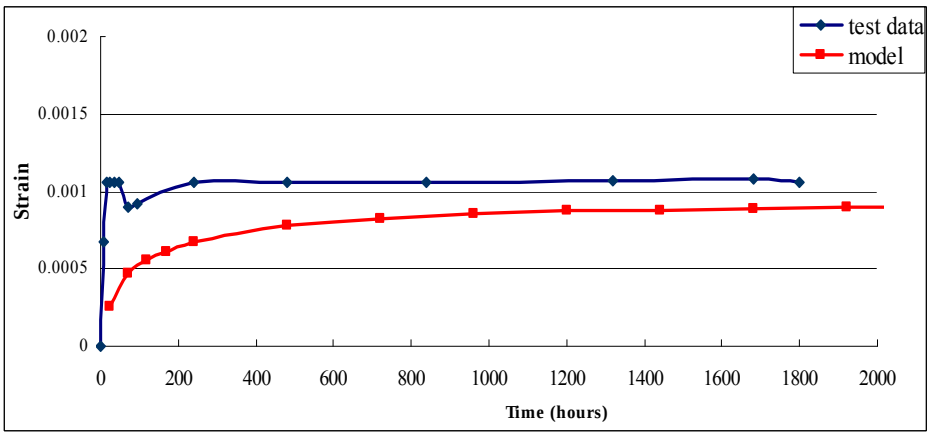

Figure 4.10 Comparison

4.12. Conclusions

(a) The models at different scale levels serve as links in the chain of a multiscale model. The multiphase model is supposed to predict the shrinkage of cement paste at the millimeter level based on parameters at the micrometer level.

(b) Spherical elements have a size gradation, and each element may contain as many phases as needed. The present multiphase model is based on the elastic solution for a boundary value problem of a two-phase composite system. The solution is then generalized for the shrinkage of multiphase materials by a recursive method.

(c) The products of C-S-H and pores, together with CH and other crystals and anhydrous phases

are regrouped into three phases according to the different roles they play in shrinkage of cement paste. Anhydrous cores, CH, and other crystals form phase 1; the inner product is phase 2; and the outer product and capillary pores constitute phase 3. The volume fractions of the three phases are then derived based on a model of hydration reaction.

(d) Only the outer product of the cement particle is considered to be a shrinking phase. Since we define phase 3 to be composed of the outer product and the capillary pores, the shrinkage of phase 3 should include the effects of two sources: one is the shrinkage of outer product in terms of age of the paste, and the other is the effect of capillary pores.

(e) From the comparison between analytical solution and test data, this multiscale chemomechanical model provides a good approach to explain, analyze, and even predict the shrinkage of recycled aggregate concrete. This model can be further developed for more material properties of recycled aggregate concrete, such as mechanical, thermal expansion, and transport properties (moisture and chloride).

Chapter 5

Chloride penetration on bridge decks

5.1. Overview

Among all components of highway bridge structures, bridge decks usually deteriorate the fastest and require the most resources for maintenance and repairs. That is because bridge decks are often exposed to severe environmental conditions, such as temperature fluctuation, moisture variation, and heavy traffic with large loads. In addition, in winter season, de-icing salts have been widely used for anti-icing and de-icing of bridge decks and pavements, which cause the chloride-induced corrosion of embedded reinforcement in bridge decks. This corrosion mechanism has historically been a long-term problem to the Department of Transportation as well as the nation's transportation management agencies in the US.

In chloride-induced reinforcement corrosion, chloride ions penetrate into concrete from the environment, and then reinforcements in concrete decks begin to corrode once the chloride concentration near rebar reaches a critical level. Using concrete with lower permeability can help resist or slow down the penetration of chloride and moisture into bridge concrete. However, this strategy cannot prevent the corrosion resulting from existing cracks. Therefore, several approaches have been developed to prevent this corrosion and prolong bridge service life.

(a) Topical protection systems:

Different materials are used as barriers to protect bridge decks from corrosion damage and prevent or slow down the penetration of water, oxygen, and chloride ions.

(b) Corrosion inhibitors:

Some particular materials are added into concrete to provide protection from by raising the critical

chloride concentration level.

(c) Corrosion protection/prevention techniques:

Use impressed current and/or external anode to protect the reinforcement. This approach is very effective even when chloride concentration near rebar is above a critical level.

(d) Alternative reinforcement steel bars:

It is feasible to use materials that electrically isolate the steel from the concrete and create a barrier against chloride ions. Those materials can protect steel and have significantly higher corrosion thresholds than conventional reinforced steels.

The first approach, topical protection systems, is commonly used on highway bridge decks. The systems provide a protective layer between bridge decks and the environments. There are many different methods used to apply a protective layer such as low-permeability concrete overlays and waterproof membranes with asphalt overlays. Various types of sealers are used in some states in the US that aim to prevent the penetration of water and chloride ions into concrete. Unlike other protection methods, concrete sealers can be applied onto bridge decks, substructure members and deck undersides. There are many sealers on the market. Sealers can be film-forming coatings, or block materials filling the capillary pores, or hydrophobic pore liner that lines the surface of the pores. Most pore blockers are not appropriate for use on bridge decks because they do not offer good skid resistance and do not hold up to traffic and the deterioration it causes (Sherman et al. 1993).

5.2. Chloride profiles

5.2.1. Motivations

Since chloride concentration in the concrete has been considered an important indicator for the effectiveness of topical protection methods, we selected and inspected several bridge decks, took concrete cores, and obtained chloride concentrations at various depths. There are three stages in the rebar corrosion process;

(a) The chloride concentration near rebar is lower than the critical value and the corrosion of rebar

has not started.

(b) The chloride concentration near rebar just reached the critical value and the corrosion of rebar just started.

(c) The chloride concentration near rebar is much higher than the critical value and the corrosion of rebar already started some time ago.

The outcomes of the inspection will show which stage a bridge deck is in, and a comparison of the outcomes will confirm the effectiveness of the topical protection methods applied on the selected bridges. Finally, five bridges were selected for inspection in the research. The following is information on the five bridges:

(a) C-16-DI – Located 6 miles west of Loveland, built in 1980, with 3 in. of asphalt wearing surface.

(b) G-22-BG – I-70, MP362.2, east of Limon, built in 1975, with 2 in. of integrated concrete surface.

(c) G-22-BH – I-70, MP362.2, east of Limon, built in 1975, with 3 in. of integrated concrete surface.

(d) G-22-BJ – I-70, MP357.77, west of Limon, built in 1972, without overlay.

(e) G-22-BL – I-70, MP361.74, east of Limon, built in 1975, without overlay.

Among the five bridges, C-16-DI and G-22-BH were selected to compare the effectiveness of asphalt and concrete overlays (with the same 3.0 in. thickness), G-22-BJ and G-22-BL were selected to compare with G-22-BG and G-22-BH on the effectiveness of concrete overlays, and finally G-22-BG and G-22-BH were selected to compare the effect of different thicknesses of concrete overlays (3.0 in. and 2.0 in. thickness). Concrete cores were taken from the bridge decks and chloride concentration profiles in the concrete cores were obtained in our laboratory. Since the inspected bridge decks are all in the first stage of the corrosion process, i.e., the corrosion of rebar has not started, just comparing the current inspection results is not sufficient to evaluate the effectiveness of the topical protection methods. What we did in this

research is to predict the future performance of the decks based on the current inspection results, and then the effectiveness of the protection methods is compared by using the predicted future performances.

In order to predict the future performance of the protection methods, the measured concentration profiles will be used later to determine chloride diffusivity rates of the concretes. The diffusivity rates determined in this way will be used in a simulation model to estimate future chloride profiles in the decks, and then the effectiveness of the topical protection methods can be evaluated by comparing the predicted future chloride concentration profiles.

5.2.2. Concrete Samples

(1) Bridge G-22-BJ and Bridge G-22-BL

Figure 5.1 and Figure 5.2 show the Bridge G-22-BL and the coring site of the Bridge G-22-BJ. For Bridge G-22-BJ, two concrete cores were taken. One core was taken from the traffic lane, 4 ft inside of the shoulder line. The core was broken into two portions during the drilling process. The top portion was numbered as J↑1L, and the bottom portion J↑2L. The other core was taken from the shoulder, 5 ft outside of the shoulder lane. The core was numbered as J↑S. There was no rebar found in the concrete cores.

The notations used for numbering the cores are as follows;

J – G-22-BJ

L (the first L) – G-22-BL

↑ - Points to the top surface.

1 and 2 – top and bottom portion.

L (the last L) – Traffic lane.

S – Shoulder.

For Bridge G-22-BL, two concrete cores were taken. One core was taken from the traffic lane, 4.5 ft inside of the shoulder line. The core was broken into two portions during the drilling process. The top portion was numbered as L↑1L, and the bottom portion was numbered as L↑2L. The other core was taken

from the shoulder, 4.5 ft outside of the shoulder line. The core was numbered as L↑S. There was no rebar found in the concrete cores. The locations of the drilled concrete cores are summarized in Table 5.1.

(2) Bridge G-22-BG, G-22-BH

For Bridge G-22-BG, The core was taken 4.1ft inside of the shoulder lane. The depth from surface to steel bars is 3.3 in. (The overlay thickness was designed to be 2.0 in.). Figure 5.3 shows the traffic control on Bridge G-22-BG.

For Bridge G-22-BH, The core was taken 3.5ft inside of the shoulder lane. When taking the cores on-site, an interface was found between new overlay and old concrete at a depth of 3.6 in (the overlay thickness was designed to be 3.0 in.). Figure 5.4 shows the coring samples on Bridge G-22-BH. The core was broken in the traffic lane.

(3) Bridge C-16-DI

Figure 5.5 shows the overview of Bridge C-16-DI. For Bridge C-16-DI, two concrete samples were taken. One core was taken from the traffic lane, 3.5 ft inside of the shoulder lane. The other core was taken from the shoulder, 5 ft outside of the shoulder lane.

When taking cores on-site, an interface was found between asphalt overlay and old concrete at a depth of 3 in. (the overlay thickness was designed to be 3.0 in.). We cut off the layer of asphalt overlay before doing the test for chloride concentration profile in our lab. Figure 5.6 shows the coring site on Bridge C-16-DI.

Figure 5.1 Bridge G-22-BL

Figure 5.2 Coring concrete samples (Bridge G-22-BJ)

Figure 5.3 CDOT traffic control (Bridge G-22-BG)

Figure 5.4 Concrete samples (Bridge G-22-BH)

Figure 5.5 Bridge C-16-DI

Figure 5.6 Take coring samples

Table 5.1 Location of taking concrete cores

Concrete Core	Location	
J↑S	G-22-BJ	Shoulder
J↑1L	West Bound	Traffic lane (Top)
J↑2L		Traffic lane (Bottom)
L↑S	G-22-BL	Shoulder
L↑1L	East Bound	Traffic lane (Top)
L↑2L		Traffic lane (Bottom)

5.2.3. Experimental results

The chloride profiles of concrete cores are shown in Figures 5.7 through 5.13.

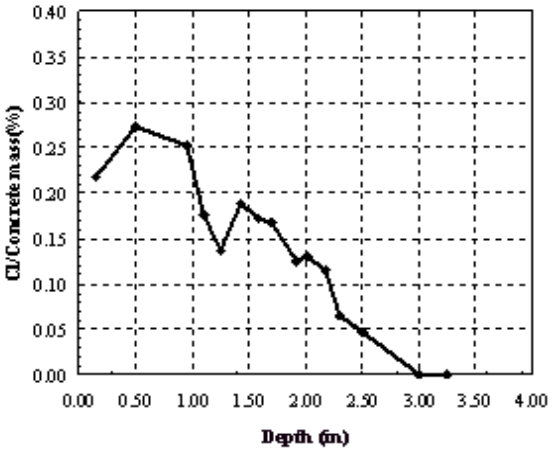

Figure 5.7 Chloride profile (Bridge G-22-BJ; shoulder lane)

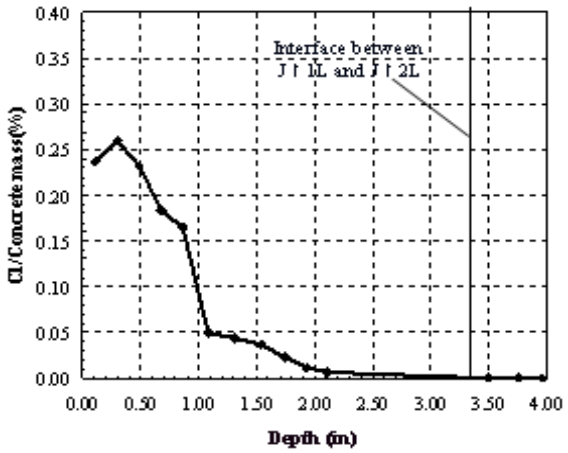

Figure 5.8 Chloride profile (Bridge G-22-BJ; traffic lane)

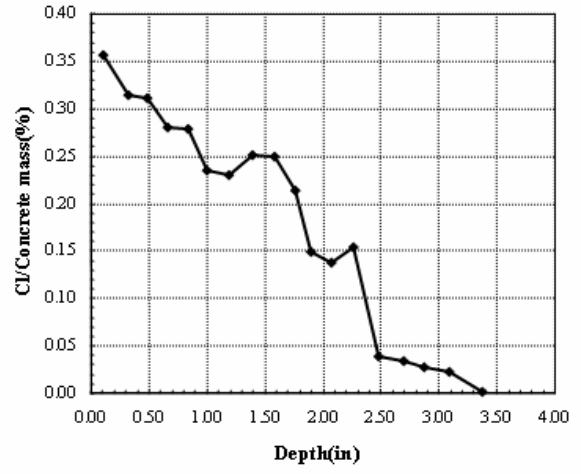

Figure 5.9 Chloride profile (Bridge G-22-BL; shoulder lane)

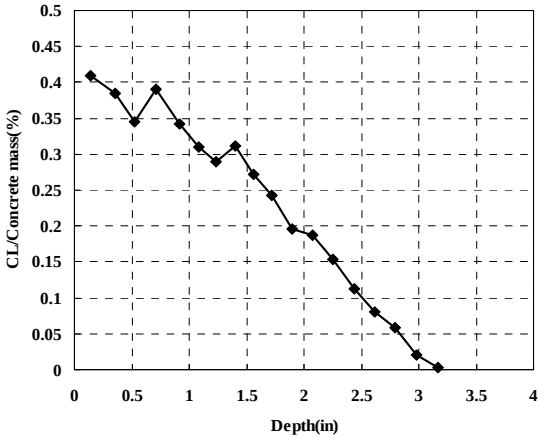

Figure 5.10 Chloride profile (Bridge G-22-BG)

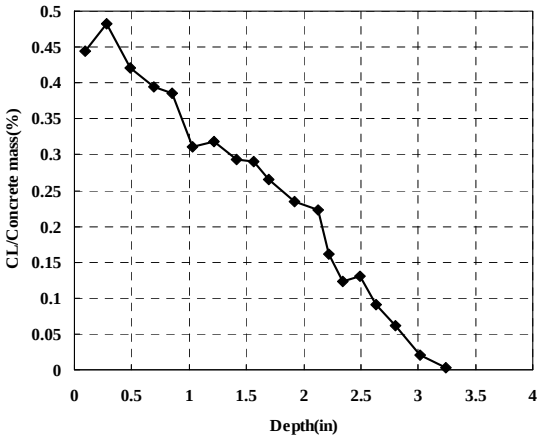

Figure 5.11 Chloride profile (Bridge G-22-BH)

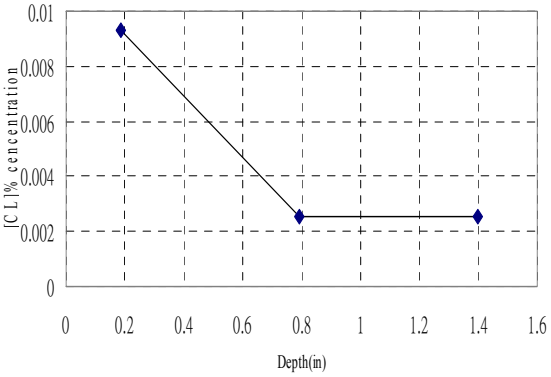

Figure 5.12 Chloride profile (Bridge C-16-DI; shoulder lane)

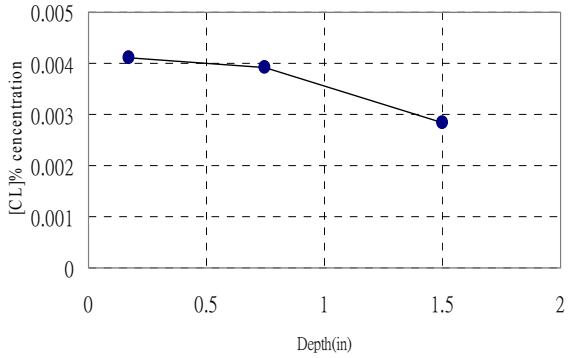

Figure 5.13 Chloride profile (Bridge C-16-DI; traffic lane)

5.3. Prediction

From the inspection results, we concluded that all bridge decks inspected are in good shape. No corrosion damage of rebar has occurred in the decks. This conclusion was based on the facts that 1) no corroded rebar were found in the coring process, and 2) the chloride concentration near rebar was much lower than the critical chloride concentration.

Although all decks are in the first stage, the inspection results can be used to predict corrosion initiation time in the future. The predicted results can be used to estimate the performance of the topical protection methods. To this end, we need to have an accurate model to predict future changes of chloride concentration profile in the bridge decks. The current inspection results are very important for the development of the prediction model, because they can be used to calibrate the model parameters.

In the next sections, we will first describe the diffusion model for characterizing the chloride penetration process, and then explain how to use the present inspection results to determine or calibrate several important parameters of the diffusion model. Finally, we will use the calibrated model to predict future chloride concentration profiles and thus predict corrosion initiation times for the bridge decks.

5.3.1. Chloride diffusion model

The penetration of chloride ions into concrete bridge decks can be described by diffusion equation (5.1). Using the Boltzman transformation as shown in equation (5.2), equation (5.1) can be solved and the solution is shown in equation (5.3).

$$\frac{\partial C}{\partial t} = D_{Cl}\frac{\partial^2 C}{\partial x^2} \qquad \text{Eq. (5.1)}$$

$$\zeta = \frac{x}{\sqrt{4D_{cl}t}} \qquad \text{Eq. (5.2)}$$

$$\frac{C - C_0}{C_{ini} - C_0} = erf\left(\frac{x}{\sqrt{4D_{cl}t}}\right) \qquad \text{Eq. (5.3)}$$

In which

C = chloride concentration in concrete in % weight of concrete

C_0 = surface concentration of concrete in % weight of concrete

C_{ini} = initial concentration of chloride in the concrete in % weight of concrete

D_{cl} = chloride diffusion coefficient in cm^2/days

x = depth in cm

t = time in days

erf is called error function. The equation (5.3) is called the error function solution of linear diffusion equation (5.1).

After the diffusion coefficient of concrete is determined and the critical chloride content is known, the error function solution can be used to predict the corrosion initiation time for the structure.

$$t_{initiation} = \frac{X_{cover}^2}{4D_{cl}}\left[erf^{-1}\left(\frac{C_o - C_{cri}}{C_o - C_{ini}}\right)\right]^{-2} \qquad \text{Eq. (5.4)}$$

C_{cri} = critical chloride concentration in concrete in % weight of concrete

X_{cover} = thickness of concrete cover in cm

5.3.2. Calibration

There are two parameters, namely the diffusion coefficient, D_{cl} , and the surface chloride concentration, C_0 , in the equations above that need to be determined by specific conditions of each deck. The diffusion coefficient of an existing concrete deck depends on many parameters related to initial

conditions of the concrete and environmental conditions of the bridge deck, including concrete mix designs, construction practice, traffic loading, and environmental loading. For different bridge decks, the diffusion coefficient of concrete varies. The surface chloride concentration depends on the amount of deicing salts applied on the deck. Since deicing salts are not applied on concrete decks all year long, the surface concentration is an average value. The best way to determine the two parameters is to calibrate the theoretical solution with the measured concentration profiles. Once these two parameters are calibrated, the chloride concentrations at any depth in the bridge decks at any time can be calculated by equation (5.3) and the future corrosion initiation time of rebar can be predicted by equation (5.4). So, the next step is to use measured data to determine the diffusion coefficient and surface chloride concentration.

Table 5.2 summarizes the useful information of the five inspected bridges. Table 5.3 lists several available critical chloride contents, C_{cri}, in the literature. C_{cri} is not a constant because the onset of corrosion of rebar does not depend only on C_{cri}. This is because the corrosion process of rebar is an electrochemical process. There are other influential parameters playing important roles in the electrochemical process, such as the moisture content of concrete and the pH value of pore solution near the rebar. In this study, we used two different values for C_{cri}. One is considered as the regular value $C_{cri} = 0.05\%$, which has been used widely in the research community, and the other is considered as the strictest critical value $C_{cri} = 0.021\%$.

Table 5.2 Information of the five bridges

No	Bridge	Location	Year	Surface (Mat &Thick)	
1	G-22-BJ	I-70, MP357.77, west of Limon	1972	IC	3.3in
2	G-22-BL	I-70, MP361.74, east of Limon	1975	IC	2.9in
3	G-22-BG	I-70, MP362.2, east of Limon	1975	IC	2in
4	G-22-BH	I-70, MP362.2, east of Limon	1975	IC	3in
5	C-16-DI	6 MI W of Loveland	1980	Asphalt	3in

Table 5.3 Critical value

	Critical chloride content
Berke (1986)	0.039%-0.043%
Browne (1982)	0.06%
FHWA	0.04%
ACI (1994)	0.02%
Cady and Weyers (1992)	0.025-0.05%

The calibration criteria for the two parameters D_{cl} and C_0 is to find the optimum values of D_{cl} and C_0 that lead to the best curve fitting of the concentration profiles between the theoretical prediction (using equation (5.3)) and the measured data. In order to do so, we tried many pairs of values for D_{cl} and C_0, compared model predictions with the measured data, and selected the optimum values for D_{cl} and C_0. Then, the two optimum values were used in equation (5.4) to predict the future corrosion initiation time. The following figures and tables show the calibration and prediction results for the five bridges in the shoulder and traffic lanes.

(1) Bridge G-22-BJ

For the chloride concentration in shoulder lane and traffic lane, the results are:

$C_0 = 0.35\%$ in shoulder lane ; $C_0 = 0.3\%$ in traffic lane; $C_{cr} = 0.05\%,0.21\%$; $C_{ini} = 0$

The depth from surface to steel bars = 3.3 in. The calibrating curves and the prediction on corrosion initiation times are shown in Figure 5.14-5.15 and Table 5.4-5.5.

(2) Bridge G-22-BL

For the chloride concentration in shoulder lane and traffic lane, the results are:

$C_0 = 0.45\%$ in shoulder lane ; $C_0 = 0.38\%$ in traffic lane; $C_{cr} = 0.05\%,0.21\%$; $C_{ini} = 0$

The depth from surface to steel bars = 2.9 in. The calibrating curves and the prediction on corrosion initiation times are shown in Figure 5.16-5.17 and Table 5.6-5.7.

(3) Bridge G-22-BG

For the chloride concentrations, the results are:

$C_0 = 0.6\%$; $C_{cr} = 0.05\%, 0.21\%$; $C_{ini} = 0$;

The depth from surface to steel bars = 3.3 in. The calibrating curves and the prediction on corrosion initiation times are shown in Figure 5.18 and Table 5.8.

(4) Bridge G-22-BH

For the chloride concentrations, the results are:

$C_0 = 0.6\%$; $C_{cr} = 0.05\%, 0.21\%$; $C_{ini} = 0$;

When taking cores on-site, an interface was found between new overlay and old concrete at the depth of 3.6 in. We considered the total depth from the surface to steel bar to be 6.6 in. The calibrating curves and the prediction of corrosion initiation times are shown in Figure 5.19 and Table 5.9.

(5) Bridge C-16-DI

For the chloride concentration in shoulder lane and traffic lane, the results are:

$C_0 = 0.01\%$; $C_{cr} = 0.05\%, 0.21\%$; $C_{ini} = 0$;

When taking cores on-site, an interface was found between the asphalt overlay and the old concrete at a depth of 3 in. We cut off the layer of asphalt overlay before conducting the chloride test in the lab. Therefore, we considered the total depth from the interface to steel bar to be 2.8 in. The calibrating curves and the prediction of corrosion initiation time are shown in Figure 5.20 and Table 5.10.

For Bridge C-16-DI, we measured three chloride concentrations at three different depths from both shoulder and traffic lanes. The measured concentrations from this bridge are quite a bit lower than the other four bridges. The bridge decks had been covered by a thick layer of asphalt overlay (more than 3 in), which may be the reason for the low chloride concentrations. In fact, even the surface chloride concentrations (0.01%) are much lower than the critical values (0.05% and 0.021%). This is why we only took readings at three different depths which were much less than the number of readings we did for other bridges.

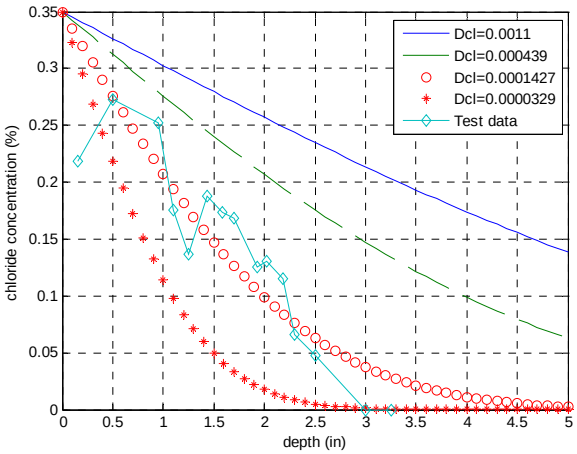

Figure 5.14 Chloride concentration profiles (Bridge G22-BJ; shoulder lane)

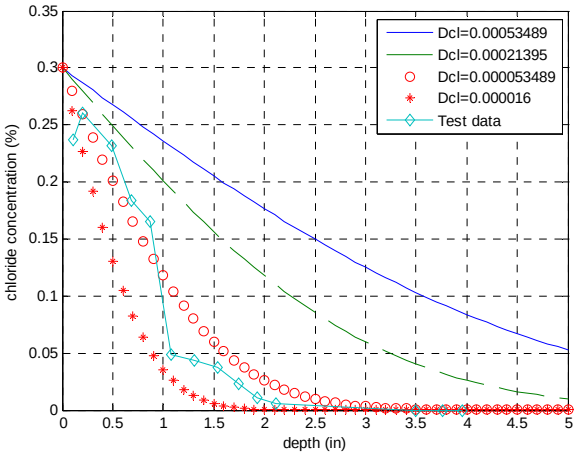

Figure 5.15 Chloride concentration profiles (Bridge G22-BJ; traffic lane)

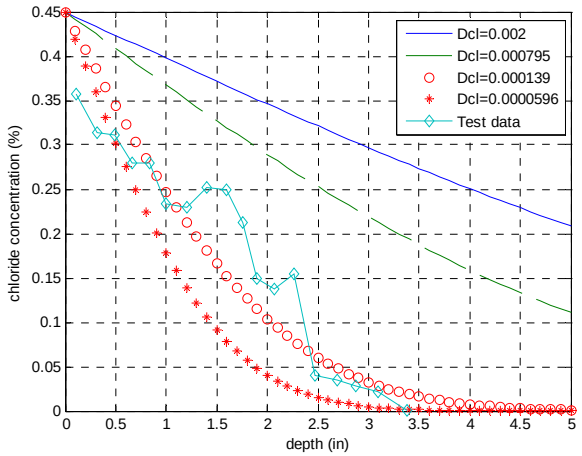

Figure 5.16 Chloride concentration curves (Bridge G22-BL; shoulder lane)

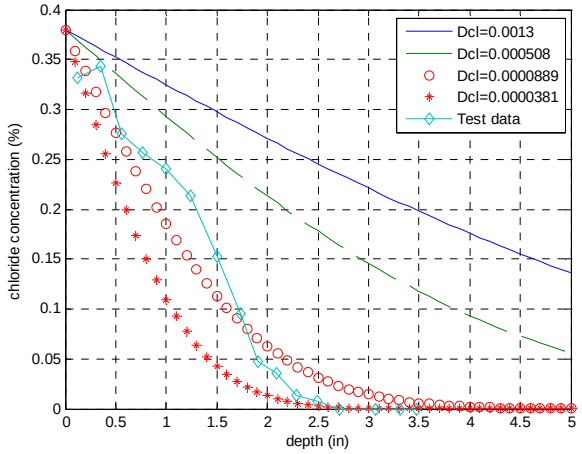

Figure 5.17 Chloride concentration curves (Bridge G22-BL; traffic lane)

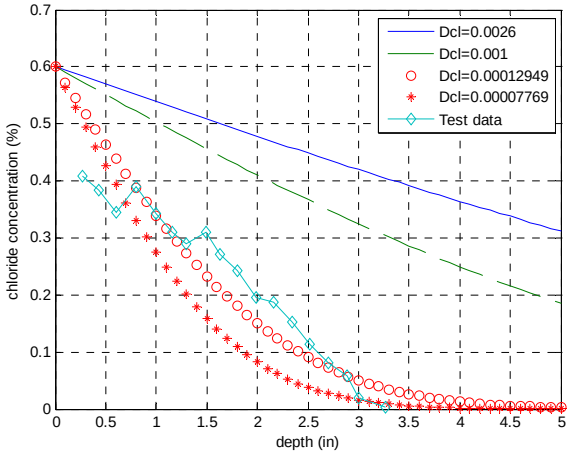

Figure 5.18 Chloride concentration curves (Bridge G22-BG)

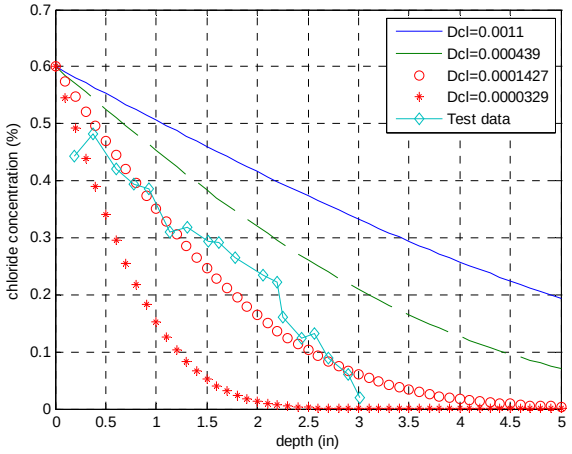

Figure 5.19 Chloride concentration curves (Bridge G22-BH)

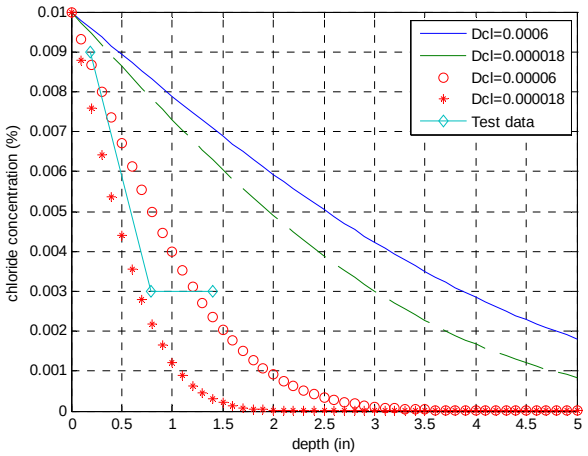

Figure 5.20 Chloride concentration curves (Bridge C16-DI)

Table 5.4 Prediction of corrosion initiation time (Bridge G22-BJ; shoulder lane)

C_{cr} (%)	C_0 (%)	D_{cl} (current) (cm^2/days)	Prediction time(years)
0.05	0.35	0.0001427	331
0.021	0.35	0.0001427	201

Table 5.5 Prediction of corrosion initiation time (Bridge G22-BJ; traffic lane)

C_{cr} (%)	C_0 (%)	D_{cl} (current) (cm^2/days)	Prediction time(years)
0.05	0.3	0.000053489	941
0.021	0.3	0.000053489	548

Table 5.6 Prediction of corrosion initiation time (Bridge G22-BL; shoulder lane)

C_{cr} (%)	C_0 (%)	D_{cl} (current) (cm^2/days)	Prediction time(years)
0.05	0.45	0.000139	246
0.021	0.45	0.000139	158

Table 5.7 Prediction of corrosion initiation time (Bridge G22-BL; traffic lane)

C_{cr} (%)	C_0 (%)	D_{cl} (current) (cm^2/days)	Prediction time(years)
0.05	0.38	0.0000889	368
0.021	0.38	0.0000889	158

Table 5.8 Prediction of corrosion initiation time (Bridge G22-BG)

C_{cr} (%)	C_0 (%)	D_{cl} (current) (cm^2/days)	Prediction time(years)
0.05	0.6	0.00012949	253
0.021	0.6	0.00012949	171

Table 5.9 Prediction of corrosion initiation time (Bridge G22-BH)

C_{cr} (%)	C_0 (%)	D_{cl} (current) (cm^2/days)	Prediction time(years)
0.05	0.6	0.0001427	253
0.021	0.6	0.0001427	170

Table 5.10 Prediction of corrosion initiation time (Bridge C16-DI)

C_{cr} (%)	C_0 (%)	D_{cl} (current) (cm^2/days)	Prediction time(years)
0.05	0.01	0.00006	NaN
0.021	0.01	0.00006	NaN

Where NaN means the calculations are infinite and out of the range

5.4. Model modification

In the chloride diffusion model shown in equations (5.3) and (5.4), we considered the chloride diffusion coefficient as a constant for each bridge (either from the traffic or shoulder lane). The value obtained in the calibration is, therefore, the best estimated chloride diffusion coefficient for each concrete

desk at the time of inspection. These estimated values for chloride diffusion coefficients can be considered as quite accurate for now. The concrete in the bridge decks is in very good condition; therefore, the predicted corrosion initiation times are all very long, more than 100 or 200 years as shown in Tables 5.4-5.10. These unrealistic predictions result from an unrealistic assumption used in the chloride diffusion model of equation (5.3). That is, the concrete will remain in the current condition without any deterioration in the next 100 or 200 years.

With various impacts of traffic loading, freeze-thawing cycles, and drying-wetting cycles, the concrete will deteriorate, the diffusion coefficients will increase significantly, and the corrosion initiation times will be much shorter than those predicted in Tables 5.4-5.10.

In this section, the diffusion model of equations (5.3) and (5.4) will be modified to take into account the deterioration process of concrete. To this end, the diffusion coefficient in equation (5.1) will be considered as a time dependent parameter (Xi et al. 2000; Mangat and Molloy 1994; Mangat and Limbachiya 1999) and at most occasions, parameter m should be negative. In addition, from previous research, the power number of time in equation (5.5) is defined at $-m$.

$$D_{cl} = D_i^{cl} t^{-m} \qquad \text{Eq. (5.5)}$$

D_i^{cl} = a reference diffusion coefficient in cm^2/days

m = empirical constant representing the rate of deterioration of concrete

Equation (5.5) shows that with increasing time, the diffusion coefficient D_{cl} increases due to the negative value of parameter m, which represents the deterioration process of concrete in bridge decks. Combine equation (5.5) and equation (5.1) gives

$$\frac{\partial C}{\partial t} = (D_i^{cl} t^{-m}) \frac{\partial^2 C}{\partial x^2} \qquad \text{Eq. (5.6)}$$

Equation (5.6) is different from equation (5.1). The solution of equation (5.6) requires some further manipulations.

$$\frac{1}{(D_i^{cl} t^{-m})} \frac{\partial C}{\partial t} = \frac{\partial^2 C}{\partial x^2} \qquad \text{Eq. (5.7)}$$

Substituting $\partial T = (D_i^{cl} t^{-m})\partial t$ into equation (5.7) gives

$$\frac{\partial C}{\partial T} = \frac{\partial^2 C}{\partial x^2} \qquad \text{Eq. (5.8)}$$

This equation is similar to the linear diffusion equation (5.1) and thus the standard error function solution, equation (5.3), can be used here (with $D_{cl} = 1$).

$$C = C_0\left[1 - erf\left(\frac{x}{2\sqrt{T}}\right)\right] \qquad \text{Eq. (5.9)}$$

Integrate $\partial T = (D_i^{cl} t^{-m})\partial t$ gives

$$T = \int_0^t D_i^{cl}\, t^{-m}\, dt \qquad \text{Eq. (5.10)}$$

And thus

$$T = \frac{D_i^{cl}}{1-m} t^{(1-m)} \qquad \text{Eq. (5.11)}$$

The new variable T can be considered as a new time scale, which is different from the regular time scale, t. Substituting equation (5.11) into equation (5.9) yields

$$C = C_0\left[1 - erf\left(\frac{x}{2\sqrt{\frac{D_i^{cl}}{1-m} t^{1-m}}}\right)\right] \qquad \text{Eq. (5.12)}$$

We rewrite equation (5.12) in the following form

$$t_{initiation}^{1-m} = \frac{(1-m)X_{cover}^2}{4D_i^{cl}}\left[erf^{-1}\left(\frac{C_0 - C}{C_0 - C_{ini}}\right)\right]^{-2} \qquad \text{Eq. (5.13)}$$

The difference between the corrosion initiation times predicted by equation (5.4) and equation (5.13) is that equation (5.13) takes into account the change of diffusion coefficient due to the deterioration of concrete.

5.5. Prediction with the modified diffusion model

Now, the main question is how to determine the values of D_i and m in equation (5.5). Since D_i is

the diffusion coefficient at a reference time, we can determine it using the current inspection results (i.e. considering the current time as the reference time). However, parameter m must be determined based on the rate of concrete deterioration by comparing the diffusion coefficients at least two different times. Figure 5.21 shows the deterioration of the diffusion coefficient at different m values. As time increases, the m value has significant effect on the diffusion coefficient. So far, we only have the estimated diffusion coefficients based on the current inspection results. It will be the best if we can conduct subsequent inspections later on the same bridges and collect another set of data to determine the second point in Figure 5.21. Once we have two different diffusion coefficients at different times, the m value can be determined for each bridge. The m values for different bridges will be different because each bridge has its own rate of deterioration, which depends on its environmental condition and traffic loading. In this way, the corrosion initiation times for the bridges can be determined better, and hence, the effectiveness of the topical protection systems can be evaluated more accurately.

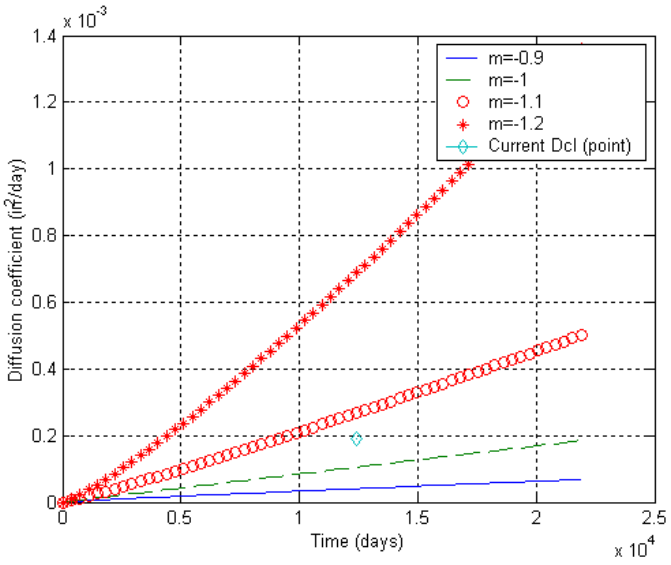

Figure 5.21 Effect of m values on D_{cl}

In previous sections, the best curve fitting of the concentration profiles between the theoretical prediction and the measured data is based on the linear model (equation (5.3)). In this section, we use the modified time dependent model (equation (5.5) and equation (5.12)) to perform the curve fitting using the

same test data. For each bridge, we adjusted two parameters m and D_i in equation (5.12) in such a way as to predict concentration profiles that will best fit the test data. The corresponding parameters are the optimum values of m and D_i .

The parameter m is mainly affected by the traffic loading and environmental conditions. The value tends to be higher when the bridge is under heavy traffic and severe environmental conditions. The parameter D_i represents the quality of concrete in the mixture process. For example, lower water to cement ratio may lead to a lower D_i value.

In equation (5.12), C_o comes from the calibration results and the time used in the calibration for each bridge is the same as the year we took cores and measured chloride concentration profiles. For example, bridge G-22-BJ was built in 1972 and we took cores in 2007. The time in equation (5.12) is 35 years. The comparisons between these predicted profiles and real on-site test data are shown in Figures 5.22 through 5.26.

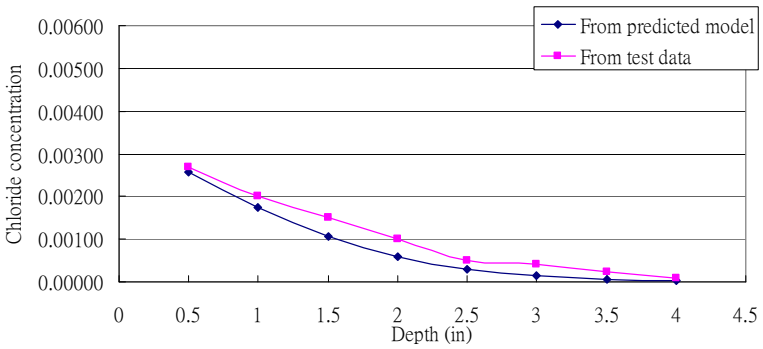

Figure 5.22 Comparison (Bridge G-22-BJ)

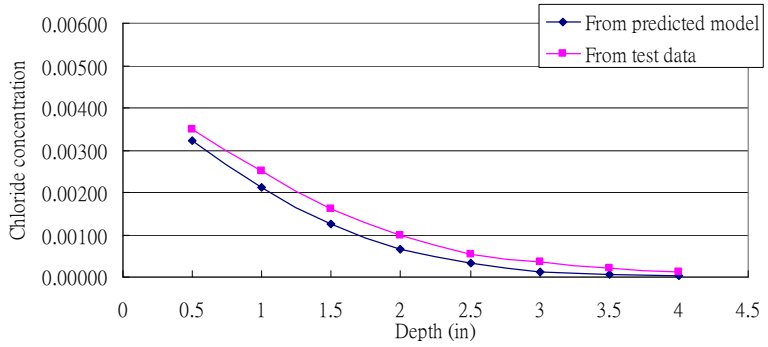

Figure 5.23 Comparison (Bridge G-22-BL)

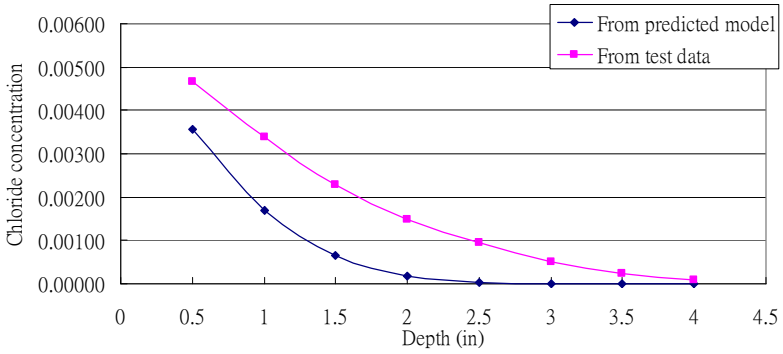

Figure 5.24 Comparison (Bridge G-22-BG)

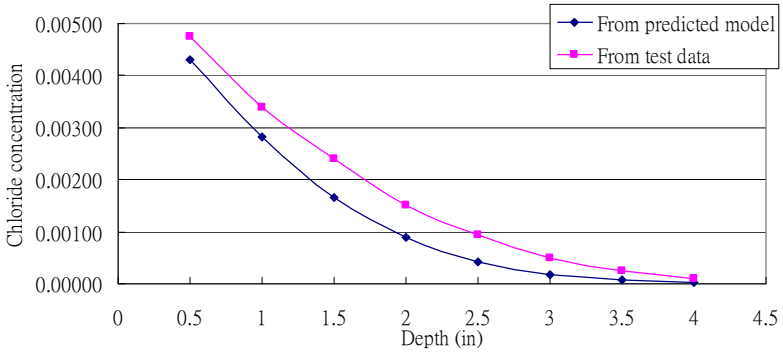

Figure 5.25 Comparison (Bridge G-22-BH)

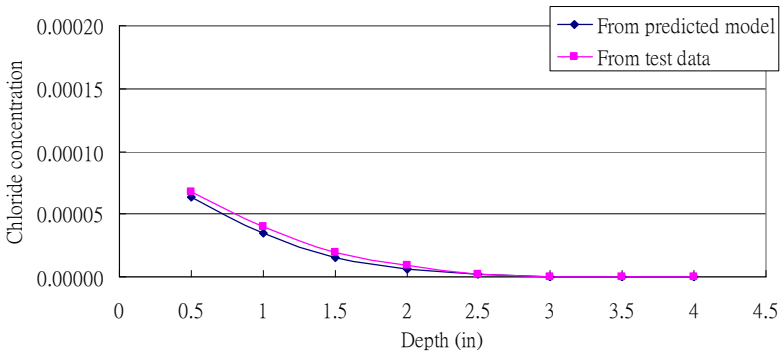

Figure 5.26 Comparison (Bridge C-16-DI)

The calibrated m , D_i values and the predicted corrosion initiation time (using equation (5.13)) based on these optimum parameters are shown as Table 5.11.

Table 5.11 Estimations of the five bridges

Bridge	m	D_{cl} (current) (in^2/days)	Initiation time from now (years)
G-22-BJ	-1.063	0.000189	16
G-22-BL	-1.05	0.000167	9
G-22-BG	-1	0.000072	6
G-22-BH	-1.05	0.000162	6
C-16-DI	-0.99	0.000078	274

5.6. Observations

(1) The corrosion initiation time is reciprocally proportional to the diffusion coefficient, as shown in equation (5.13). This means that the corrosion initiation time will be reduced to 1/10 of the current value, if the diffusion coefficient increases 10 times. In the practice, 10 times increase in the diffusion coefficient is highly possible under heavy traffic and severe environmental conditions.

(2) With the two different critical chloride concentration values, we can obtain a range of the corrosion initiation time. With the lower critical value (0.021%), we can determine a shorter corrosion initiation time, which can be considered as the lower bound of the initiation time. With the higher critical value

(0.05%), we can determine a longer corrosion initiation time, which can be considered as the upper bound of the initiation time. In practice, the actual corrosion initiation time of a bridge deck may be between the two bounds.

(3) While comparing the surface chloride concentrations among the five bridges, we found that Bridge G-22-BH has the highest concentration (0.6%) and Bridge C-16-DI has the lowest (0.01%). These values represent an average of the surface chloride concentration, which is an indication of the amount of deicers used on the bridge decks over the years.

(4) At the same bridge, the surface chloride concentration values from shoulder lane and from traffic lane are different, but the difference is not large.

(5) For the predicted corrosion initiation time, Bridge C-16-DI is the longest, which means the current bridge deck condition for this bridge is the best in terms of corrosion damage of rebar. Another important reason for the much longer predicted corrosion initiation time for this bridge is that the traffic loading on the bridge is much lower than the traffic loadings of other bridges on I-70. All the other bridges have shorter initiation times ranging from 6 to 16 years. Given the uncertainties in the prediction model, the conditions of the other four bridges may be considered as the same.

(6) In order to have a more accurate estimation of the rate of concrete deterioration, i.e. a better estimation for parameters m and D_i (see equation (5.13) and Figure 5.21), we must conduct another inspection of the same bridges in the future. Once we have two different diffusion coefficients corresponding to two different times, we can better define the curve in Figure 5.21, obtain a better estimation on the value for m, and predict more accurately the corrosion initiation time of rebar for the bridge decks. Only then, the effectiveness of the topical protection systems used on the five bridges can be evaluated accurately.

Chapter 6

Evaluation of Bridge Deck Sealants

6.1. Overview

Many older bridges and even new bridges suffer excessive deterioration on the surface of their decks. Although some substances such as deicing salts, graffiti and oil might cause damage or disfigure concrete surfaces, deicing salts are the most destructive material among them. Much of the deterioration is caused by the penetration of water and chloride ion from deicing salt into the concrete.

Deicing salts, which are generally mixtures of sodium chloride and calcium chloride, are commonly spread over bridge decks during winters. As ice melts, it mixes with the deicing salts to form a salt water solution, which remains on the surface of bridge decks. Although some bridges built in the last 15 to 25 years already have the sealer coating system, chloride ions may still penetrate into the decks through existing cracks, and then induce the corrosion of the steel substructure or rebar.

The existing cracks in bridge decks provide a convenient avenue for chemical ions and water to penetrate concrete and thus speed up the corrosion of rebar so crack sealers were first developed and used to seal cracks in bridges. In some snow-belt states, moisture content stays inside cracks and contributes to deterioration during freeze-thawing cycles. As the water in the cracks freezes into ice, the larger volume of ice forces the concrete apart.

Therefore, American Concrete Institute identifies the crack sizes, which are bigger than 0.18 mm, must be sealed by better crack sealers or must provide a system for prohibiting chloride ions from penetrating the decks (American Concrete Institute Manual of Practices 1997). It is found that a crack in the range of 0.3 mm to 0.64 mm allows a saline solution to leak through the concrete too swiftly (John D. and Wenzlick, P.E. 2007).

Over the past several decades, approximately 16 generic types of crack sealers and more than 450 concrete sealers have been used to seal larger cracks. The sealers were applied in an attempt to seal the surface and prevent or to slow down the penetration of water and chloride ions. Each sealer has specific properties to deal with specific problems. In order to verify the feasibility and performance of these sealers, various test procedures are performed.

6.2. Literature reviews

Chemical sealers, applied on the top of concrete surfaces, are employed by many states' Departments of Transportation (DOT) for waterproofing new and existing bridge decks which don't have membranes and asphalt overlays on them. Chemical sealers can be categorized as deck sealers and crack sealers, including silanes, HMWM, siloxanes, epoxy, methacrylate, and other potential sealer products. By comparing the test results on-site or in the laboratory for these sealers' penetration depth, bond strength, expected durability, ability to withstand freeze-thaw cycles, and resistance, we selected appropriate sealers in our research.

6.2.1. Crude tar and coal tar

Crude tar has been an important component of seal coating for the past 50 years (Heydorn, Allan. 2007). However, there have been problems with availability of crude tar in recent years which has resulted in shortages or delivery delays of coal tar sealer. This kind of availability problem plagued coal tar producers, sealer producers and sealer coating contractors in 2006 and earlier so the industry can only attempt to predict what may happen in the future.

Production of coal tar has decreased in the last decade due to strikes, plants closings and production cutbacks. In addition, most coal tar is sold to the aluminum industry, which is a growing market, further reducing the sealer coating market's share.

Sealer coating supply companies are reacting by distributing coal tar to their contractor customers on an as-needed basis, increasing production of asphalt-coal tar blends, and increasing production and marketing of asphalt-based sealers. There are few indications that supplies of coal tar will improve in

coming years. Therefore, although coal tar sealer has been the most popular pavement sealer in the past, limited availability is forcing contractors to explore alternative products.

Asphalt emulsion sealer is one of the asphalt-based sealers that have been used (Heydorn, Allan. 2007). It has been the primary alternative to coal tar for many years. However, these sealers perform very differently from coal tar sealers and currently there are no industry specifications for asphalt-based sealers.

Contractors and producers both generally consider asphalt-based sealers to be inferior to coal tar sealers in terms of durability, drying time, and consistency. Products that blend asphalt and coal tar are also available. The handling and use of these products is determined by which gradient dominates the blend. Blended sealers generally take longer to cure than either 100% asphalt or 100% coal tar products. Some producers refuse to make blended products because they feel that the two products are chemically incompatible.

A few producers are using ceramics with asphalt material to produce what could be a new and stronger pavement sealer. The sealer has the same characteristics of coal tar, but without its drawbacks. Set and cure times generally are quicker than coal tar, and the cost is comparable to that of asphalt sealers.

Due to budget constraints, the Arizona Department of Transportation (ADOT) sought an alternative to using asphalt for a roadway rehabilitation project in Yavapai County (James Information Media 2003). By mixing recycled asphalt pavement (RAP) with a polymer-modified asphalt surface sealer (PASS), the county found a RAP/PASS method that enabled them to find an inexpensive way to meet the ADOT's minimum stability requirements. Costs were further reduced by adding 6% more mixing water while increasing the mixing time. The correct moisture-to-emulsion ratio was maintained and the results of the procedure proved satisfactory.

6.2.2. HMWM

HMWMs are adhesives composed of methacrylate monomers (Meggers, D. A. 1998). Curable methacrylate adhesives were first developed in West Germany in the late 1960s. Curing of the methacrylate monomers is accomplished by adding an initiator and a promoter to create an oxidation–

reduction chain reaction. An intermediate free radical allows the monomer to build a high molecular weight polymer (Damico 1990).

The California Department of Transportation (Caltrans) began the use of HMWM resin for sealing cracks in bridge decks in 1981 (Krauss, 1985). Initially, the cracks to be treated in the bridges were very large. In October 1981, Caltrans treated the first bridge deck with a topical application through the use of squeeze bottles. HMWM resin was batch mixed and applied to each crack individually. The method successfully treated cracks as deep as 76 mm.

Caltrans had developed a specification and the application of the material that has been adopted in part, or whole, by a number of Departments of Transportation, including the Kansas Department of Transportation. Another example is the Mississippi River Bridge at Keokuk, Iowa that was completed and opened to traffic in November 1985 by the Iowa DOT. HMWM was applied to the bridge deck for the first time in October 1986. The Iowa DOT adopted the Caltrans specification, with some changes to reflect the Iowa climate. However, leakage occurring soon after the first application indicated that the cracks had not been sufficiently sealed, although the flow had been reduced. A second application of the material was done in November 1987. In June 1988, the leakage was further reduced by the second application (Marks, 1988).

Recently, HMWM has been frequently used as a crack sealer with millions of dollars spent annually on work involving methacrylate applications on some state-owned bridges (Rahim, Ashraf M. et al. 2007). In these states, a thorough review of previous research regarding the effectiveness of concrete bridge deck sealers has been done in conjunctions with a nationwide survey investigating sealer effectiveness. They have also reviewed practices for using methacrylate as a crack/surface sealer and developing guidelines concerning the use of HMWM along with other potential successful sealers.

HMWM sealers may be more effective in penetrating into the existing cracks in bridge decks due to their extremely low viscosity and low surface tension. A wide range of application temperature was reported in the literature. However, a range of application temperature between 45 and 85 degree F is

recommended. It is also recommended that HMWM sealer be applied every 4-5 years or as recommended by a bridge inspection team. For areas not subjected to deicing chemicals/a chloride-laden environment, the use of HMWM as a crack sealer can help restore the structural bond strength and the flexural strength of decks, but only for narrow and contaminant free cracks.

6.2.3. Epoxy/ Water-borne epoxy/ Polar-Epoxy / Solvent-based epoxy

Epoxies are adhesives based on a reaction between versatile biphenol A and epichlorohydrin (Meggers, D. A. 1998). Epoxy adhesives are perhaps the most versatile of structural adhesives. Various formulations can create epoxies with a wide range of physical properties (Behm and Gannon. 1990).

The New Jersey Highway Authority (Goldberger, 1961) used epoxy as a bridge deck sealer on several structures as early as 1959 and 1960. The initial application in 1959 was completed mostly by hand and was relatively expensive. After the application of the epoxy material, a layer of crushed emery was spread on the fresh epoxy to create a skid resistant surface. It should be noted that application rates and procedures developed in 1961 are very similar to those in use today.

There is minimal information available as to the effectiveness of the material used to seal the decks or the longevity of the treatment. However, it is stated that the Turnpike Authority intended to treat all other bridges on the Garden State Parkway. No information is readily available to determine if the applications were performed.

6.2.4. Linseed oil

In the past several years, some departments of transportations have experienced problems with excessive amounts of cracking on some concrete bridges. Various concrete sealer products are used to seal cracks. Between them, linseed oil became the concrete sealer listed in the standard specifications, and is used for scaling new bridge decks (John D. and Wenzlick, P.E. 2007).

6.2.5. Silanes and Siloxanes

Most of the concrete deck sealers in use are based on silicone technology primarily silanes and siloxanes. These materials are derivatives of silicone with molecules small enough to penetrate and bond

to the concrete, creating a hydrophobic layer in the treated region.

Since they are sealers and not membranes, they do not provide an impenetrable physical barrier, but rather reduce water inflow by inducing a chemical repulsion of the concrete to water (Aitken and Litvan 1989). Silanes and siloxanes are usually supplied as a solution or as a suspension in a solvent.

6.2.6. Potential sealer products

The North and South Grand Island Bridges, near Niagara Falls, New York, are in the process of receiving much-needed facelifts. The coating system for the North Grand Island Bridges project, the first of the Grand Island bridges to be tackled, features Zinc Clad IV, is an organic two-component polyamide epoxy zinc-rich coating (Scranton Gillette Communications 1998).

Its low VOC level and wide curing temperature range of 40 to 120 degree F at an 85% relative humidity combined with 85% zinc dust pigment in its dried film has made zinc clad IV ideal for this type of application.

In addition, Zinc Clad IV has exhibited years of proven corrosion resistance on other similar structures. The zinc-based coating was a top coating with low-viscosity Macropoxy 920 PrePrime that penetrated hard-to-reach areas of the structural steel, such as crevices and tight corners.

Epoxy Mastic Aluminum II was applied next. The high–build mastic is ideal for added corrosion resistance and provides additional film build. In late October 1997, Polar-Epoxy, an epoxy amine adduct mastic coating capable of recoating in 24 to 36 hours at temperatures as low as 20 degree F, was substituted for the epoxy mastic.

The final coat, Corothane II Polyurethane Gloss, is a two-component, VOC-component, aliphatic acrylic-modified polyurethane. In addition to color and gloss retention, it also provided exceptional abrasion and salt spray resistance. The project was completed in the summer of 1999.

6.2.7. Others

Some other sealer products are also used commercially or still in the process of laboratory test, such as,

(1) Lithium hydroxide (Krauss, Paul. Et al. 2006),

(2) Methacrylate (Krauss, Paul. Et al. 2006),

(3) Methyl Methacrylate (Chang, L.M. 1992),

(4) Asphalt/rock composite material (Bose, A. and Li, W. 2002),

(5) Styrene acrylic-modified cementitious coating (Technology Publishing Company and Steel Structures Painting Council 2000),

(6) Aliphatic acrylic-modified polyurethane (Scranton Gillette Communications 1998),

(7) Urethane (Transportation Research Record 1995),

(8) Aluminum (Curra, W. 1990),

(9) Acrylics (Damico, Dennis J. 1990),

6.2.8. Additives

Additives are often added to sealers to enhance the performance properties of the sealers in terms of better flexibility, toughness, fuel and chemical resistance and overall longevity (Dubey, G. 2002). Specifications that delineate the proper ratios of various components, including additives in the mix design are important for the optimum performance of seal coats. The article provides an overall review of the polymeric, latex and rubber additives that can be used in seal coats to accomplish the following: thickening, fast drying, uniform dry color, sand/ aggregate suspension and performance improvement.

6.3. Experimental setup

CDOT has identified structure E-17-QM as the bridge to be used for the field evaluation. This bridge was built in 1998 and is located on a busy highway; part of the interchange of U.S. 36, I-270, and I-25. The structure consists of two traffic lanes and one shoulder lane which goes to the ramp of South I-270. It is 841 feet long with 6.6-foot-deep steel box girders. Access inside the box girders can be achieved by walking up the paved slope and entering through a hatch. Figure 6.1 is the bird's eye view of the testing section on E-17-QM. Figures 6.2 through 6.4 show the structure of this bridge.

Figure 6.1 Bird's eye view on Bridge E-17-QM

Figure 6.2 Side view of this bridge structure

Figure 6.3 Two traffic and one shoulder lanes of the bridge

Figure 6.4 A hatch beneath the bridge for passing through

Based on the previously mentioned literature review, four sealers were chosen as follows:

(1) HMWM: Sika Pronto 19- HMWM (2 component)

(2) Epoxy 1: Super low viscosity, low modulus epoxy

(3) Epoxy 2: Low Viscosity, high modulus epoxy

(4) Silanes : Tamms Baracade 244-Silane Sealer

Before spreading sealer products on bridge decks, the deck condition assessment must be made. First, we inspect the concrete substrate and pay attention to the presence of contaminants at the location of surface cracks. For surface preparation, in general, we follow the manufacturer's recommendations. In

our case, the decks were washed and power swept to remove all dirt, sand, clay and other debris prior to applying sealer (Figure 6.5). We mixed several chemical solutions to form the sealer products and spread those on deck surfaces. Meanwhile, extremely fine sand was spread on the surface. Figures 6.6 - 6.8 show the detail of the process of applying sealers.

Figure 6.5 Smooth the surface

Figure 6.6 Mix chemical solutions

Figure 6.7 Sealer application

Figure 6.8 Spread extremely fine sands

For the location of applying sealer products, we divided the longitudinal direction of one traffic lane into five areas. Areas 1-4 are sealed with the sealer products above and area 5, which has no sealer, is used to compare the performance with the other four. The location of sealer application is shown as Figure 6.9.

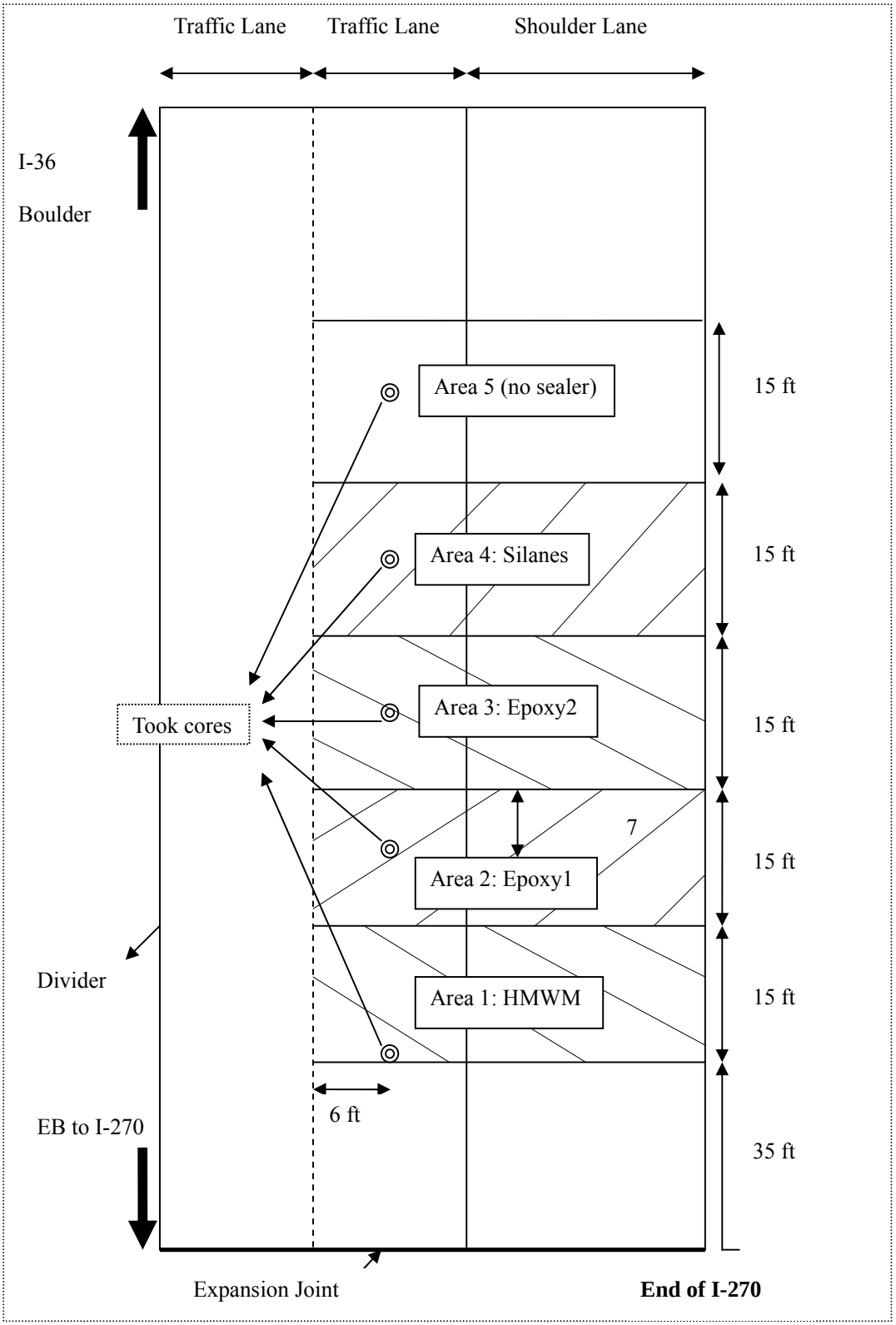

Figure 6.9 Application of sealer products

After spreading sealer products on the surface of bridge decks, skid resistance measurements were taken right after the sealer application and one year later. The chloride concentration test was performed in the lab every six months. For moisture and temperature, integrated sensors were installed at different depths of the bridge decks so that the vertical distributions of both internal moisture content and temperature could be obtained.

Based on the four above parameters, we can compare and rank their performance. More details about the four parameters are discussed below.

6.3.1. Skid resistance

6.3.1.1. Background

Worldwide, more than one million people are killed yearly due to traffic accidents. There are about 42,000 fatalities on the road in the US each year. Although a high percentage of these accidents are due to driver error, conditions of highways have a significant effect. In regards to traffic accident rates, the most important factor in highways' conditions is skid resistance. Hence, accidents due to pavement skid resistance deficiencies are a major concern for the highway construction industries and governments.

Actually, skid resistance is a technical term for the cumulative effects of snow, ice, water, loose material and the road surface on the traction produced by the wheels of a vehicle. Road slipperiness can be measured either in terms of the friction between a freely-spinning wheel and the ground or vehicle braking distance and is related to the coefficient of friction between the tire and the road.

Skid resistance is developed when vehicle tires are fully or partially prevented from rolling under lubricated conditions and start to slide along a pavement surface. The roughness of a pavement surface is correlated to its serviceability. In this research, skid resistance is one of the four parameters we use to evaluate sealers' performance on bridge decks. Measurements were taken when sealers were initially applied and one year later.

6.3.1.2. Test apparatus and test methods

The test apparatus and corresponding standards are shown below,

(1) Yaw Mode Method (Mu-meter)

(2) Stopping Distance Method: ASTM E445 (Locking 4 wheels) and E303 (Locking diagonal wheels)

(3) Slip Mode Method (Swedish Road Research Skid meter)

(4) Portable Field Tester – ASTM E303 British Pendulum

(5) Locked-wheel trailer– ASTM E 274-97

6.3.1.3. British pendulum tester

We selected the British Pendulum Tester (BPT) from the four previously mentioned tests. The BPT is a stationary type of skid testers. It comprised a support frame that can be leveled on the road. Attached to the support frame is a swinging arm, at the bottom of which is a spring loaded ASTM rubber measuring foot. This swinging arm, when released from a fixed point, sweeps across the surface underneath. From that position, the pendulum contains potential energy. When released, the potential energy is converted to kinetic energy that is dissipated by friction on the rubber shoe, which slides over the surface. The skid resistance of the surface determines how far the arm swings up on the follow-through. The arm also moves a measuring that gives a value on the attached scale. Figure 6.10 shows the BPT being used on this research.

Figure 6.10 British Pendulum Tester

In this research, we use a BPT to take measurements when sealers were initially applied and one year later. The purpose of the first measurement is to tell us which sealer product can provide the best skid resistance and whether or not all the sealer products have better skid resistance than the area without sealer immediately after applying sealer. From the second measurement, we can gather skid resistance measurements on sealed areas after one year traffic loading.

6.3.1.4. IRI and PSR rating

The pavement condition ratings are derived from one of two measurements;

(1) International Roughness Index (IRI)

(2) Present Serviceability Rating (PSR)

Between them, IRI measures the cumulative deviation from a smooth surface in inches per mile and PSR is a subjective rating system based on a scale of 0 to 5. Lower IRI values represent a smoother road condition. Table 6.1 contains a description of qualitative pavement condition terms and corresponding quantitative PSR and IRI values. The translation between PSR and IRI is not exact; IRI values are based on objective measurements of pavement roughness, while PSR is a subjective evaluation of a broader range of pavement characteristics.

Table 6.1 Pavement conditions (RSR and IRI)

	IRI Rating	PSR Rating
Good	<95	≥3.5
Acceptable	≤170	≥2.5
Not Acceptable	>170	<2.5

For example, a given paved section of interstate could have an IRI rating of 165, but might be rated a 2.4 on the PSR scale. Such a section would be rated as acceptable based on its IRI rating, but would not have been rated as acceptable had PSR been used. Thus, the mileage of any given pavement condition category may differ depending on the rating methodology.

In our research, the IRI is chosen to use for our adjustment of the extent of bridge decks' skid resistance. The skid resistance test is shown as Figure 6.11.

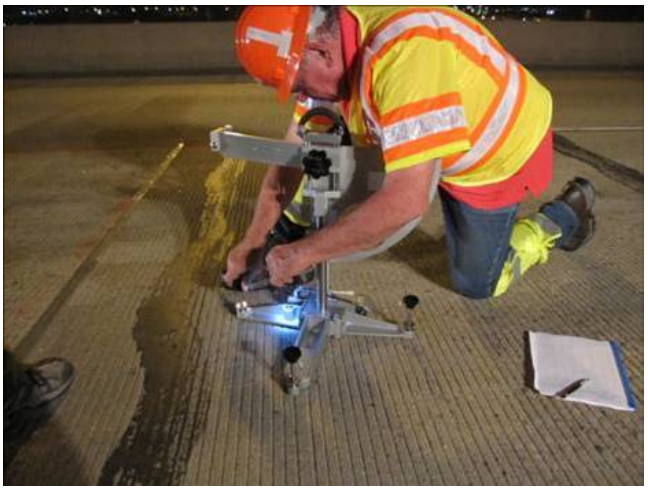

Figure 6.11 Conduction of skid resistance test

6.3.2. Integrated sensor and data acquisition system

6.3.2.1. Integrated sensor

One integrated relative humidity and temperature sensor (SHT7X) was used in this research. The SHT7X is a single chip that measures relative humidity and temperature in a multi-sensor module with a calibrated digital output. For the five divided areas, we installed sensors at different depth alternating between 3 and 4 sensors for each area. Our objective was to obtain the vertical profiles for moisture and temperature inside concrete decks. We alternated sensors as follows: area 1 (HMWM), area 2 (epoxy 1), area 3 (epoxy 2), area 4 (Silanes), and area 5 (no sealer) respectively. All sensor installation was done through the confined space (steel box girder) beneath the bridge decks as we drilled upwards into decks (Figure 6.12).

The total depth of the bridge decks is 9.5 in and the written numbers next to sensors in Figure 6.12 represent the drilling distances. However, the varied values of inner moisture and temperature are mainly caused by environmental issues from above the bridge decks. All comparisons and analysis of those readings are based on the distance from the deck surface to the location of the sensors. For example, in

Figure 6.12, the third number from the left, 6.5 in, should be treated as 3 in from surface.

Figure 6.12 Sensor installations

6.3.2.2. Data logger

The data logger (EK-H3)/evaluation kit with the SHT7X, allow for applying 20 sensors to be simultaneously reading relative humidity, temperature and calculated dew point. In this research, we connected 18 sensors from five areas to the datalogger and then took readings with software from a computer. The setup is shown in Figure 6.13 and Figure 6.14.

Figure 6.13 Setup (1)

Figure 6.14 Setup (2)

In this research, we use the setup above to take monthly readings for one year. Based on these readings, we analyzed each chemical sealer's ability to slow down the diffusion of moisture inside concrete and we measured temperature variation to compare the effect of different sealers.

6.3.3. Chloride concentration experiments

Chloride concentration in concrete is important because the main function of the chemical sealers is to block the penetration of chloride ions. Through the research, we took concrete cores from bridge decks for four times as detailed in Table 6.2. The first measurement was taken six months before spreading sealer products on the deck surfaces and so the chloride profiles from areas 1 through 4 are supposed to be the same. The date for the second measurement was taken promptly after we applied sealer products. The third and fourth measurements represent the 6-month mark and one year after the initial application of sealers.

Table 6.2 Dates of taking concrete cores

	Date	Take core number	Deck surface condition
1	11/04/2009	4	No sealer
2	05/26/2010	5	Right after sealer application
3	11/06/2010	5	Six months after sealer application
4	05/04/2010	5	One year after sealer application

Each time the above measurements were taken, concrete cores (4 in. in diameter) were taken from test locations (Figure 6.9) to determine chloride content at an interval of 0.25 in below the surface following ASTM C1218M-99. Figure 6.15 shows the process of taking cores from bridge decks.

Figure 6.15 Taking cores from bridge decks

6.4. Skid resistance measurements

6.4.1. Test results

The skid resistance tests were preformed on 05/04/2010 and 06/02/2011 with the British Pendulum Tester (PFTS). Some details about the measurements were recorded below and the test results are shown in Tables 6.3-6.4. Details for the first test:

(1) Tested dry (no rain, no water).

(2) Sections 1 and 2 were very oily.

(3) Section 2 was not completely set, but the PFTS didn't move the sealers.

(4) All tests were done in the area of the right wheel path.

(5) The changing lane width made the wheel path very vague and not well defined.

(6) Tests done with the pendulum traveling in the direction of traffic.

Table 6.3 Skid resistance (measurement 1)

06/02/2010 (same time to apply sealers)	Average
Area 1 (HMWM)	86.35
Area 2 (Epoxy 1)	57.4
Area 3 (Epoxy 2)	96.1
Area 4 (Silanes)	96.15
Area 5 (No sealer)	100.7

Details for the second test:

(1) Tested with water.

(2) All tests were done in the area of the right wheel path.

(3) The changing lane width made the wheel path very vague and not well defined.

(4) Tests done with the pendulum traveling in the direction of traffic.

Table 6.4 Skid resistance (measurement 2)

05/04/2011	Readings					Average
Area 1 (HMWM)/1	72	70	71	70	70	73.9
/2	78	77	77	77	77	
Area 2 (Epoxy 1)/1	60	59	59	58	57	61.2
/2	63	64	64	64	64	
Area 3 (Epoxy 2)/1	90	89	89	89	89	82.9
/2	78	77	76	76	76	
Area 4 (Silanes) /1	92	92	93	93	94	91.2
/2	88	89	90	90	91	
Area 5 (No sealer) /1	89	88	88	88	88	88
/2	87	88	88	88	88	

6.4.2. Analysis

According to the test results above and the pavement conditions in terms of IRI values in Table 6.1, the ranking of these four sealer products right after application and after one year's usage are shown in as Table 6.5 and Table 6.6.

Table 6.5 Rankings of skid resistance (measurement 1)

Sealer	Epoxy1	HMWM	Epoxy2	Silanes	No sealer
Number	57.4	86.35	96.1	96.15	100.07
Ranking	1	2	3	4	5

Table 6.6 Rankings of skid resistance (measurement 2)

Sealer	Epoxy1	HMWM	Epoxy2	No sealer	Silanes
Number	61.2	73.9	82.9	88	91.2
Ranking	1	2	3	4	5

From the ranking, we can make comments below:

(1) Sealer products did improve skid resistance and provide safer transportation condition.

(2) The ranking right after application and after one year's usage are consistent, the only changes occurred in areas with Silanes and without sealer.

(3) Epoxy 1 and HMWM are apparently much better than the other three sealers.

(4) Comparing Epoxy 1 and Epoxy 2, Epoxy 1 has a super low viscosity and low modulus epoxy. Epoxy 2 has a low viscosity and high modulus epoxy formulation. The first one has an obvious advantage in regards to transportation safety concern.

6.5. Temperature readings

From the eighteen installed sensors, we got monthly readings for internal temperature and moisture. Between them, temperature has less effect than moisture on rebar corrosion. For temperature readings, we did the comparisons in four ways:

(1) Comparisons between daytime and night time.

(2) Comparisons for hourly readings in five areas.

(3) Comparisons of different sealer area at the same depth.

(4) Comparisons for bimonthly readings.

6.5.1. Comparisons between daytime and night time

The trend in all five areas between daytime and night time is consistent. The temperature decreases during the day time and increases at the night time. Figures 6.16 through 6.20 show the trend for sealed and unsealed areas. The only difference between them is the temperature variation near the

surface. At the depth of 1.5 in has 5 to 8 degree C difference at sealed areas and just has 2 degree C difference at unsealed area. The sealer products slow down the temperature diffusion, but it is limited near the surface. At deeper locations, such as 3 and 6 inches, there is no significant temperature difference among these five areas.

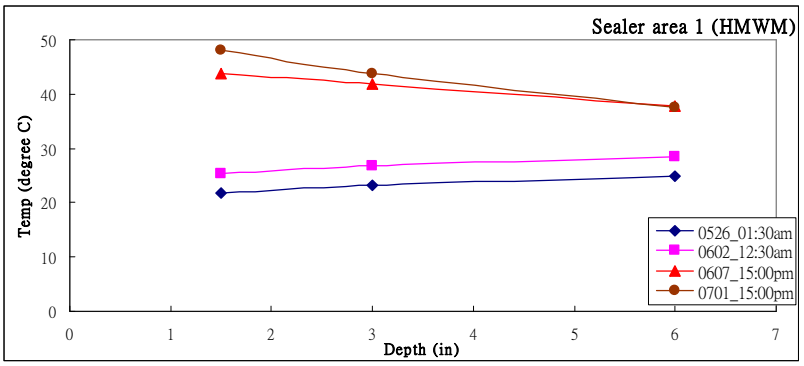

Figure 6.16 Comparisons (daytime and night time (HMWM))

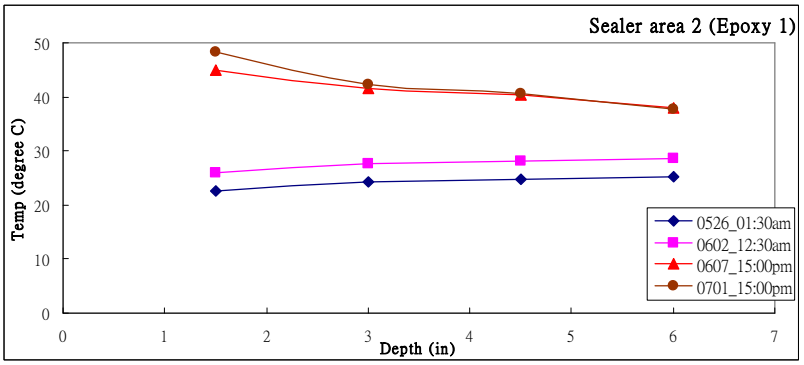

Figure 6.17 Comparisons (daytime and night time (Epoxy 1))

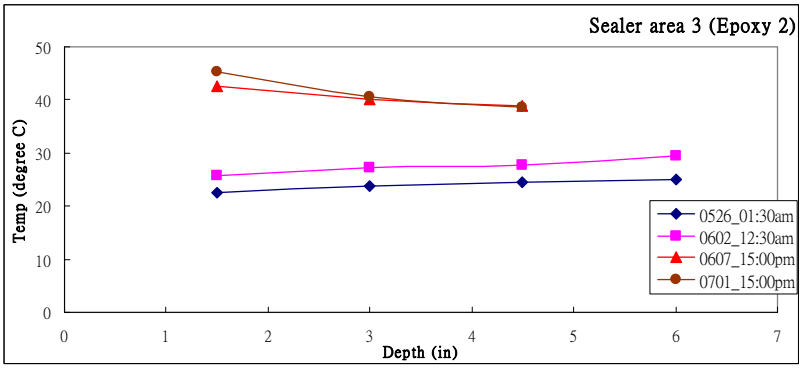

Figure 6.18 Comparisons (daytime and night time (Epoxy 2))

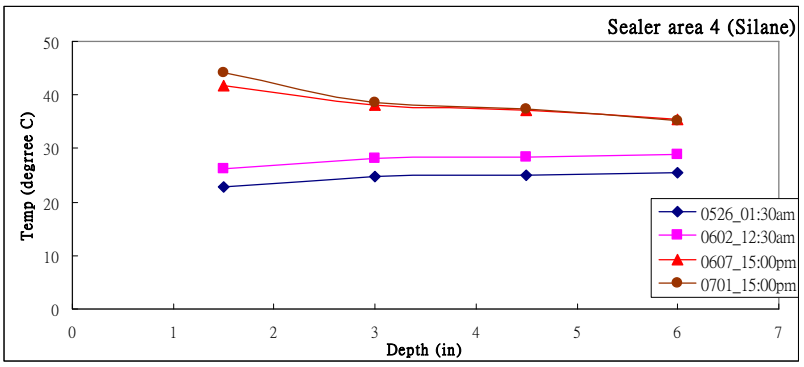

Figure 6.19 Comparisons (daytime and night time (Silanes))

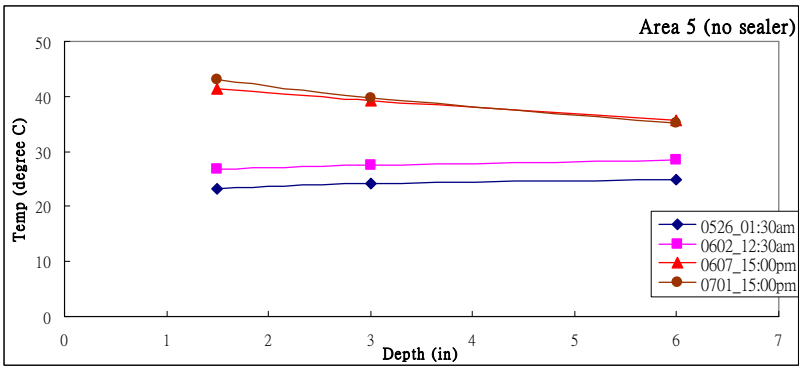

Figure 6.20 Comparisons (daytime and night time (no sealer))

6.5.2. Comparisons for hourly readings in five areas

Figure 6.21-6.25 show hourly readings for these five areas. Please see some comments below:

(1) 08:30am-16:30pm, temperature distribution is: 1.5in>3in>4.5in>6in

(2) 16:30pm-08:30am, temperature distribution is: 6in>4.5in>3in>1.5in

(3) The difference at day time (8 degree C) is higher than during the night (3 degree C)

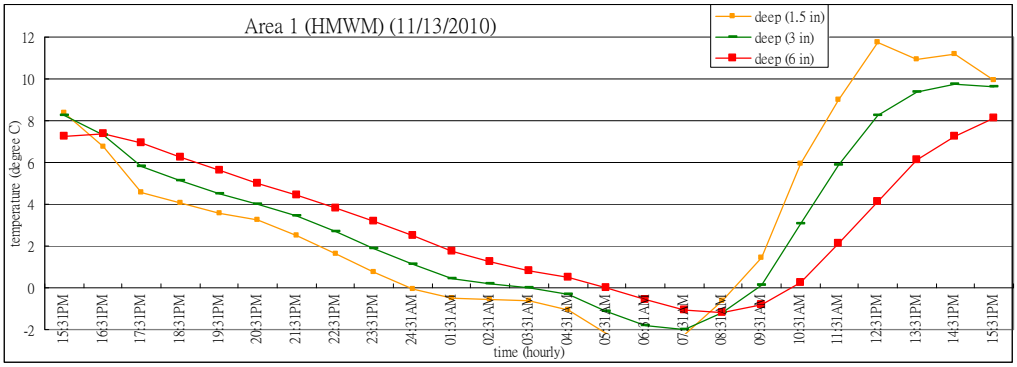

Figure 6.21 Comparisons (hourly readings (HMWM))

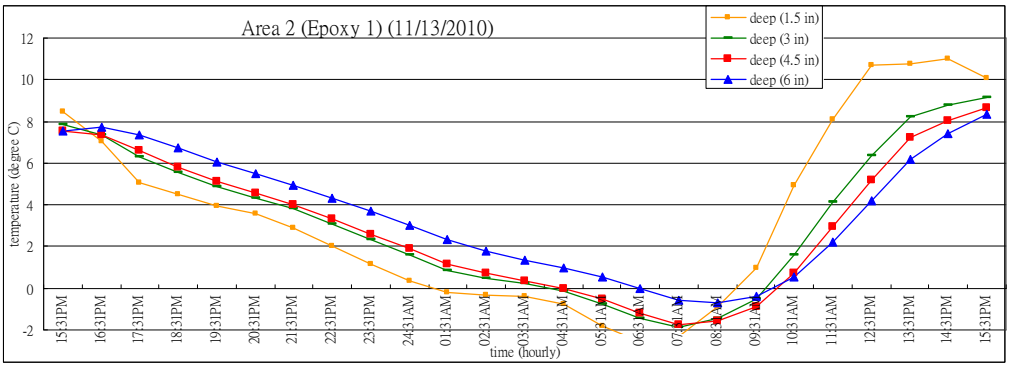

Figure 6.22 Comparisons (hourly readings (Epoxy 1))

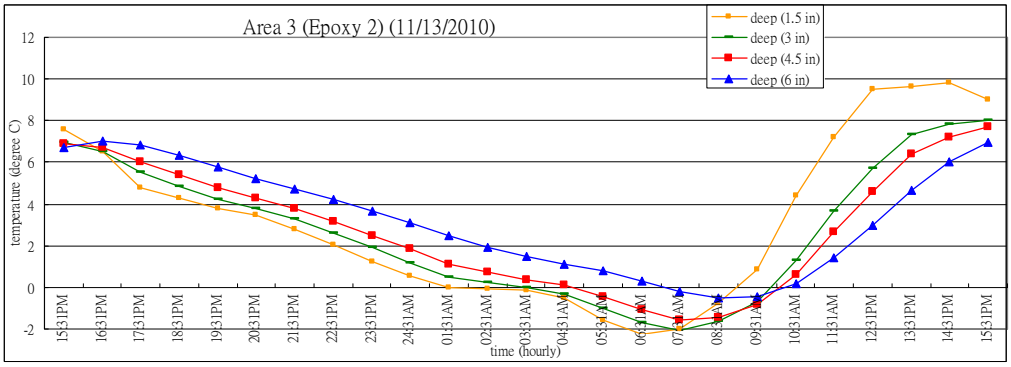

Figure 6.23 Comparisons (hourly readings (Epoxy 2))

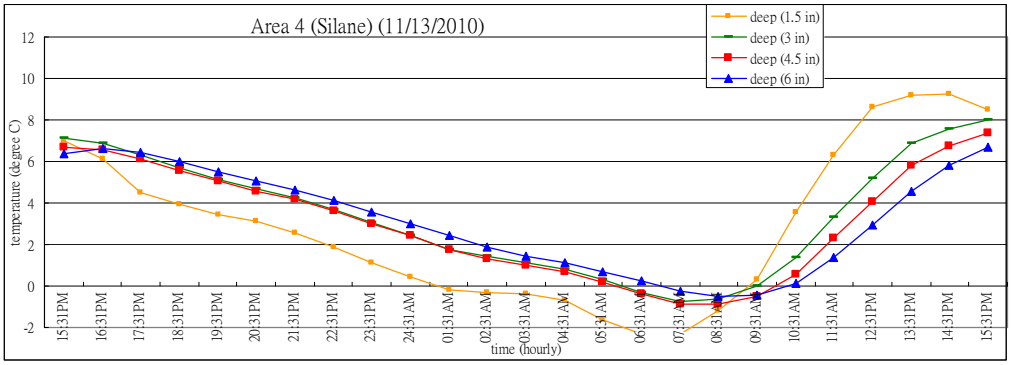

Figure 6.24 Comparisons (hourly readings (Silanes))

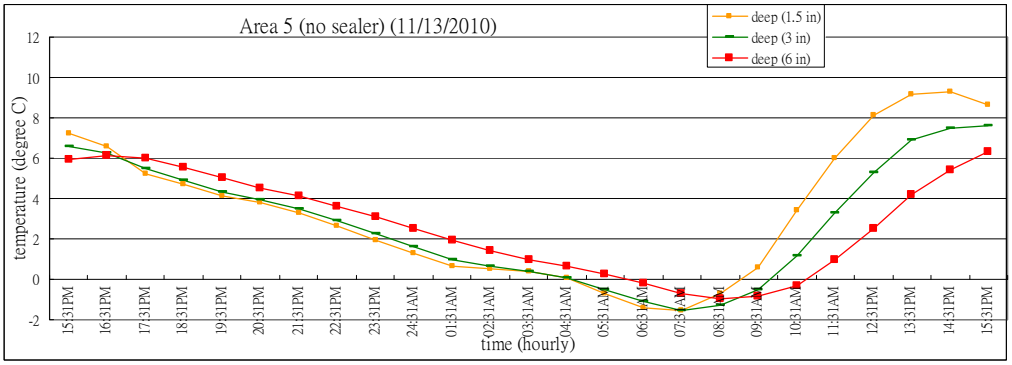

Figure 6.25 Comparisons (hourly readings (no sealer))

6.5.3. Comparisons of different sealer area at same depth

Figures 6.26-6.29 show hourly readings for these five areas. Please see some comments below:

(1) Day time: 1(HMWM)>2(Epoxy1)>3(Epoxy2)>4(Silane)>5(no sealer).

(2) Nighttime: no big difference.

(3) Near the location of rebar location (3 in): area 4(Silane) has the highest reading at night.

(4) Near the location of rebar location (3 in): area 1(HMWM) has the highest reading during the day.

(5) Near the surface and rebar locations, area 5 (no sealer) is the lowest during the day.

(6) Near the surface and rebar locations, area 5 (no sealer) is in the middle of the data for nighttime.

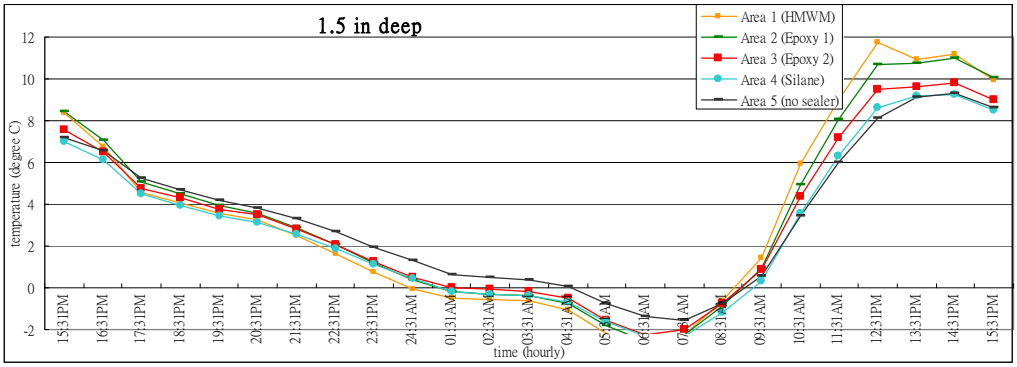

Figure 6.26 Comparisons (different sealer area (1.5 in))

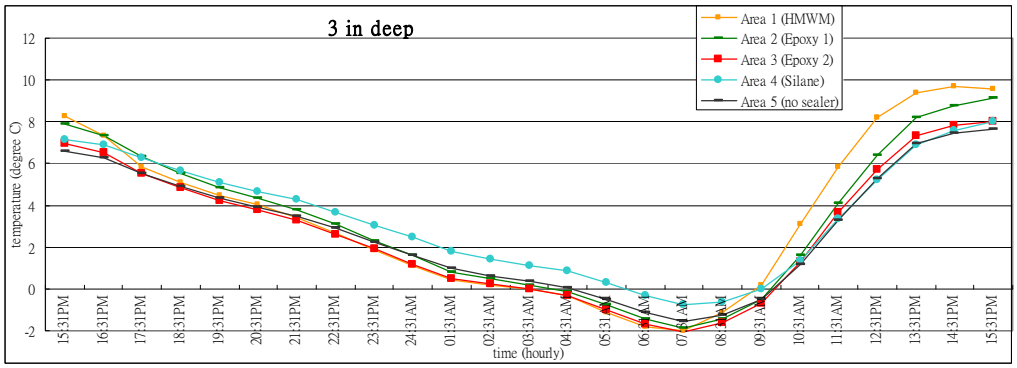

Figure 6.27 Comparisons (different sealer area (3 in))

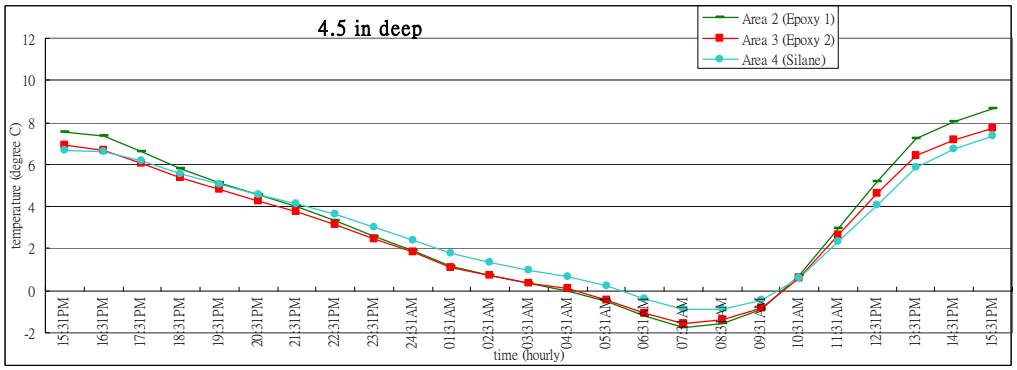

Figure 6.28 Comparisons (different sealer area (4.5 in))

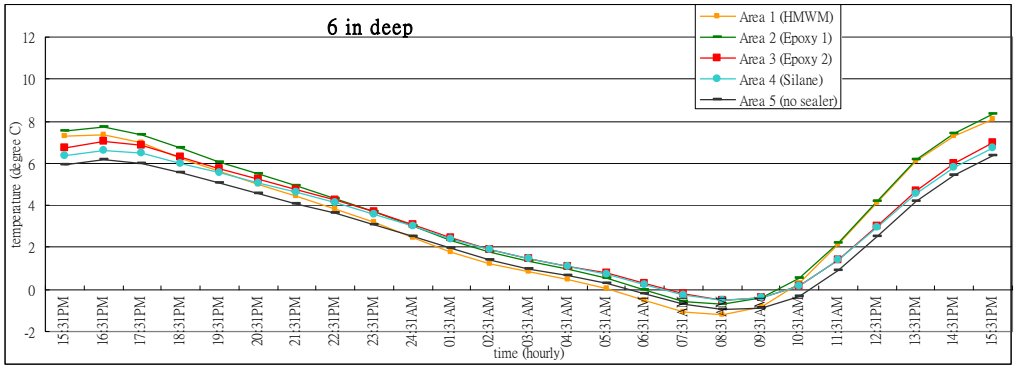

Figure 6.29 Comparisons (different sealer area (6 in))

6.5.4. Comparisons of bimonthly readings

Figures 6.30-6.34 show bimonthly readings for the five areas, but we could not figure out the difference from those. In Figure 6.35, we rearrange the readings and have comments below:

(1) The highest and lowest temperatures are in July and February.

(2) Near the rebar, temperature varies among 3 to 40 degree C.

(3) Temperature varied the most in area 2 (Epoxy 1).

(4) In summer: Silanes < no sealer < Epoxy2 << HMWM < Epoxy1.

(5) In winter: no sealer < Silanes < Epoxy1 < Epoxy2 <<HMWM.

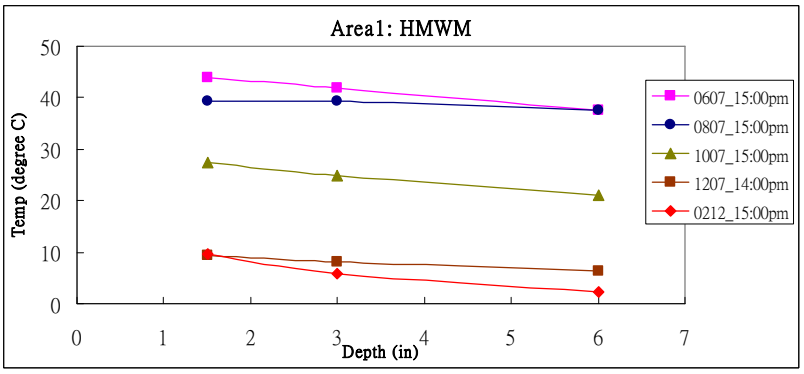

Figure 6.30 Comparisons (bimonthly readings (HMWM))

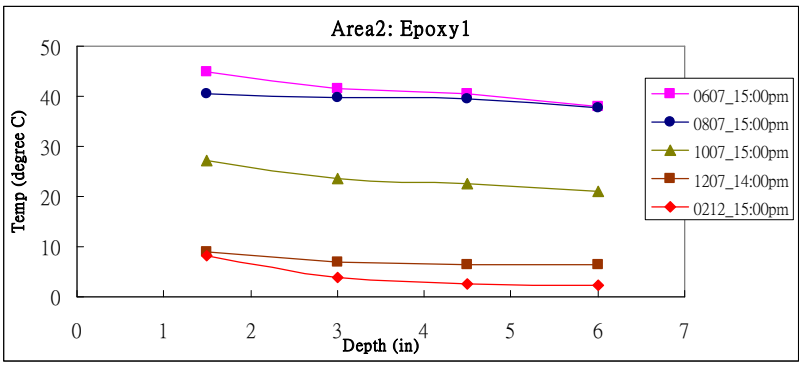

Figure 6.31 Comparisons (bimonthly readings (Epoxy 1))

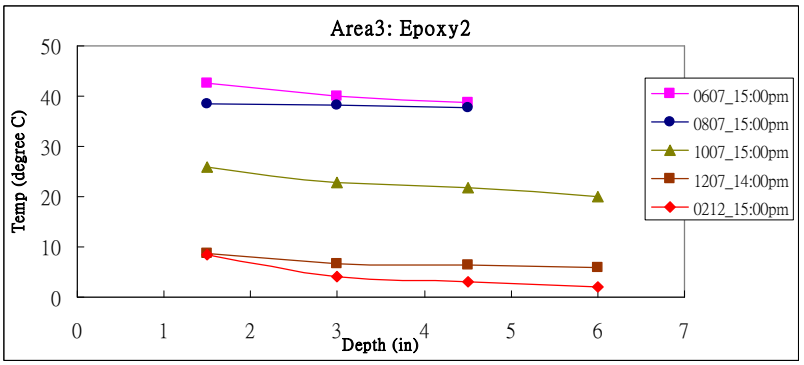

Figure 6.32 Comparisons (bimonthly readings (Epoxy 2))

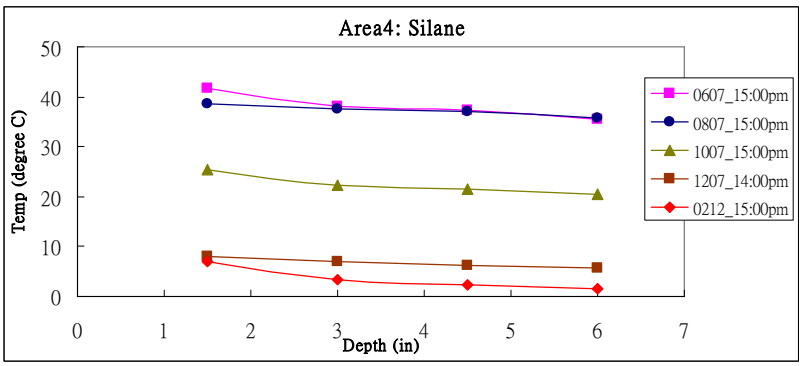

Figure 6.33 Comparisons (bimonthly readings (Silanes))

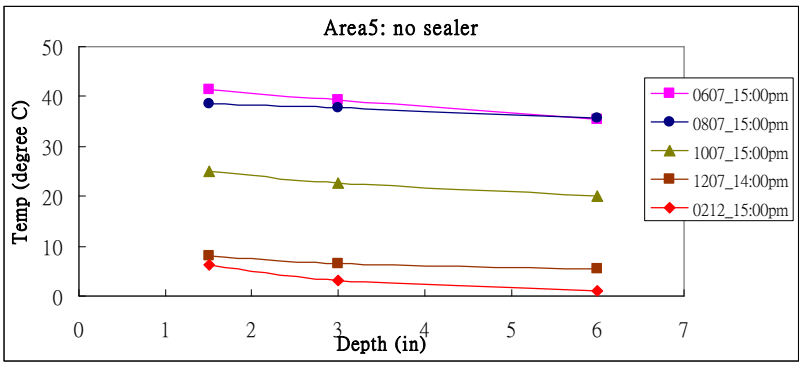

Figure 6.34 Comparisons (bimonthly readings (no sealer))

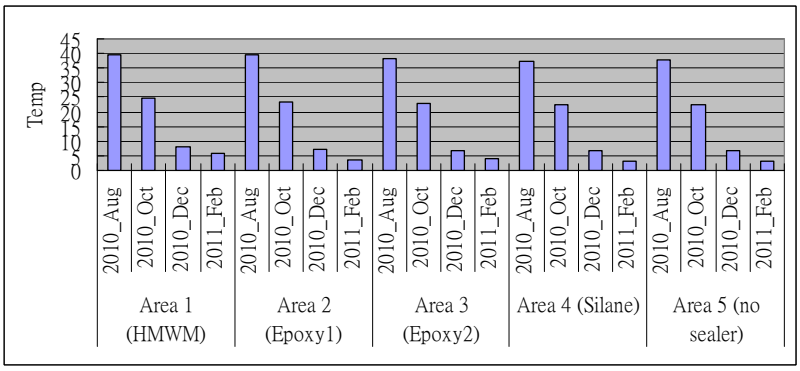

Figure 6.35 Comparison (bimonthly readings)

6.6. Moisture readings

In rebar's corrosion mechanism, internal moisture near rebar location plays a more important role than temperature. Higher internal moisture content might lead to more serious corrosion or even shorten the corrosion initiation time. For moisture readings, we compared them in four ways:

(1) Water repellent capability after rains.

(2) Comparisons of bimonthly readings.

(3) Comparisons of different sealer areas at the same time.

(4) Comparisons at the rebar location.

6.6.1 Water repellent capability after rains

The moisture mostly comes from the surrounding environment issues, such as rain. Therefore, we first observe the water repellent capability of the sealer after rain for the five areas. In Figures 6.36-6.40,

the sealer products were spread on the top surface before 05/27/2010. The readings for all five areas are supposed to be the same. It rained between 05/27/2010 and 06/02/2010, so the relative humidity (RH) values jump sharply during this period. There was no raining from 06/02/2010 to 06/07/2010, so the internal moisture content inside concrete decks diffused to deeper locations. Meanwhile, because there was no new rain coming from outside, the higher RH inside concrete implies that moisture content moves toward the outside environment. In regards to Figures 6.36-6.40, there are some comments below:

(1) Without sealer, decreased RH is not significant. That corresponds to real situation.

(2) Near surface, area 2 (epoxy 1), 3 (epoxy 2), and 4 (silane) work well.

(3) Two epoxies and silanes show better water repellent capabilities than HMWM's near surface.

(4) Area 1(HMWM) and 4 (silane) show better performance than sealer 2 (epoxy 1) and 3 (epoxy 2) in a deeper location.

(5) HMWM gradually dissipates moisture content along the profile.

(6) Epoxy shows better water repellant capability near surface.

(7) Silanes works better near the surface and worse at deeper locations.

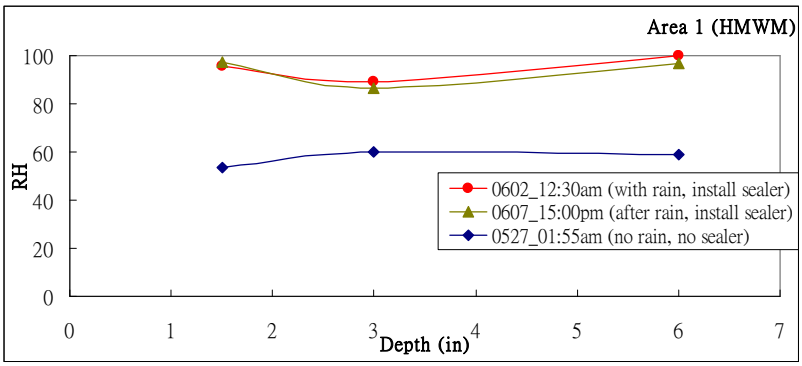

Figure 6.36 Water repellent capabilities after rains (HMWM)

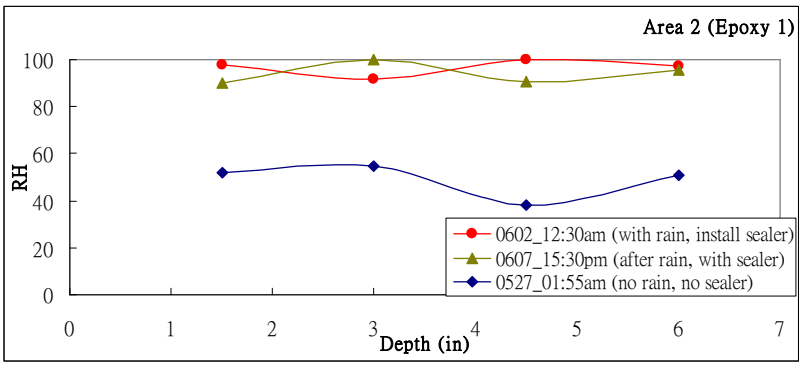

Figure 6.37 Water repellent capabilities after rains (Epoxy 1)

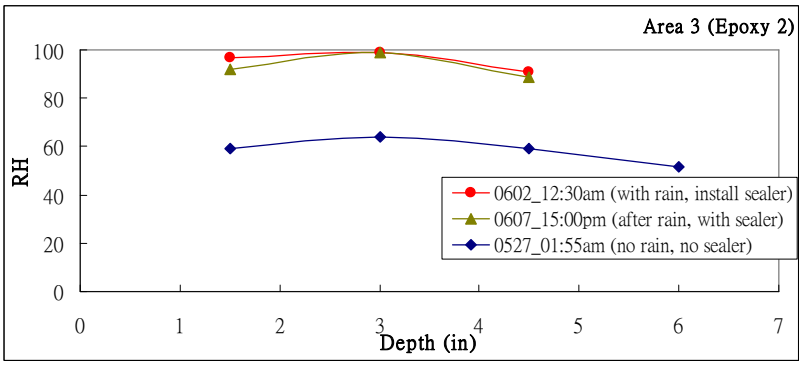

Figure 6.38 Water repellent capabilities after rains (Epoxy 2)

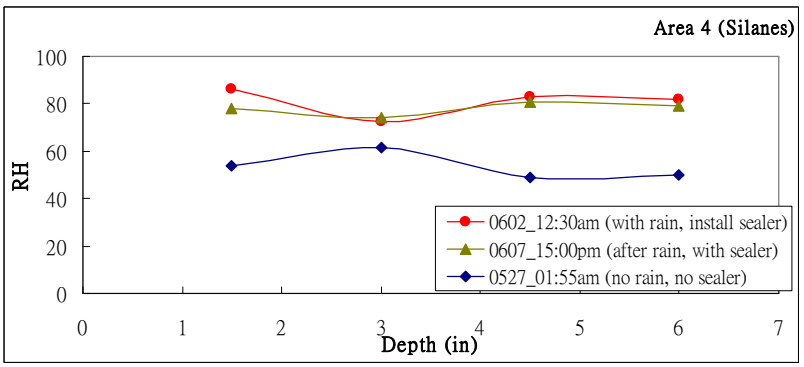

Figure 6.39 Water repellent capabilities after rains (Silanes)

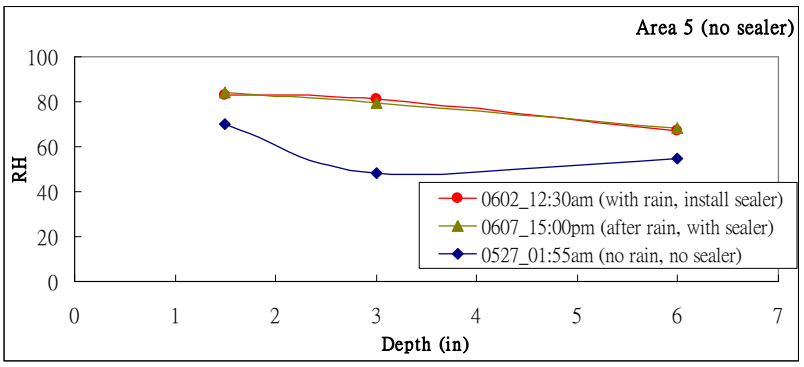

Figure 6.40 Water repellent capabilities after rains (no sealer)

6.6.2 Comparisons for bimonthly readings

Also for Figures 6.41-6.45, see comments below:

(1) In a deeper location, area3 (Epoxy 2) and area4 (Silane) are the least effective.

(2) At 4.5 in, RH in the silane area jumps to 72.

(3) At 4.5 in, the Epoxy 2 area is as low as 65.

(4) Area 4 (Silanes) shows relatively low RH in June (below 80).

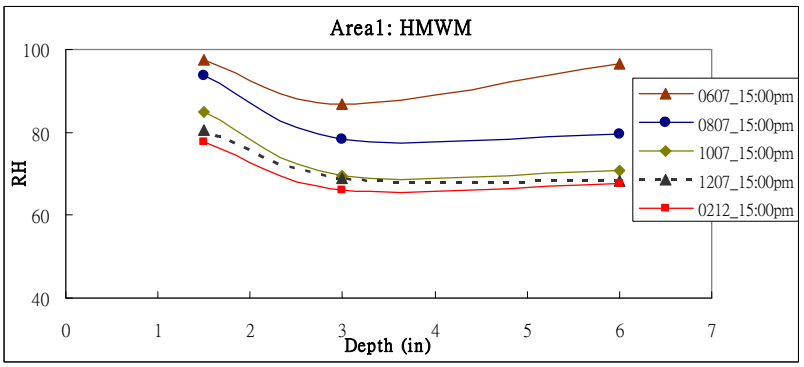

Figure 6.41 Comparisons (bimonthly readings (HMWM))

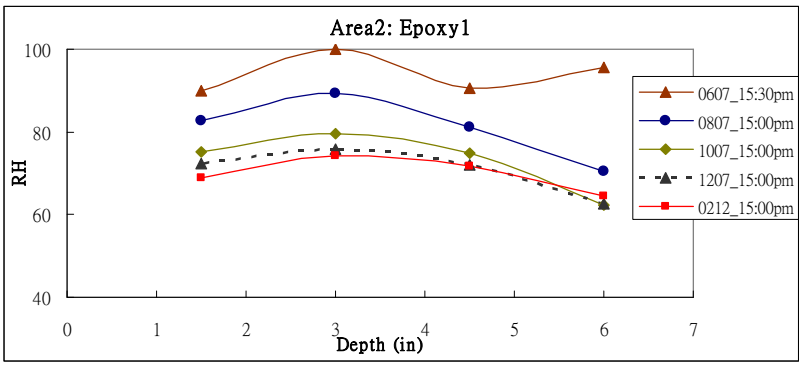

Figure 6.42 Comparisons (bimonthly readings (Epoxy 1))

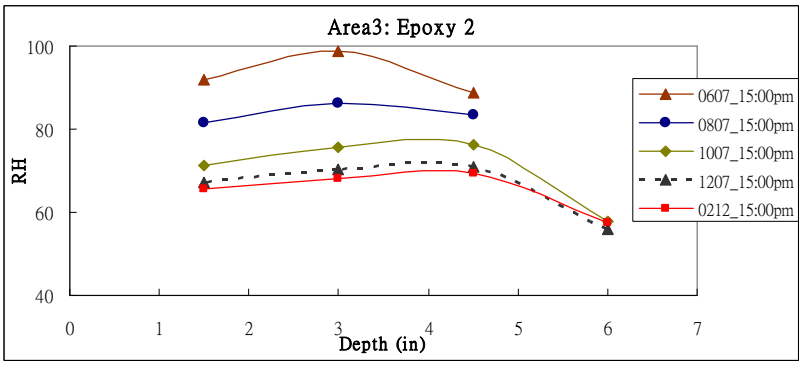

Figure 6.43 Comparisons (bimonthly readings (Epoxy 2))

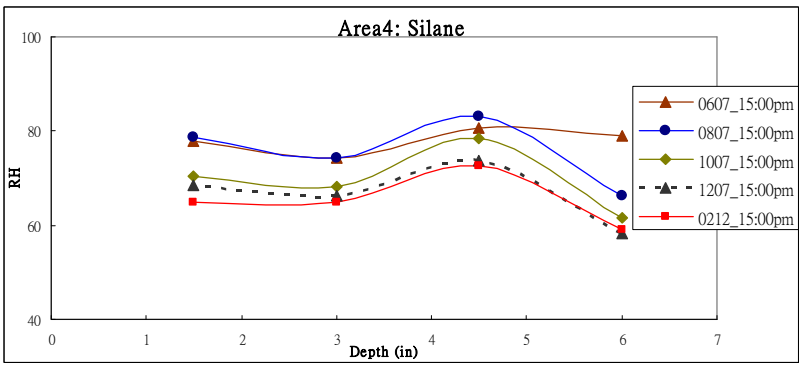

Figure 6.44 Comparisons (bimonthly readings (Silanes))

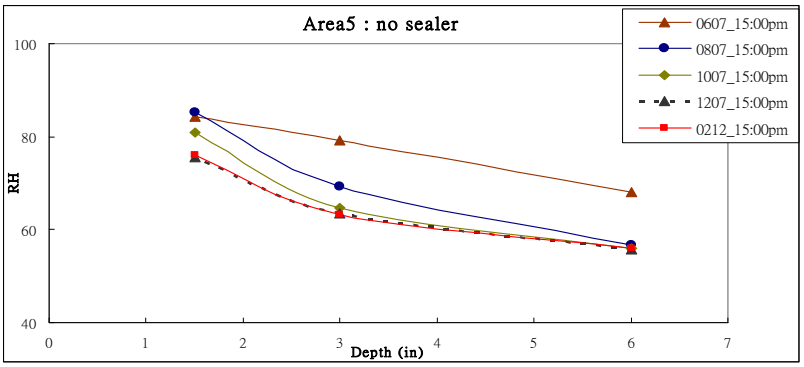

Figure 6.45 Comparisons (bimonthly readings (no sealer))

6.6.3 Comparisons of different sealer area at same time

From Figures 6.46-6.49, see comments below:

(1) Near the surface, the RH value at area 1(HMWM) is higher than other four.

(2) Along the profile, HMWM shows higher RH than the other three.

(3) Near the surface, areas 2-4 show lower RH (62-70) than area 5 (78).

(4) Near the rebar, areas 2-4 show higher RH (65-75) than area 5 (63).

(5) The applications of sealer products (epoxy 1, 2, silanes) have lower RH near the surface, but have higher RH near rebar and at deeper locations.

(6) The original trend has changed (slowly decreasing along whole profiles).

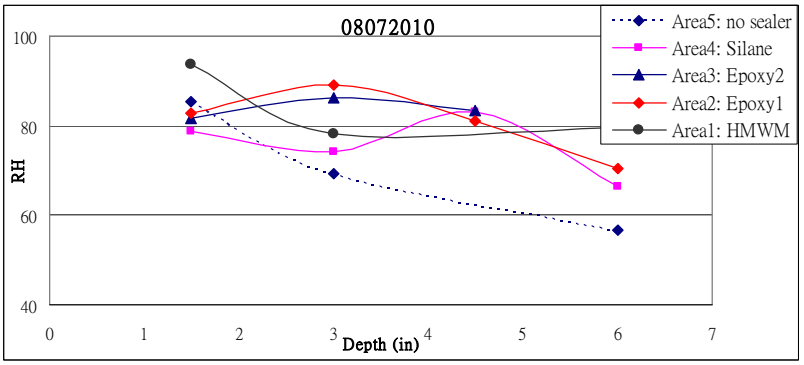

Figure 6.46 Comparisons (different sealer area (08/07/2010))

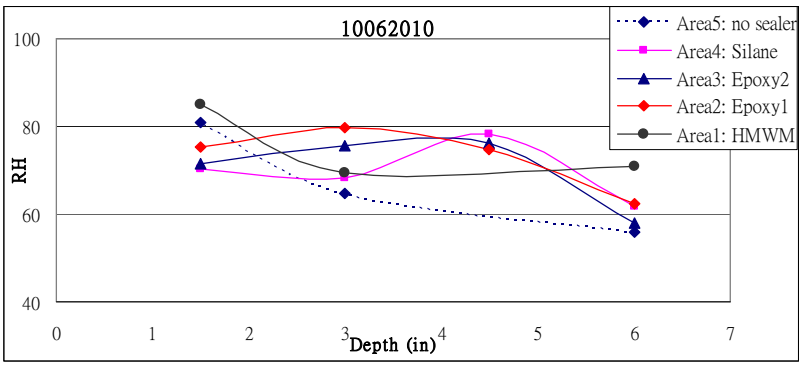

Figure 6.47 Comparisons (different sealer area (10/06/2010))

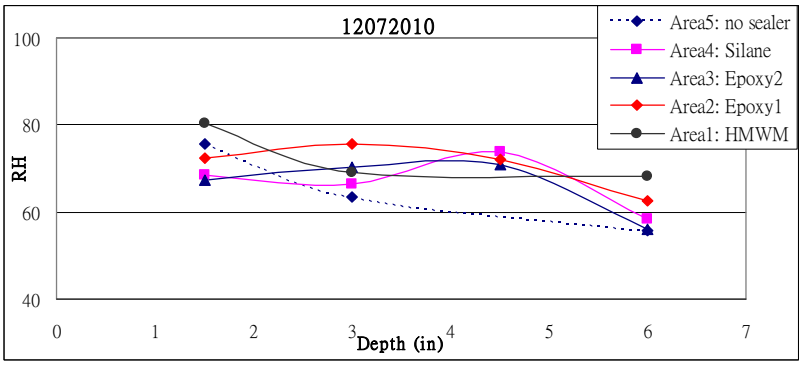

Figure 6.48 Comparisons (different sealer area (12/07/2010))

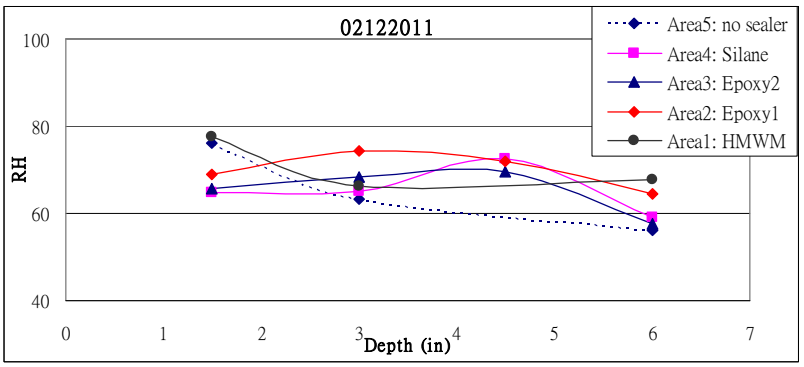

Figure 6.49 Comparisons (different sealer area (02/12/2011))

6.6.4 Comparisons at rebar location

Higher RH values near rebar might cause serious corrosion problems, so we pay more attention to this area. In order to observe the RH dissipation at different sealer areas in Figure 6.50, the y axis represents the RH difference between each month and the reading on June 2010. Figure 6.51 represents

the bimonthly readings. The higher values mean bigger fluctuation. From the two comparisons, we get the results below:

(1) RH fluctuates: Silanes < no sealer < HMWM < Epoxy 1 < Epoxy 2.

(2) In summer: no sealer < Silanes < HMWM < Epoxy 2 < Epoxy 1.

(3) In winter: no sealer, Silanes, Epoxy1, Epoxy2 < Epoxy1.

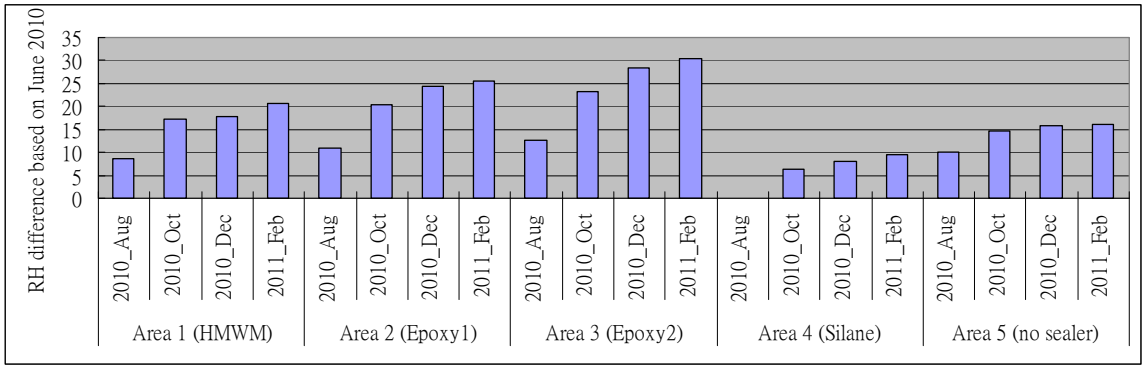

Figure 6.50 RH difference

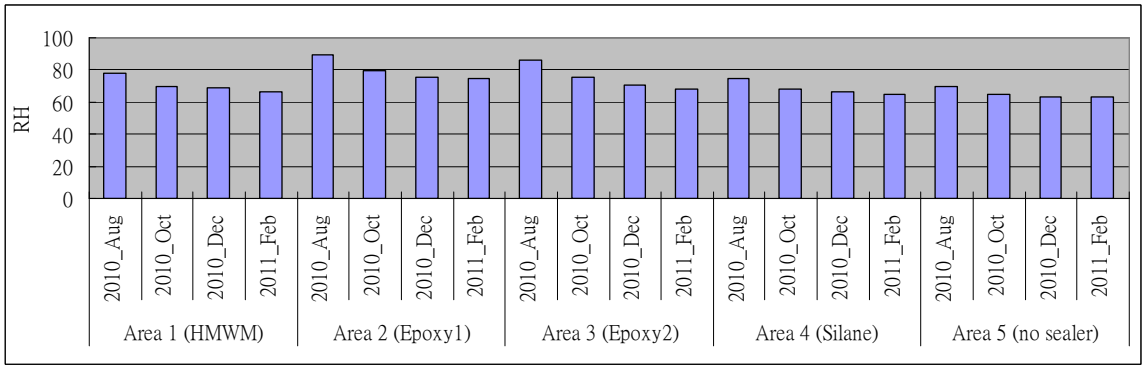

Figure 6.51 Bimonthly readings

6.7. Chloride concentration results

Among the four parameters we used to verify sealer products' performance, chloride concentration plays the most important role in rebar's corrosion mechanism. In addition, some researchers compared sealers' performance for slowing down chloride diffusion in concrete between sealed and unsealed specimens in the laboratory. They conclude that the growing rates of chloride concentration level on sealed and controlled specimens were inconsistent. In some cases, the sealed specimens even had higher

increasing rate than the controlled ones.

In our research, we took concrete cores from bridge decks four times as shown in Table 6.2. The first samples of concrete cores were taken six months before spreading sealer products on the deck surface. The date for the second taking of samples is right after we applied sealer products. The third and fourth times represent six months and one year after application of sealers. We verified the sealers' performance in terms of chloride diffusion in concrete decks in two ways:

(1) Comparisons of each area at different time stage.

(2) Comparisons of each time stage for different areas.

6.7.1 Comparisons of each area at different time stage

The interval between the first and second time, which was conducted on 11/04/2009 and 05/26/2010, respectively, is around six months. Since we had not applied sealer products on the surface, the chloride distribution for the whole bridge decks are ideally supposed to be the same, so we took four at the first time. Due to different environmental and traffic conditions, the chloride concentrations at each area for the third and fourth times should be different. From Figures 6.52-6.56, see the comments from comparisons of the first and second measurements:

(1) As mentioned above, for the first measurement, the chloride distribution for area 1 (HMWM), area 3 (Epoxy 2), and area 4 (Silanes) are similar, but it is higher in area 2 (Epoxy 1). The difference is 30 % near the surface (0.25 in).

(2) For the second measurement, the chloride distribution for area 1 (HMWM), area 2 (Epoxy 1), and area 3 (Epoxy 2) are similar, but it is lower in area 4 (Silanes) and area 5 (no sealer). The difference is 25 % near the surface (0.25 in).

(3) During this winter season, deicing salts were applied on deck surface. Therefore, the environmental chloride ion concentration outside bridge decks should be higher.

(4) At area 1 (HMWM) and area 3 (Epoxy 2), the whole profiles increase. At area 2 (Epoxy 1), the chloride concentration decreases near the surface (0.25 in) and increases at deeper location

(0.75 to 1.75 in). The trend shows that the chloride ions diffuse into bridge decks as time passes. At area 4 (Silanes), the chloride concentration keep the same near the surface and slightly fluctuates at deeper locations.

(5) Even though the trends at these areas are different, they are reasonable. The total chloride content under the curves increases with increasing time. That means the chloride ions keep moving from outside into decks.

Secondly, the comments are at the period of the second and third measurements:

(1) During the period, the weather was fair because it was not during the winter season. Therefore, without the spread of deicing salts, the environmental chloride concentration is supposed to be much lower than previous one.

(2) The reason above can explain why test results showed relatively low chloride content at area 1 (HMWM), area 2 (Epoxy 1), and area 3 (Epoxy 2). At the three areas, the chloride concentration near the surface is constant (0.25 in), but just a few at deeper depths. Part of the chloride ions inside decks disappear during this period.

(3) At area 4 (Silanes) and area 5 (no sealer), the trends are similar and are distinct from the other three. The chloride concentration increases at almost every depth inside decks. The transportation mechanism could be treated as the chloride ions continue moving and penetrating into concrete decks

Details on the comparison of the third and fourth measurements:

(1) Again, during this period, the environmental chloride concentration should be higher due to the spread of deicing salts. The five areas show two different trends this time.

(2) At area 2 (Epoxy 1) and area 3 (Epoxy 2), the chloride content increase with time near the surface and keep the same at deeper locations. The transportation mechanism can be treated as the chloride ion continue moving and penetrating into concrete decks

(3) At area 1(HMWM), area 4 (Silanes) and area 5 (no sealer), the chloride concentration

decreases considerably through the whole profile.

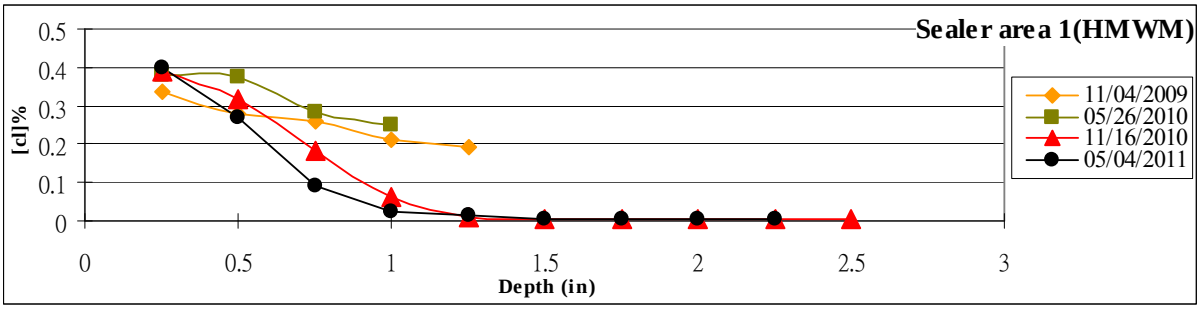

Figure 6.52 Chloride concentrations (HMWM)

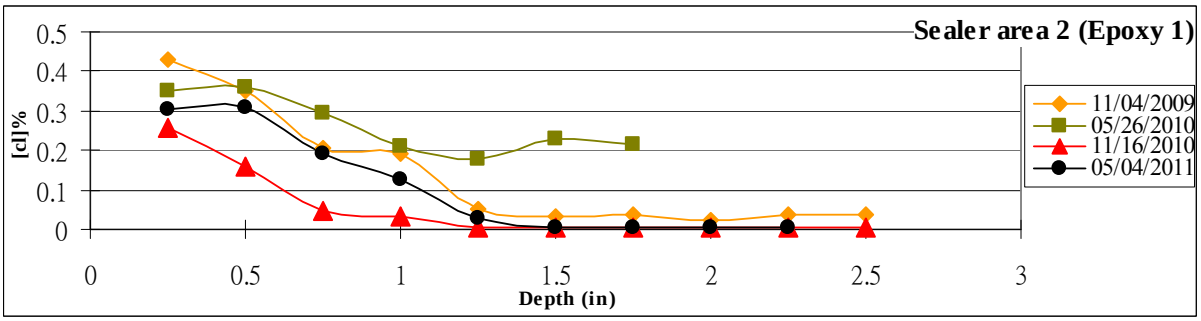

Figure 6.53 Chloride concentrations (Epoxy 1)

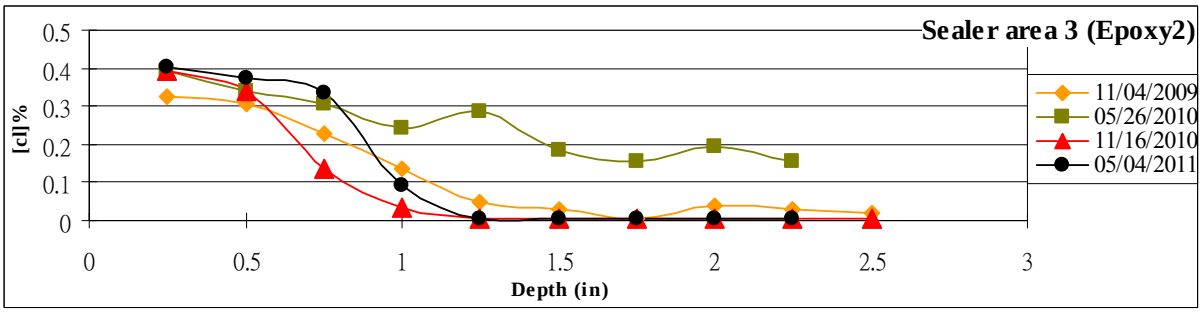

Figure 6.54 Chloride concentrations (Epoxy 2)

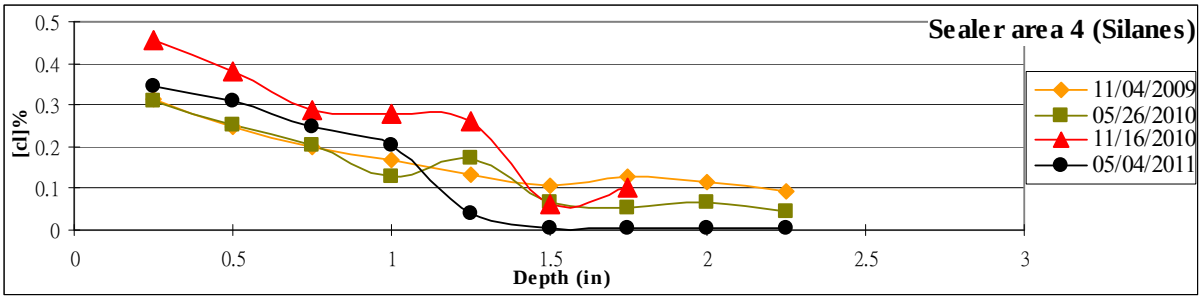

Figure 6.55 Chloride concentrations (Silanes)

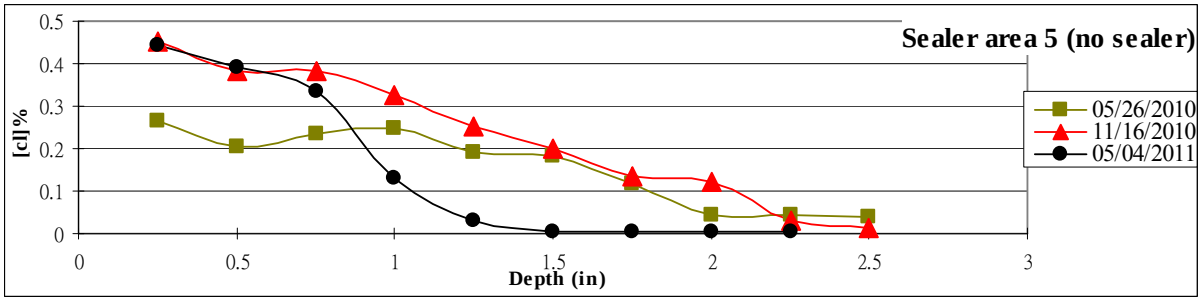

Figure 6.56 Chloride concentrations (no sealer)

6.7.2 Comparisons of each time stage for different areas

In Figures 6.57 and 6.58, the first (11/04/2009) and second (05/26/2010) measurements are represented. Before applying sealer products on the surface, the chloride concentration at the same depth doesn't change significantly. That means the test results are very consistent for the five areas before applying sealers.

For details on the comparison of the second (05/26/2010), third (11/16/2010), and fourth (05/04/2011) measurements, see comments below:

(1) At area 1 (HMWM), it is difficult to explain why the total chloride content under the curves reduce as time passes. However, with HMWM, the chloride concentration near the surface stays almost the same (0.38 %) at the second, third, and fourth measurements, but this value at one inch deep significantly decreases from (0.25 %) to (0.07 %) and (0.02 %). The chloride concentrations near rebar are extremely low in each of the five areas. Hence, we compare each sealer's effectiveness at slowing the chloride ion penetration at one inch deep.

(2) At area 2 (Epoxy 1), the curve is almost the same as that in area 1 (HMWM) at the second sampling time. With Epoxy 1, the chloride concentration near surface decrease from (0.43 %) to (0.35 %), and the value significantly decrease from (0.21 %) to (0.03 %), then jump to (0.13 %) at one inch deep.

(3) At area 3 (Epoxy 2), after applying Epoxy 2 for six months, the chloride concentration decreases considerably and the difference (from 0.25% to 0.03%) is much larger than HMWM. That implies Epoxy 2 indeed has good performance. However, during the period between the third and fourth sampling times, the chloride concentration increases the most (from 0.035% to 0.09%).

(4) At area 4 (Silanes), its performance looks like the worst of the above three sealers. At the second core sampling, the chloride concentration is lower, but it increases at the third sampling time. Its value is relatively higher at the fourth time.

(5) At area 5 (no sealer), the trend is reasonable. The value of chloride concentration is highest at the third time (0.32 %) at one inch deep due to the fact that there is no barrier between the deck surface and the environment. The chloride ions penetrate into the deck more easily. Even at the fourth time, the whole chloride concentration profile is still higher than other four areas.

(6) From the discussions above, sealed parts of concrete deck (areas 1 through area 4) did have better performance for slowing down the chloride ion penetration than the unsealed decks (area 5).

(7) Comparing these four sealer products during the period 05/26/2010 and 11/16/2010, which doesn't have a high concentration of chloride ions in the surrounding environment; Epoxy 2 works better than Epoxy 1 and HMWM to repel chloride ions. Silanes is the least effective sealer.

(8) During the period between 11/16/2010 and 05/04/2011, which has a high concentration of chloride ions in the surrounding environment from deicing salts, HMWM is more effective

than Epoxy 1, then Epoxy 2 and Silanes.

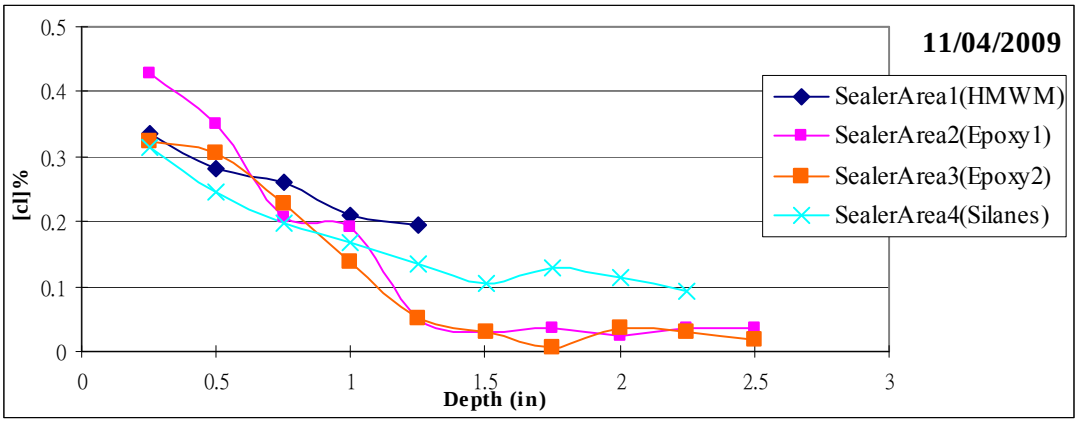

Figure 6.57 Chloride concentrations (11/04/2009)

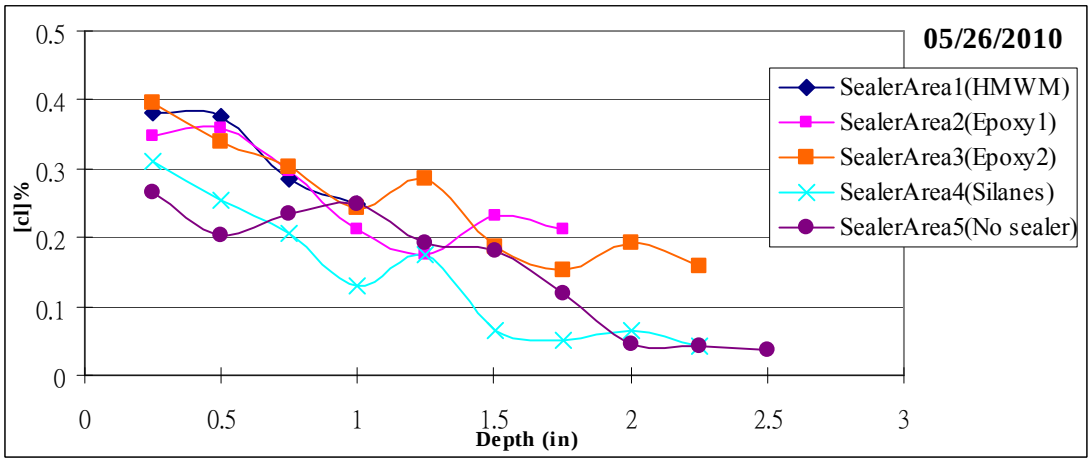

Figure 6.58 Chloride concentrations (05/04/2010)

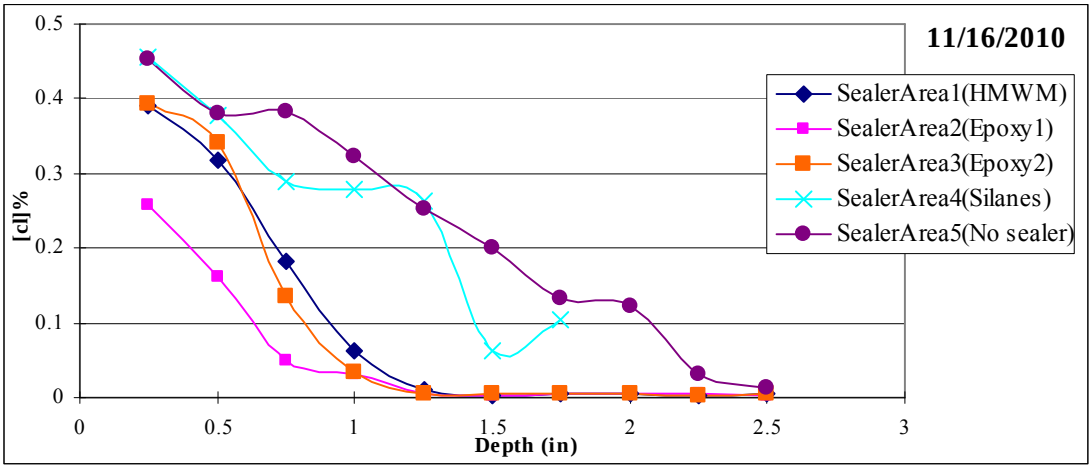

Figure 6.59 Chloride concentrations (11/16/2010)

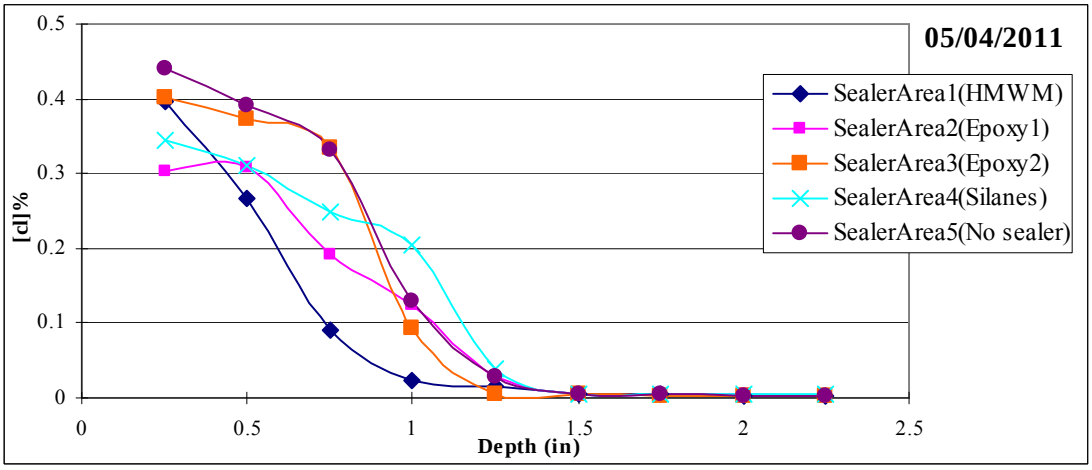

Figure 6.60 Chloride concentrations (05/04/2011)

6.8. Conclusions

From the analysis and comparisons of the four parameters; skid resistance, temperature, moisture, and chloride concentration, we ranked the performance for sealed and unsealed concrete decks on Bridge E-17-QM. Four sealer products, HMWM, Epoxy 1, Epoxy 2, and Silanes were used on the top surface to slow down or even stop moisture and chloride ion penetration from the outside environment. Meanwhile, the internal temperature readings were taken to verify the effect of sealers, and the skid resistance measurements were taken two times; right after the application of sealers and one year after that, to check their performance in regards to concerns about driving safety.

For internal moisture and temperature, we monitored the monthly readings from eighteen sensors we installed and embedded in concrete decks at different depth for five areas. From the long-term monitoring, we obtained one full year of complete measurements and whole profiles of variables for the vertical direction of bridge decks.

The skid resistance of the sealers is important to driving safety, and is relatively an independent issue in comparison to the other three variables. Regarding the mechanism of rebar corrosion, chloride concentration and moisture content play the most important roles. They are both much more important than the temperature inside the concrete. Therefore, in the comparisons, we would like to propose a reasonable weighting range for these parameters and by combining those, provide further rankings and suggestions. The weighting we use is shown in Table 6.7.

Table 6.7 Weightings

Concerns	Parameters	Weighting (%)
Driving Safety	Skid resistance	100
Corrosion Mechanism	Chloride concentration	40-60
	Moisture	30-50
	Temperature	5-10

From the readings of internal chloride concentration, the results show two different trends from the period of 05/26/2010 to 11/16/2010, which doesn't have high concentration of chloride ion from the surrounding environment (mostly from deicing salts) and the period of 11/16/2010 to 05/04/2011 (which has higher outside chloride ion concentration from deicing salts). The rankings of the sealers' performance varied during these two periods. We proposed the first ranking for driving safety and the corrosion mechanism shown in Table 6.8 and Table 6.9, and then we combined the rankings above and the weightings in Table 6.7 and concluded with the final rankings shown in Table 6.10.

In Table 6.8, for example, if we only consider the skid resistance, Epoxy 1 is ranked number 1

among the four chemical sealer products plus one unsealed deck area. In Table 6.9, during the summer season that implies lower environmental chloride concentration, Epoxy 2 performed the best. During the winter season, at which we spread deicing salts on bridge decks lead to higher environmental chloride concentration, HMWM performed the best. In Table 6.10, because the skid resistance individually belongs to the driving safety concern and the other three parameters relate to the corrosion mechanism, we show the rankings in terms of corrosion mechanism at the last column and the driving safety at the second column to clearly point out the different rankings based on different considerations.

Table 6.8 Rankings (driving safety)

Sealer	Driving Safety
HMWM	2
Epoxy 1	1
Epoxy 2	3
Silanes	5
Unsealed	4

Table 6.9 Rankings (corrosion mechanism)

	Chloride		Moisture	Temperature
Sealer	Low outside environmental chloride concentration	High outside environmental chloride concentration		
HMWM	3 or 4	1 or 2	3	3
Epoxy 1	2 or 3	2 or 3	5 or 4	2
Epoxy 2	1 or 2	3 or 4	4 or 3	1
Silanes	4	4	2	4
Unsealed	5	5	1	5

Table 6.10 Ranking (driving safety and corrosion mechanism)

Sealer	Driving Safety	Corrosion Mechanism				
		Chloride Moisture		Moisture	Temp	Combination
		Outside(Low)	Outside(High)			
HMWM	2	3 or 4	1 or 2	3	3	1 or 2
Epoxy 1	1	2 or 3	2 or 3	5 or 4	2	2
Epoxy 2	3	1 or 2	3 or 4	4 or 3	1	3 or 4
Silanes	5	4	4	2	4	4
Unsealed	4	5	5	1	5	5

Chapter 7

Theoretical Modeling the Effect of Damage on Diffusion Coefficient

7.1. Overview

Chapter 5.4 suggested that in order to have a more accurate estimation of the rate of concrete deterioration, i.e. a better estimation for parameters m and D_i, we must conduct another inspection of the same bridges. Once we have two different diffusion coefficients corresponding to two different time stages, we can better define the curve and obtain a better estimation of the m value, and predict more accurately the rebar corrosion initiation time in bridge decks.

The parameter m for different bridges should be varied because each bridge has its own rate of deterioration, which depends on its environmental conditions and traffic loading. The absolute value of parameter m tends to be higher when the bridge is under heavy traffic and severe environmental conditions. The derivation of equation (5.5) through equation (5.13) in Chapter 5.4 shows that when the absolute value of m is high, its corresponding corrosion initiation times will reduce greatly.

In Chapter 6, we applied four chemical sealer products on the surface of bridge decks, and then through long-term performance monitoring, in which four parameters were adopted to analyze the sealers' performance, we proposed rankings. Among the four parameters, chloride ion concentration played the most important role in the corrosion mechanism. Unlike the one time measurement in Chapter 5, the chloride concentration profiles in Chapter 6 were taken four different times at six-month intervals. That allowed us to observe and analyze the changing m parameters.

In this chapter, we continue the derivation of time dependent diffusion equations in Chapter 5.4 and use the four sets of on-site test data of chloride ion concentrations in Chapter 6 to derive a certain m value representing each chemical sealer product. Each m value represents the damage status of each

sealer area. Through this methodology, we can not only provide a more reasonable ranking of sealer areas in terms of chloride ion penetration based on their unique m values, but also extend this concept, using m values to represent the damage status of any bridge deck. In addition, in this chapter, we will consider varied boundary conditions, such as higher environmental chloride concentration in winter seasons due to the application of deicing salts.

7.2. Chloride concentration profiles

In Chapter 5, we took concrete cores from the sealed and unsealed areas four times (Table 7.1). The first measurement was taken six months before spreading sealer products on deck surfaces, and therefore the chloride profiles from areas 1 through 4 were supposed to be the same. The second measurement was taken shortly after we applied sealer products. The third and fourth measurements represent the six-month mark and one year after the initial application of sealers. The chloride concentration profiles categorized with different sealer areas and the first two or three measurements are shown from Figure 7.1 through Figure 7.5.

Table 7.1 Dates of taking concrete cores

	Date	Number of cores taken	Deck surface condition
1	11/04/2009	4	No sealer
2	05/26/2010	5	Right after sealer application
3	11/16/2010	5	Six months after sealer application
4	05/04/2011	5	One year after sealer application

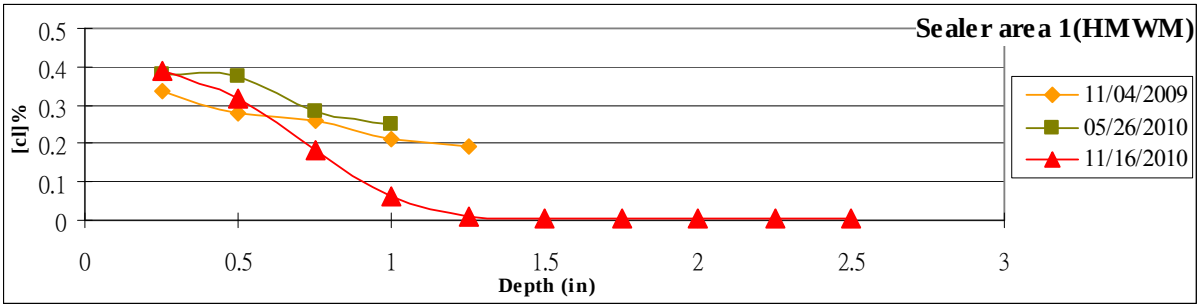

Figure 7.1 Chloride concentrations (HMWM)

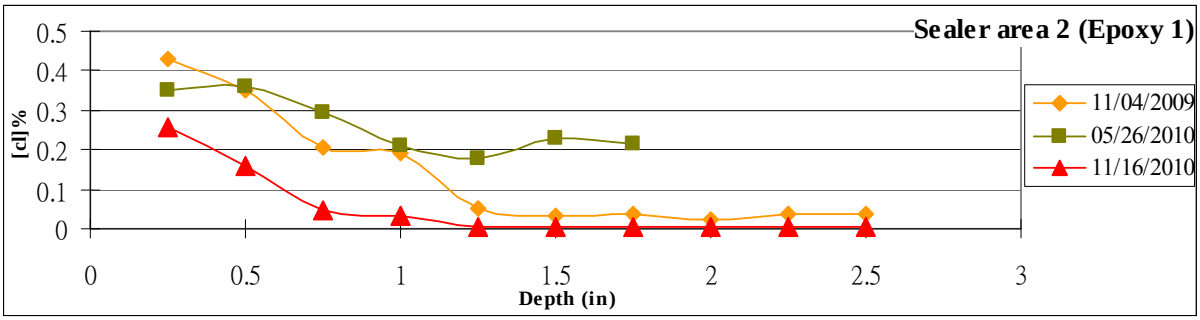

Figure 7.2 Chloride concentrations (Epoxy 1)

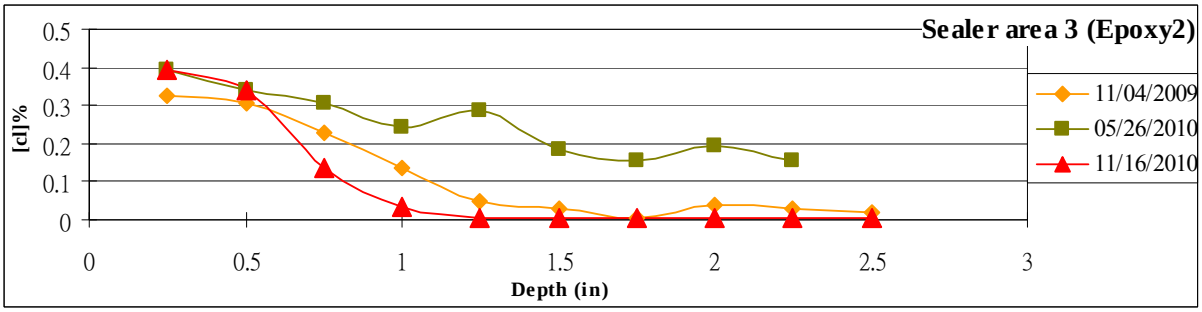

Figure 7.3 Chloride concentrations (Epoxy 2)

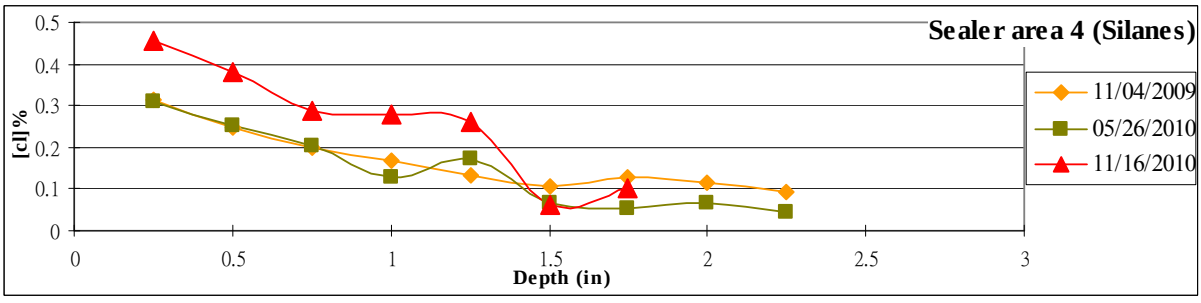

Figure 7.4 Chloride concentrations (Silanes)

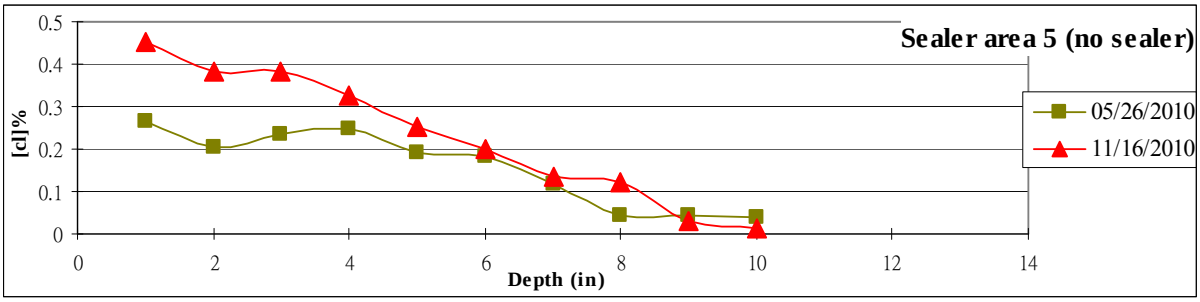

Figure 7.5 Chloride concentrations (no sealer)

In Chapter 5, we ranked their performance by comparing the chloride ion concentration near rebar, but actually the sealers' performance should be based on their capability of blocking chloride ion penetration. In the next section, we will analyze the total amount of chloride ions inside concrete decks. For four sealed areas with different sealer products and one unsealed area, there are different m values representing varied damage statuses. Therefore, the second task is to propose m values for the above areas. The third task is to consider the varied boundary conditions and propose the average m values.

7.3. Observations

From Figure 7.1 through Figure 7.5, we observed the total amount of chloride ions inside concrete decks and compared the trend of chloride profiles at different periods, and then drew conclusions as follows:

(1) During the winter season (11/04/2009-05/26/2010), the deicing salts were applied on the deck surface, but the four chemical sealer products had not been spread on them.

(2) In this period, area 1 (HMWM) and area 3 (Epoxy 2) showed the same trend: the whole profile increased as time passes. At area 2 (Epoxy 1), the trend showed the chloride ions diffused into bridge decks. At area 4 (Silanes), the chloride distribution stayed the same.

(3) The trend above is reasonable because the total chloride amount under the curves increased, which means the chloride ions kept moving from the outside environment into the concrete decks.

(4) During the summer season (05/26/2009-11/16/2010), the deicing salts were not being applied

on the deck surface, but the four chemical sealer products had already been spread on them for six months.

(5) From the second measurement to the third measurement, the weather was fair because it was not during the winter season. Therefore, without the application of deicing salts, the environmental chloride concentration was supposed to be much lower than the previous period.

(6) At area 4 (Silanes) and area 5 (no sealer), the trends were similar and were distinct from the other three. The chloride concentration increases at almost every depth inside the concrete decks, which implied that the chloride ions continued moving and penetrating into the concrete decks.

(7) At area 1 (HMWM), area 2 (Epoxy 1), and area 3 (Epoxy 2), the total chloride amount under the curves decreased, which means the chloride ions moved out from the bridge decks into the outside environment. The reason is that the vehicle wheels actively pull out the chloride ions from the existing cracks in the concrete decks into the environment, especially when the cars drive at high speeds.

7.4. Derivations

The problem of chloride ion penetration into concrete decks can be described in equation (7.1). After substituting equation (7.2) into equation (7.1), we get equation (7.3) and the original problem can be transferred to equation (7.4). In equation (7.4), the new variable T can be considered as a new equivalent time scale.

$$\begin{gathered}\frac{\partial C}{\partial t} = D(t)\frac{\partial^2 C}{\partial x^2} \\ C(0,t) = g(t), C(\infty,t) = C_0 \\ C(x,0) = C_0\end{gathered} \qquad \text{Eq. (7.1)}$$

$$\frac{dT}{dt} = D(t) \qquad \text{Eq. (7.2)}$$

$$\frac{\partial C}{\partial t} = \frac{\partial C}{\partial T} \cdot \frac{dT}{dt} = D(t)\frac{\partial C}{\partial T} = D(t)\frac{\partial^2 C}{\partial x^2} \qquad \text{Eq. (7.3)}$$

$$\frac{\partial C}{\partial T} = \frac{\partial^2 C}{\partial x^2}$$

$$C(0,T) = g\left(F^{-1}(T)\right)G(T),\ C(\infty,T) = C_0 \qquad \text{Eq. (7.4)}$$

$$C(x,0) = C_0$$

For the special case (D_{cl} =constant), the analytical solution is shown in equation (7.5). Furthermore, if D_{cl} is the same as 1, the analytical solution is shown in equation (7.6).

$$C(x,t) = C_0 erf\left(\frac{x}{2\sqrt{D_{cl}t}}\right) + \frac{x}{2\sqrt{D_{cl}\pi}}\int_0^t g(t-u)\frac{1}{u\sqrt{u}}e^{-\frac{x^2}{4D_{cl}u}}du \qquad \text{Eq. (7.5)}$$

$$C(x,T) = C_0 erf\left(\frac{x}{2\sqrt{|T|}}\right) + \frac{x}{2\sqrt{\pi}}\int_0^T G(T-u)\frac{1}{u\sqrt{u}}e^{-\frac{x^2}{4u}}du \qquad \text{Eq. (7.6)}$$

When we treat the chloride diffusion coefficient as a time dependent variable, the problem can be described in equation (7.7). With the derivation of equation (7.2) through (7.4), equation (7.8) and equation (7.9) can be obtained. Combining those equations above, we get the general solution of this problem in equation (7.10).

$$\frac{\partial C}{\partial t} = \frac{D_0}{t^m}\frac{\partial^2 C}{\partial x^2}$$
$$C(0,t) = g(t), C(\infty,t) = C_0 \qquad \text{Eq. (7.7)}$$
$$C(x,0) = C_0$$

$$T = F(t) = \int_0^t \frac{D_0}{s^m}ds = \frac{D_0}{1-m}t^{1-m}(m \neq 1) \qquad \text{Eq. (7.8)}$$

$$G(T) = g\left(F^{-1}(T)\right) = g\left(\left[\frac{T(1-m)}{D_0}\right]^{\frac{1}{1-m}}\right) \qquad \text{Eq. (7.9)}$$

$$C(x,t) = C_0 erf\left(\frac{x}{2\sqrt{\frac{D_0}{|1-m|}t^{1-m}}}\right) + \frac{x}{2\sqrt{\pi}}\int_0^{\frac{D_0}{1-m}t^{1-m}} \frac{1}{u\sqrt{u}} e^{-\frac{x^2}{4u}} g\left(\left[t^{1-m} - \frac{1-m}{D_0}u\right]^{\frac{1}{1-m}}\right) du \qquad \text{Eq. (7.10)}$$

In equation (7.7), if the boundary condition $g(t)$ is constant, the analytical solution can be solved in equation (7.11).

$$C(x,t) = C_s + (C_0 - C_s) erf\left(\frac{x}{2\sqrt{\frac{D_0}{|1-m|}t^{1-m}}}\right) (m \neq 1) \qquad \text{Eq. (7.11)}$$

Treating the chloride diffusion coefficient as a time dependent variable (equation (7.7)), we get the analytical solution in equation (7.11), which is the same as the solution in equation (5.12) in Chapter 5.4. However, both equations can only be applied to a situation with a constant boundary condition. In this section, equation (7.10) can be used as the general analytical solution with varied boundary conditions. In future work, equation (7.10) can have more broad applications to real problems with much more complicated boundary conditions.

7.5. Calculations

First we consider the fixed environmental chloride ion concentration and through equation 7.11, the m value corresponding to each sealer area is shown in Table 7.2. In Table 7.2, the second column through the sixth column individually represent the data from which time we adopted, initial m value, initial diffusion coefficient, m values, and the least square values.

Table 7.2 The m value of each sealer area (fixed boundary condition)

	Time	mo	Do	m	S
Sealer area 1 (HMWM)	2	-1.105	0.01368578523419	0.15281902371285	0.00114625739175
	3	-1.308	0.00025820405715	-0.9027265009163	0.00259448119850
	4	-1.8	0.00000036744125	-1.8819451478297	0.02058090577326
Sealer area 2 (Epoxy 1)	2				
	3	-1.41	0.17025584222811	0.76509876838218	0.00906201260534
	4	-1.89	0.00000009267443	-1.9613929056732	7.553362309e-004
Sealer area 3 (Epoxy 2)	2				
	3	-1.355	0.12981351569452	0.55056646544732	0.00670528732232
	4	-1.7	0.00000280604629	-1.436141758129	0.02903312967855
Sealer area 4 (Silanes)	2	-1.2	0.07175670725073	0.81497983866386	0.01202808227699
	3	-1.51	0.04409474991190	0.68084473331612	0.00661095092139
	4	-1.89	0.00000519714166	-1.639478900269	0.03147108581644
Sealer area 5 (No sealer)	2				
	3	-1.87	0.00055305474688	-0.56289013176	0.02263738755852
	4	-1.995	0.00000434601642	-1.715795712026	0.04054415852381

In most occasions, the environmental chloride concentration is not constant. During the winter season, due to the application of deicing salts, the value should be higher. In Figure 7.6, the upper graph and lower graph represent the concept of taking the boundary conditions as a fixed one and a varied one.

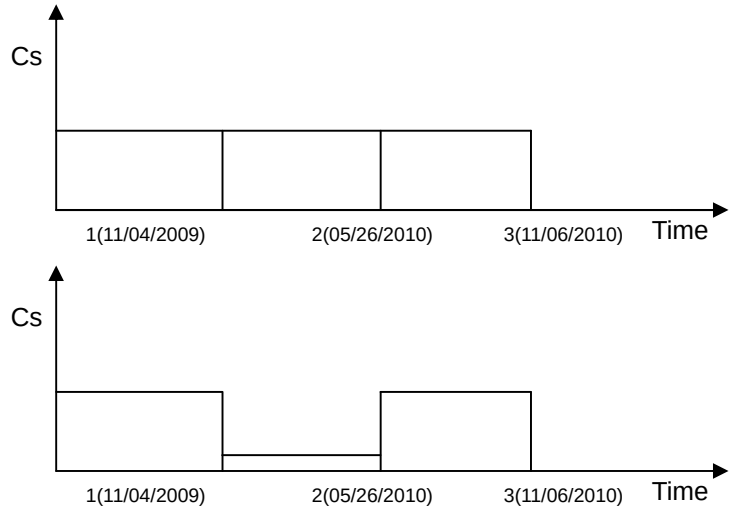

Figure 7.6 Boundary conditions

We also consider the varied environmental chloride concentrations and do the calculations by using equation 7.11 for each period. The m value for each sealer area is shown in Table 7.3, whose second column represents the time stages at which we took measurements and the proposed environmental chloride concentration. For example, in sealer area 1 (HMWM), we use the test data from the third measurement and treat the environmental chloride concentration as 0.05 % listed at the first line, and then use the test data from the fourth measurement and treat the environmental chloride concentration as 0.5 % at the second line. In addition, the average m values from the curve fittings are shown in Figure 7.7 through Figure 7.11. The dashed lines in those figures represent the average m values.

Table 7.3 The m value of each sealer area (varied boundary condition)

	Varied B.C.	mo	Do	m	Average m
Sealer area 1 (HMWM)	3 (0.05 %)	-1.3	0.73089830983290	-1.7195626682	-1.80
	4 (0.5 %)	-1.8	0.00000036744125	-1.8819451478	
Sealer area 2 (Epoxy 1)	3 (0.05 %)	-1.91	10.05355106196500	-3.409429440396	-2.69
	4 (0.5 %)	-1.89	0.00000009267443	-1.961392905673	
Sealer area 3 (Epoxy 2)	3 (0.05 %)	-1.1	1.42290638939568	-2.345022919842	-1.89
	4 (0.5 %)	-1.7	0.00000280604629	-1.436141758129	
Sealer area 4 (Silanes)	3 (0.05 %)	-1.7	0.67338603171734	-1.976910267612	-1.81
	4 (0.5 %)	-1.89	0.00000519714166	-1.639478900269	
Sealer area 5 (No sealer)	3 (0.05 %)	-1.845	0.59972000078843	-3.964535508533	-2.84
	4 (0.5 %)	-1.995	0.00000434601642	-1.715795712026	

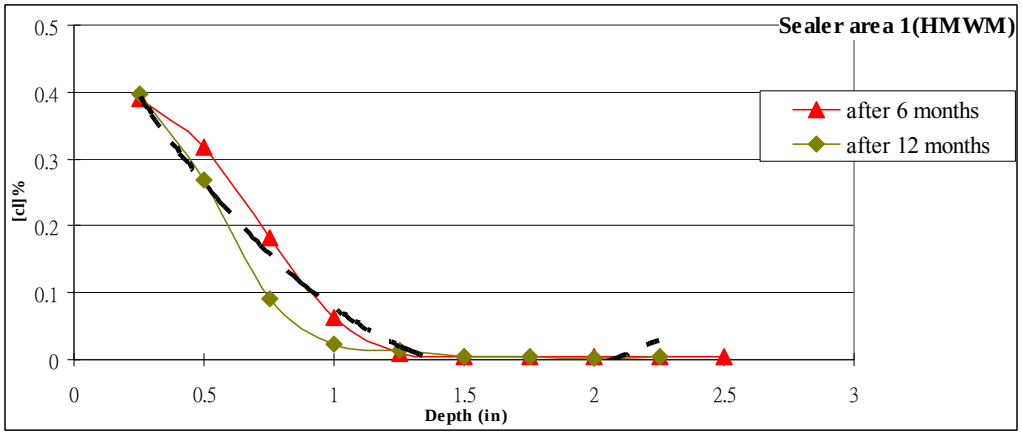

Figure 7.7 Chloride concentration (HMWM)

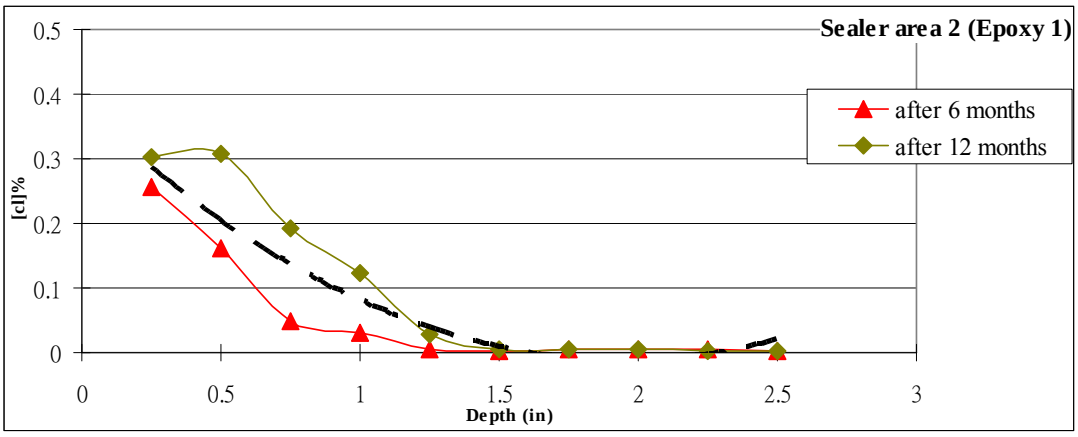

Figure 7.8 Chloride concentration (Epoxy 1)

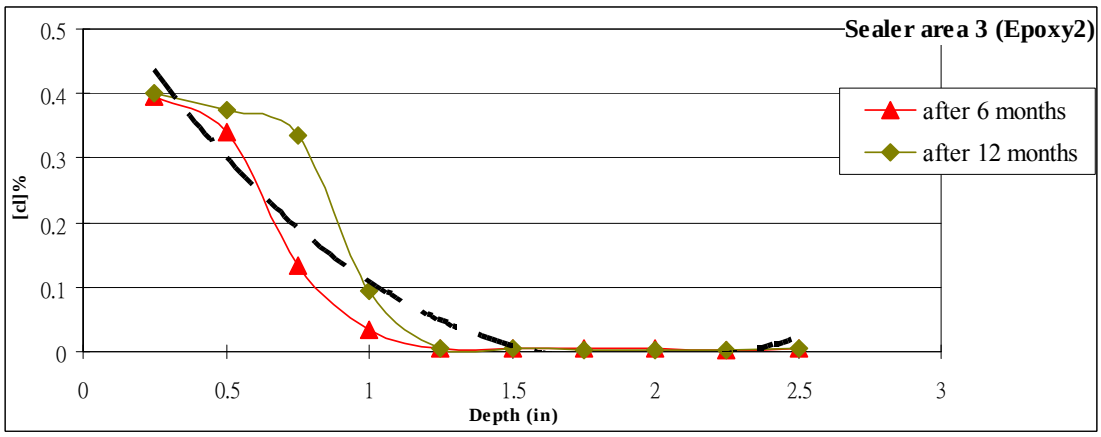

Figure 7.9 Chloride concentration (Epoxy 2)

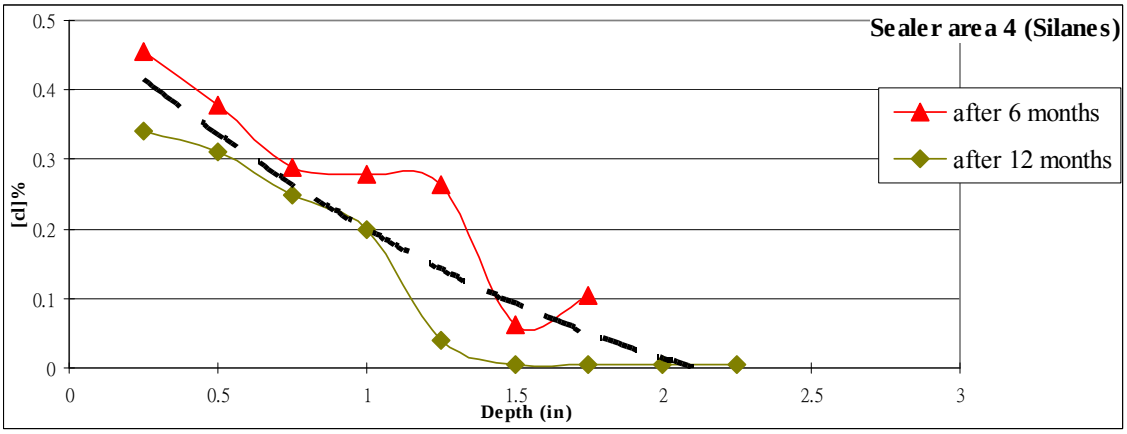

Figure 7.10 Chloride concentration (Silanes)

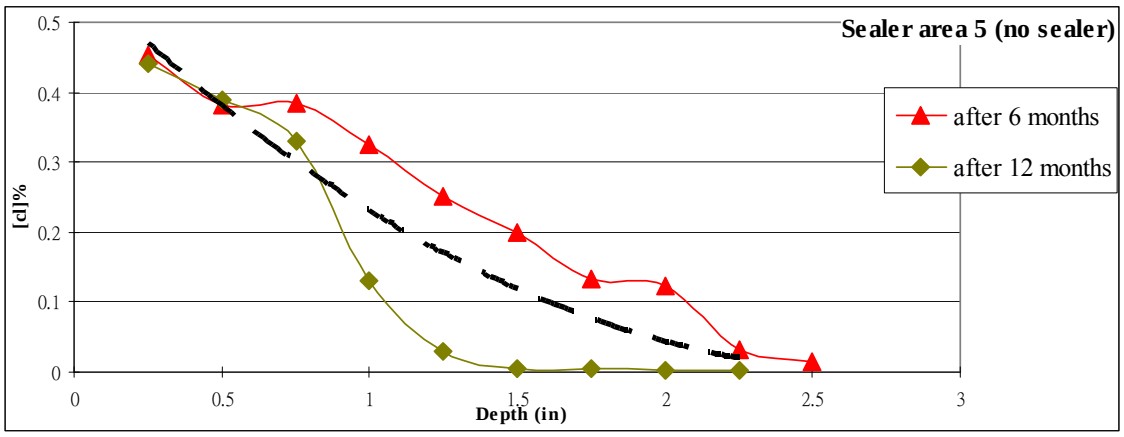

Figure 7.11 Chloride concentration (no sealer)

7.6. Composite damage model

A theoretical model for the diffusion coefficient can be developed using the composite damage mechanics approach (Xi and Nakhi 2005; Xi et al. 2006), in which the distressed concrete can be represented by many concentric spherical elements as shown in Figure 7.12. The cores (the inclusions) are the damaged concrete and the rings (the matrix) are original concrete without damage. In the following equation (equation (7.12)), d is the damage parameter ranging from 0 to 1. When $d = 0$, there is no damaged concrete, and when $d = 100\%$, there is no original concrete. Both D_d and Do are constants. The subscript d is for the damaged concrete, and the subscript o is for the original concrete without damage.

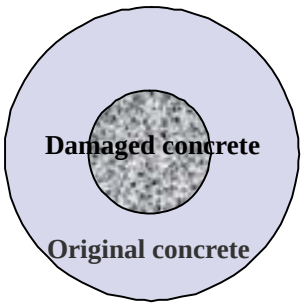

Figure 7.12 Three-phase model

$$D_{eff} = D_o\left[1+\frac{d}{\frac{(1-d)}{3}+\frac{D_o}{(D_d-D_o)}}\right] \qquad \text{Eq. (7.12)}$$

Since d varies from 0 to 1, we use the equation (7.13) to calculate d.

$$d = 1-e^{t\times m_d} \qquad \text{Eq. (7.13)}$$

Here m_d is the parameter that represents the damage status and can be calculated by dividing the m values of five sealants by a certain constant. Another parameter that can be adjusted is D_d.

Equation (7.14) represents the damage evolution in concrete due to traffic and environmental conditions such as temperature fluctuation and humidity variation. When t=0, d=0, so $D_{eff}=D_0$, there is no damage in concrete. When $t\to\infty$, d= 1, so $D_{eff}=D_d$, there is no original concrete.

Substituting equation (7.13) into equation (7.12), we can get the following equivalent time as equation (7.14) and (7.15). Then substitute T into equation (5.9) in Chapter 5.4, the chloride concentration profile can be obtained as equation (7.16).

$$T=\int_0^t D_{eff}\,dt=\int_0^t D_o\left[1+\frac{d}{\frac{1-d}{3}+\frac{D_o}{D_d-D_o}}\right]dt=\int_0^t D_o\left[1+\frac{1-e^{-t\times m_d}}{\frac{e^{-t\times m_d}}{3}+\frac{D_o}{D_d-D_o}}\right]dt \qquad \text{Eq. (7.14)}$$

$$T = \frac{D_d\,t}{D_0}-\left(\frac{2D_0+D_d}{D_0 m_d}\right)\times\left(\log\frac{3D_0+(D_d-D_0)e^{t\times m_d}}{2D_0+D_d}\right) \qquad \text{Eq. (7.15)}$$

$$C = C_0\left[1-erf\left\{\frac{x}{2\sqrt{\left(\frac{D_d\,t}{D_0}\right)-\left(\frac{2D_0+D_d}{D_0 m_d}\right)\left(\log\frac{3D_0+(D_d-D_0)e^{t\times m_d}}{2D_0+D_d}\right)}}\right\}\right] \qquad \text{Eq. (7.16)}$$

We applied the equations above to the test results of four sealed sealer areas and one unsealed sealer area, and then got the results as Figures 7.13 through 7.15.

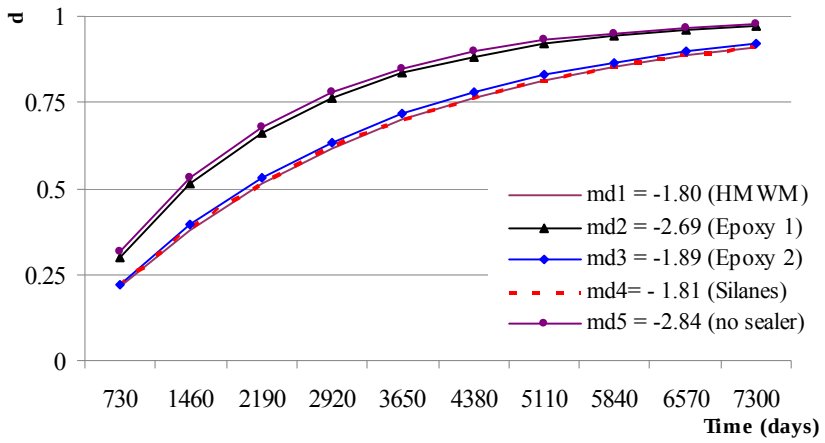

Figure 7.13 Combine with three-phase model (d vs time)

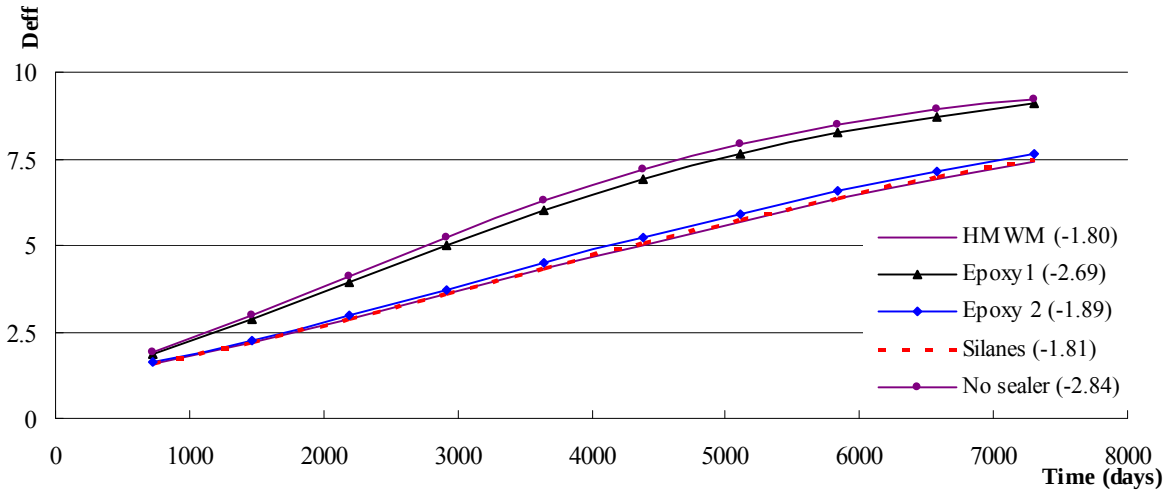

Figure 7.14 Combine with three-phase model (Deff vs time)

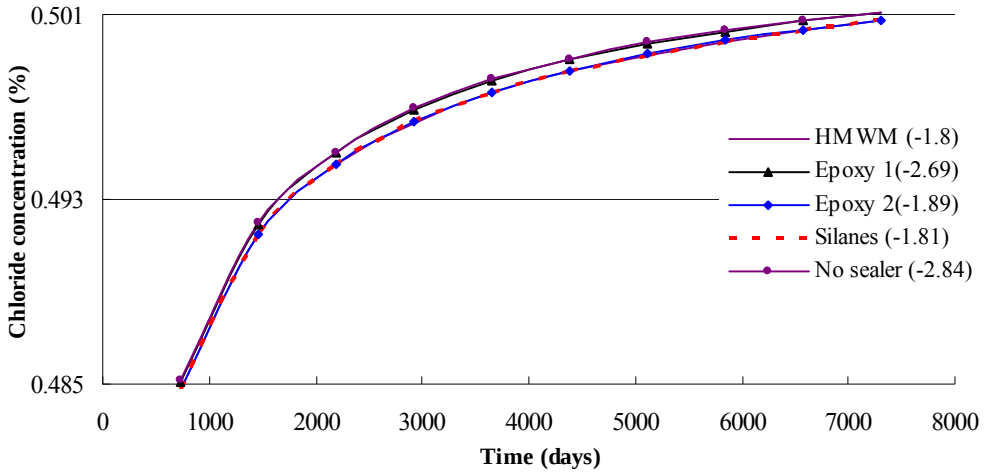

Figure 7.15 Combine with three-phase model (concentration profiles)

7.7. Conclusions

(1) In Table 7.2, the absolute values of m increase as time passes. For example, in sealer area 1 (HMWM), the m values changes from 0.1528 to -0.9, and then to -1.88. Apply these m values in equation (5.5) in Chapter 5.4, and the increasing rate of the current D_{cl} value at each of the three time stages is larger than 10. The same results occur at sealer area 2 (Epoxy 1), sealer area 3 (Epoxy 2), and sealer area 5 (no sealer).

(2) That implies the damage status of the concrete deck is getting serious, which matches the conclusion made in Chapter 5: the corrosion initiation time is reciprocally proportional to the diffusion coefficient. This means the corrosion initiation time will be reduced to 1/10 of the current value, if the diffusion coefficient increases 10 times. In practice, the increasing rate is more than 10 times the diffusion coefficient which is highly possible under heavy traffic and severe environmental conditions.

(3) In Table 7.3, we consider the varied boundary condition as well and compare the sealers' performance based on their average m values. Sealer area 5 (no sealer) and sealer area 2 (Epoxy 1) show worse performance because their absolute values of the m parameter are higher, implying a more serious damage status than the other three. Sealer area 1 (HMWM) and sealer area 4 (Silanes) performed better than sealer area 3 (Epoxy 2).

(4) The problem can be combined with the three-phase damage model. From Figure 7.13 and Figure 7.14, the concrete decks with HMWM, Epoxy 2, and Silanes show better performance than the concrete decks with Epoxy 1 and unsealed one. From Figure 7.15, we can further predict the chloride concentration profiles based on the damage model and get an idea about how many years the application of sealer products can extend the corrosion initiation time, which is denoted as the chloride concentration near rebar reaching the critical value (0.5%).

Chapter 8

Summary and Suggestions for Future Work

8.1. Summary

This dissertation covers two themes: one for experimental and theoretical studies of recycled aggregate concrete (RAC) and the other for the performance evaluation of chemical sealers applied to reinforced concrete (RC) bridge decks.

At the first theme, we find a better mixing approach, better water to cement ratio, and more appropriate surface treatment methods for improving mechanical properties of RAC, and then we check its durability properties. Also, a multiscale chemomechanical coupled analytical model is described for characterizing the shrinkage property of RAC. Composite mechanics models are used at the selected scale levels to characterize effective properties of RAC. The volume fractions of different constituents in the old and new concrete are calculated based on the degrees of hydration of old and new cements.

At the second theme, first we focus on the experimental study and theoretical analysis of chloride penetration. Then, the service life of concrete decks in terms of rebar's corrosion initiation time is proposed. By calibrating the parameters in the analytical model with the chloride concentration profiles obtained from bridges, a more reliable prediction model was established. Second, from the long-term monitoring, we compare the performance of four chemical sealer products and give the rankings. Finally, we continue the derivation of time dependent diffusion equations and use the on-site test data to derive certain m values. Finally, we combine the concrete composite damage model and give the prediction of chloride concentration and rebar's corrosion initiation time.

8.2. Future work

(1) In Chapter 2, the optical micrographic images provide us good understanding of recycled aggregate

concrete at the microstructure level. In the future, micrographs can be taken by scanning electron microscopes (SEM) and the micrographs can be further used in finite element analysis. The results of the finite element analysis can be used to compare with the obtained test data.

(2) In Chapter 4, from the comparison between analytical solution and test data, this multiscale chemomechanical model provides us a good approach to explain, analyze, and even predict the shrinkage of recycled aggregate concrete. In the future, this model can be further developed for more material properties of recycled aggregate concrete, such as mechanical, thermal expansion, and transport properties (moisture and chloride).

(3) In Chapter 7, we can predict the chloride concentration profiles based on the damage model and get an idea about how many years the application of sealer products can extend the corrosion initiation time, which is denoted as the chloride concentration near rebar reaching the critical value (0.5%). In the future, from the next CDOT (Colorado Department of Transportation) project, we can get more test data, which is longer than one year, to calibrate the damage model with the same bridge. Also, the accuracy and consistency of this damage model with different period can be checked.

Bibliography

Abbas, A., Fathifazl, G., Isgor, O. B., Razaqpur, A. G., Fournier, B., and Foo, S. (2006) "Environmental benefits of green concrete," *EIC Climate Change Technology, 2006 IEEE*, Ottawa, Ont., Canada, 1–8.

ACI Committee 201 (1994), "Guide to durable concrete, Chapter 4 Corrosion of steel and other materials embedded in concrete," *Manual of Concrete Practice, Part I*.

Aitken, C., and Litvan, G. (1989) "Laboratory investigation of concrete sealers," *Concrete International*, Vol. 11, Issue 11, pp.37-42.

Allais, L., Bretheau, T., and Zaoui, A., (1992) "Experimental and Theoretical Approach of the Influence of Morphology on a Two-Phase Material Mechanical Behavior", *Macroscopic Behavior of Heterogeneous Materials from the Microstructure, Proc. of the Winter Annual Meeting of ASME*, Anaheim, California, Nov. 8-13, Ed. Torquato, S., and Krajcinovic, D., 13-25, 1992.

American Association of State Highway and Transportation Officials (2004) "Standard method of test for resistance of concrete to chloride penetration," AASHTO Designation T 259-02, Washington, D.C

American Association of State Highway and Transportation Officials (2004) "Standard test method for sampling and testing for total chloride ion in concrete and concrete raw materials," AASHTO Designation T 260-02, Washington, D.C

American Society of Testing and Materials (2004) "Standard test method for splitting tensile strength of cylindrical concrete specimens," ASTM Designation C 496-96, West Conshohocken, Pennsylvania.

American Society of Testing and Materials (2004) "Standard test method for resistance of concrete to rapid freezing and thawing," ASTM Designation C 666-97, West Conshohocken, Pennsylvania.

American Society of Testing and Materials (2004) "Standard test method for scaling resistance of concrete surfaces exposed to deicing chemicals," ASTM Designation C 672-03, West Conshohocken,

Pennsylvania.

American Concrete Institute Manual of Practices (1997) “Crack widths in concrete bridge deck,” ACI 224R, 4.4

Ann, K.Y., Moon, H.Y., Kim, Y. B., and Ryou, J. (2008) “Durability of recycled aggregate concrete using pozzolanic materials,” *Waste management*, 28, 993-999

ASTM C 1202 “Standard Test Method for Electrical Indication of Concrete's Ability to Resist Chloride Ion Penetration”

ASTM C 157 “Standard Test Method for Length Change of Hardened Hydraulic-Cement Mortar and Concrete”

ASTM C 597 “Standard Test Method for Pulse Velocity through Concrete”

ASTM C 666 “Standard Test Method for Resistance of Concrete to Rapid Freezing and Thawing”

Behm, Dean T., and John Gannon (1990) “Epoxies,” In Adhesives and Sealants, Engineered Materials Handbook, Vol. 3, ASM International, p.94-102.

Bergstrom, T.B., Sujata, K., Xi, Y., and Jennings, H.M., (1997) “The Drying Shrinkage of Cement Paste as Measured in an Environmental Scanning Electron Microscope”, *J. Amer. Cer. Soc.*, submitted.

Berke, N.S. (1986) "Corrosion Rates of Steel in Concrete," *ASTM Standardization News*, 14, 3, 57-61.

Bose, A., and Li, W (2002) “Characterization and manipulation of asphalt adhesion to rock,” Federal Highway Administration, FHWA-RIDOT-RTD, 11p

Browne, R. (1982) "Design Prediction of the Life for Reinforced Concrete in a Marine and Other Chloride Environment," *Durability of Building Materials*, 1, 2, 113-125.

Cady, P.D., and Weyers, R.E. (1992) “Predicting service life of concrete bridge decks subject to reinforcement corrosion,” *In Corrosion Forms & Control for Infrastructure*, San Diego, CA.

Chang, L.M. (1992). “Laboratory evaluation of generic concrete sealer and coating systems,” Transportation Research Record, No.1335, p.1-9

Christensen, R.M., (1979) “Mechanics of Composite Materials”, Wiley-Interscience, New York

Christensen, R.M., and Lo, K.H., (1979) "Solutions for Effective Shear Properties in Three Phase Sphere and Cylinder Models", *J. Mech. Phys. Solids*, 27, 315-330.

Curra, W. (1990) "Evaluation of sealers for concrete bridge decks," Texas State Department of Highways & Public Transportation, 47p

Damico, Dennis J. (1990). "Acrylics," Adhesives and Sealants, Engineered Materials Handbook, Vol. 3, ASM International, p. 119-125.

Dhir, R. K., Limbachiya, M. C., and Leelawat, T. (1999) "Suitability of recycled aggregate concrete for use in BS 5328 designated mixes," *Proceedings of the Institution of Civil Engineers*, 134(3), 257–274.

Diamond, S. and Bonen, D., (1993) "Microstructure of Hardened Cement Paste—A New Interpretation", *J. Am. Ceram. Soc.*, 76 [12] 2993-99

Dubey, G. (2002). "Improving sealer using additives," *Pavement magazine: Advancing the World of Pavements*, Vol. 17, No. 1, 4p.

Etxeberria, M., Vazquez, E., Mari, A., and Barra, M. (2007) "Influence of amount of recycled coarse aggregates and production process on properties of recycled aggregate concrete," *Cement and Concrete Research*, 37, 735-742

Goldberger, Harold W. (1961) "Corrective measures employing epoxy resins on concrete bridge deck," Highway Research Board Vol. 40, National Academy of Sciences- National Research Council, Washington, DC, p. 489-496.

Gomez Soberon, J. M. V. (2002a) "Shrinkage of concrete with replacement of aggregate with recycled aggregate concrete," *SP-209: ACI 5th Int. Conf. on Innovation in Design with Emphasis on Seismic, Wind and Environmental Loading, Quality Control, and Innovation in Materials/Hot Weather Concreting,* V. M. Malhotra, ed., 475–495.

Gomez Soberon, J. M. V. (2002b) "Creep of concrete with substitution of normal aggregate by recycled aggregate concrete," *SP-209: ACI Fifth Int. Conf. on Innovation in Design with Emphasis on Seismic, Wind and Environmental Loading, Quality Control, and Innovation in Materials/Hot Weather*

Concreting, V. M. Malhotra, ed., 441–464.

Gomez Soberon, J. M. V. (2002c) "Porosity of recycled concrete with substitution of recycled aggregate concrete: An experimental study," *Cement and Concrete Research*, 32(8), 1301–1311.

Hamel, S. (2005) "Effects of Freezing and Freeze-Thaw Damage to the Transport Properties of Concrete". M.S. Thesis of the University of Colorado at Boulder

Henry, G. (2004) "Penetrating water-repellent sealers", Concrete International information, Vol. 26 No. 5, pp 81-83

Herve, E., and Zaoui, A., (1990) "Modeling the Effective Behavior of Nonlinear Matrix-Inclusion Composites," *Eur. J. Mech.*, A/Solids, 9(6), 505-515

Heydorn, Allan. (2007) "Understanding sealer options", *Pavement Magazine*, Vol. 22, No. 3, pp18-26

Heydorn, Allan. (2007) "What happened to coal tar in 2006", *Pavement Magazine*, Vol. 22, No. 1, pp12-19

James Information Media (2003) "Recycled sealer meets rural road resurfacing requirements", Better Roads information, Vol. 73, No. 11, p86-87.

Jennings, H.M., and Tennis, P.D., "A Model for the Developing Microstructure in Portland Cement Pastes", *J. of Amer. Ceram.Soc.*, 77 (12), 3161-72, 1994. Correction published in the J. of Ameri. Cera. Soc., 78 (19), page 2575, 1995

Jennings, H.M., and Xi, Y., (1993) "Microstructurally Based Mechanisms for Modeling Shrinkage of Cement Paste at Multiple Levels", Proc. of the 5th Int. RILEM Symp., ed. by Zdenek P. Bazant and Ignacio Carol, (E& FN Spon., London) 22, 85-102.

Jiusu, L., Hanning, X., Yong, Z. (2009) "Influence of coating recycled aggregate surface with pozzolanic powder on properties of recycled aggregate concrete," *Construction and Building Materials*, 23: 1287-1291

John D. and Wenzlick, P.E. (2007) "Bridge deck concrete sealers", Final report RI04-051, Missouri Department of Transportation

Katz, A. (2004) “Treatments for the improvement of recycled aggregate”, Journal of materials in civil engineering,” *ASCE*, 16(6), 597-603

K. Eguchia, K. Teranishib, A. Nakagomea, H. Kishimotoa, K. Shinozakia and M. Narikawac. (2007) “Application of recycled coarse aggregate by mixture to concrete construction,” *Construction and Building Materials*, 21: 1542–1551

Kou, S.C., Poon, C.S., and Chan, D. (2007) “Influence of fly ash as cement replacement on the properties of recycled aggregate concrete,” *Journal of Materials in Civil Engineering*, 19(9), 709-717.

Krauss, Paul., and Mallela, Jaqannath., and Aho, Brian. (2006) ”Highway concrete pavement technology development and testing: volume I - field evaluation of strategic highway research program (SHRP) C-202 Test Sites (Alkali-Silica Reaction (ASR))”, Final Report FHWA-RD-02-082, Federal Highway Administration.

Krauss, P.D., and Boyd, S.R. (1999) “Cracking repair trials: City Island Bridge at US 61 and 151 Over the Mississippi River”, WJE No. 971345, Iowa Department of Transportation.

Kuauss, P. D. (1985). “New materials and techniques for the rehabilitation of Portland cement concrete”, FHWA/CA/TL-85/16, Office of Transportation Laboratory, California Department of Transportation, Sacramento, Calif., p. 46-59.

Lamond, J. F., et al. (2002) “Removal and reuse of hardened concrete,” *ACI Material of Journal*, 99(3), 300–325

Limbachiya, M.C., Leelawat, T., and Dhir, R.K. (2000) “Use of recycled aggregate concrete in high-strength concrete,” *Materials and Structures*, 33 (9), 574–580

Limbachiya, M.C., Marrocchino, E., and Koulouris, A. (2008) “Chemical-mineralogical characterization of coarse recycled aggregate concrete,” *Waste Management*, 27, 201-207

Mandal, S., Chakarborty, S., and Gupta, A. (2002) “Some studies on durability of recycled aggregate concrete,” *Indian Concrete Journal*, 76(6), 385–388

Mangat, P.S., and Molloy, B.T. (1994) ”Prediction of long term chloride concentration in concrete,”

Materials and Structure 27, p338-346.

Mangat, P.S., and Limbachiya, M.C. (1999) "Effect of initial curing on chloride diffusion in concrete repair materials," *Cement and Concrete Research 29*, 1475–1485.

Marks, Vernon J. (1988) "High molecular weight methacrylate sealing of a bridge deck", Final Report for Iowa DOP Project HR-2031 FHWA Project DTFH 71-86-948-1A-25

Meggers, D. A. (1998) "Crack sealing and repair of older serviceable bridges using polymer sealers", *Kansas Department of Transportation*, 131p.

Meyer, C. (2009) "The greening of concrete industry," *Cement and Concrete Composites*, 31: 601–605

Mueller A, Sokolova SN, Vereshagin VI. (2008) "Characteristics of lightweight aggregates from primary and recycled raw materials," *Construction and Building Materials*, 22(4):703–12.

Oikonomou ND. (2005) "Recycled aggregate concretes," *Cement and Concrete Composites*, 27(2):315–8.

Otsuki, N., Miyazato, S.I., and Yodsudjai, W. (2003) "Influence of recycled aggregate on interfacial transition zone, strength, chloride penetration and carbonation of concrete," *Journal of Materials in Civil Engineering*, *ASCE*, 15(5), 443-451

Pincheira, Jose A., and Dorhorst, Melissa A. (2005) "Evaluation of concrete deck and crack sealers", *Final Report WHRP 06-09, University of Wisconsin-Madison & Wisconsin Department of Transportation*, 159p.

Primer GASB 34, (2000), *FHWA-IF-00-010*, 48p

Rahal K. (2007) "Mechanical properties of concrete with recycled coarse aggregate," *Building and Environment*, 42(1):407–15

Rahim, Ashraf M., and Jansen, D., and Abo-Shadi, N., and Simek, J. (2007) "Use of high molecular methacrylate to seal bridge deck cracks: overview of research", *Transportation Research Board 86th Annual Meeting*, 17p.

Scranton Gillette Communications (1998) "Cold-weather coating battle winter's chill", *Roads & Bridges information*, Vol. 36, No. 4, p.72-74.

Shah, S.P., and Li, Z., (1992) "Bond Properties in Fiber-Cement and Aggregate-Cement Paste Interfaces," *Proc. of First Int. Conf. on Fracture Mechanics of Concrete Structures*, Ed. Bazant, Z.P., Breckenridge, Colorado, U.S.A., 1-5 June, Elsevier, England.

Sherman, M.R., Carrasquillo, R.L., and Fowler, D.W. (1993) "Field Evaluation of Bridge Corrosion Protection Measures," *Report No. FHWA/TX-93+1300-1*, Texas Department of Transportation, Austin, Texas

Shoenberger, J.E. (2002). "A new test method for coal-tar sealer mixtures", *Designing, Constructing, Maintaining, and Financing Today's Airport Projects*, *Proceedings of the Twenty-Seventh International Air Transport Conference*, 9p

Stanish, K.D., Hootan, R.D., Thomas, M.D.A., (1997) "Testing the Chloride Penetration".

Sun, Y.M., Liang, M.T ., and Chang, T.P., (2010) "Time/Depth Dependent Diffusion and Chemical Reaction Model of Chloride Transportation in Concrete", *Applied Mathematical Modelling*, Volume 36, Issue 3, March, Pages 1114–1122

Tabsh, S.W., and Abdelfatah, A.S. (2009) "Influence of recycled aggregate concretes on strength properties of concrete," *Construction and Building Materials*, 23, 1163-1167

Tam, V. W. Y., Gao, X. F., and Tam, C. M. (2005) "Microstructural analysis of recycled aggregate produced from two-stage mixing approach," *Cement and Concrete Research*, 35(6), 1195–1203.

Tam, V. W. Y., and Tam, C. M. (2007) "Assessment of durability of recycled aggregate concrete produced by two-stage mixing approach," *Journal of Material Science*, 42, 3592-3602

Tam, V. W. Y., and Tam, C. M. (2008) "Diversifying two-stage mixing approach (TSMA) for recycled aggregate concrete: TSMAs and TSMAsc," *Construction and Building Materials*, 22, 2068-2077

Tam, V. W. Y., and Tam, C. M. (2009) "Parameters for assessing recycled aggregate and their correlation," *Waste Management & Research*, 27, 52-58

Taylor, H.F.W., (1987) "A Method for Predicting Alkali Ion Concentration in Cement Pore Solutions", *Adv. Cem. Res.*, 1(1), 5

Technology Publishing Company and Steel Structures Painting Council (2000) “Sealing and coating of concrete floor resolved moisture problem at airport”, *Journal of Protective Coatings & Linings*, Vol. 17 No. 9, 3p.

Torquato, S., and Stell, G., (1982) “Microstructure of Two-Phase Random Media. I. The N-point Probability Functions”, *J. of Chem. Phys.*, 77(4), 15 Aug., 2071-2077, 1982

Torquato, S., (1986) “Microstructure Characterization and Bulk Properties of Disordered Two-Phase Media”, *J. of Statistical Physics*, 45(5/6), 843-873, 1986

Transportation Research Record (1995) “Service lives of concrete sealers,” *Transportation Research Record*, No.1490, p.54-59.

Tu TY, Chen YY, Hwang CL. (2006) “Properties of HPC with recycled aggregates,” *Cement and concrete research*, 36(5):943–50

Wijeyewickrema, A. C. and Leungvichcharoen, S., (2003) “Prediction of interphase properties of a three-phase composite using three-phase and four-phase composite models”, *Proceedings of the 16th Engineering Mechanics Division Conference, ASCE*, EM2003, July 16-18, Seattle, CD-ROM Paper No. 194, 12 pages.

Xi, Y., Eskandari-Ghadi, M., Suwito, and Sture. S. (2006) “A Damage Theory Based on Composite Mechanics”, *Journal of Engineering Mechanics*, *ASCE*, 132(11), 1-10

Xi, Y., and Jennings, H.M. (1997) “Shrinkage of Cement Paste and Concrete Modeled by a Multiscale Effective Homogeneous Theory”, *Materials and Structures (RILEM)*, 30, July, 329-339.

Xi, Y. and Nakhi, A. (2005) “Composite Damage Models for Diffusivity of Distressed Materials”, *Journal of Materials in Civil Engineering*, *ASCE*, May/June, 17(3), 286-295.

Xi, Y., Willam, K., and Frangopol, D. (2000) “Multi-scale Modeling of Interactive Diffusion Processes of Concrete”, *Journal of Engineering Mechanics*, *ASCE*, 126(3), 258-265

Zheng, J., and Zhou, X. (2008) “Analytical Solution for the Chloride Diffusivity of Hardened Cement Paste”, *Journal of Materials in Civil Engineering*, 20(5), 384–391.